11-24-2014 12:00 AM

Controls on Syenite-Hosted Gold Mineralization in the Western Timmins Camp

Robert A. Campbell, *The University of Western Ontario*

Supervisor: Bob Linnen, *The University of Western Ontario*

A thesis submitted in partial fulfillment of the requirements for the Master of Science degree in Geology

Controls on Syenite-Hosted Gold Mineralization in the Western Timmins Camp

(Thesis format: Monograph)

by

Randy Campbell

Graduate Program in Earth Sciences

A thesis submitted in partial fulfillment

of the requirements for the degree of

Master of Science

The School of Graduate and Postdoctoral Studies

The University of Western Ontario

London, Ontario, Canada

ABSTRACT

The Abitibi granite-greenstone belt has long been known for its' world-class Archean lode gold deposits. While a spatial relationship between felsic intrusions and gold deposits has been noted for some time, it is not clear whether porphyries are genetically related to gold mineralization or just provided a brittle host for unrelated mineralization. The Thunder Creek deposit and Hwy-144 gold prospect are two recently discovered and exploited syenite-associated gold plays in the Timmins Camp. Currently the Thunder Creek deposit is the only syenite-hosted deposit being mined in the Timmins Camp. While syenite-hosted deposits have been well characterized and exploited in the Kirkland Lake area and Eastern (Quebec) portion of the Abitibi, the discovery and exploitation of Lake Shore Gold's Thunder Creek deposit provides renewed interest into the Western portion of the Timmins Camp.

The research compares the Thunder Creek and Hwy-144 properties providing new observations regarding the controls on gold mineralization. Both properties show broad similarities like; syenite hosted mineralization and quartz vein + pyrite associated hosting mineralization; but there are differences including alteration assemblages and pyrite geochemistry. Disseminated pyrite crystallization at Thunder Creek is synchronous with early gold mineralization. This style of mineralization is overprinted by V_1 and V_2 quartz veins that host the bulk of gold mineralization in medium to coarse vein-hosted pyrite. Vein-formation at Thunder Creek occurred in response to D_3 deformation in the adjacent Rusk Shear Zone, with silicification being the main alteration style. At Hwy-144, hematitic and potassic alteration vary in intensity and are weakly associated with gold mineralization. Pyrite geochemistry reveals that pyrite crystallized out of a gold-poor fluid. Gold mineralization is restricted primarily to vein-hosted pyrite grains with inclusions of gold deposited by late auriferous fluids that corroded pyrite grains.

Keywords: syenite, lode-gold, Timmins, pyrite, alteration

Acknowledgements

I would like to take a brief moment to acknowledge those who aided in the improvement and completion of this project. First and foremost I would like to thank my supervisor Dr. Bob Linnen. I would like to thank Bob for finding the project and assisting me from start to finish. I would also like to thank Bob for his unmatched, instantaneous responses through email correspondence. I would like to thank Lake Shore Gold Corporation for providing financial, logistical and field support. I am especially grateful for the field/industry experience Lake Shore provided. Specifically I would like to thank Keith Green, Jacques Samson and Eric Kallio. All of the above provided encouragement and built the foundation for my current understanding of the Abitibi and Thunder Creek/Hwy-144 properties. My uncle Bob Barnett deserves a big thank you for taking the time to review my drafts, assisting with petrography and for instigating arguments over the importance of mineral chemistry. I'd like to thank Mark Beauchamp for the assistance in generating spectacular trace element pyrite maps and spot analyses using the electron microprobe. Finally I'd like to thank my dad Andy Campbell for reluctantly introducing me the industry and for patiently guiding me from undergrad to today.

Table of Contents

Abstract **II**

Acknowledgements **III**

Table of Contents **IV**

List of Figures **VIII**

List of Tables **XV**

1.0 Introduction **1**

1.1 Thesis Objectives 2

2.0 Regional Geology **4**

2.1 Abitibi Subprovince 5

2.2 Tectonic Evolution of the Timmins Camp 6

2.3 Metamorphism 8

3.0 Methods **9**

3.1 Sampling Strategy 9

3.1.1 Thunder Creek Mine 9

3.1.2 TC05-21-EXT 10

3.1.3 Hwy-144 10

3.1.4 Vein Density Calculations 16

3.2 Whole Rock Geochemistry 16
3.3 Laser Ablation Induced Coupled Mass Spectrometry 17
3.4 Electron Microprobe Analyses 18
3.5 Secondary Ion Mass Spectrometry 18

4.0 Local Geology 19
4.1 Thunder Creek 19
4.1.1 Mafic Volcanics 20
4.1.2 Pyroxenite 21
4.1.3 The Rusk Zone 23
4.1.4 Transitional Lithologies 24
4.2 Thunder Creek Syenite (Mine) 25
4.2.1 TC280m Level 26
4.2.2 TC695m Level 26
4.3 Thunder Creek Syenite Stock 26
4.4 Structure 27
4.5 Vein Types 28
4.6 Hwy-144 Exploration Target 29
4.6.1 Mafic Volcanics 30
4.6.2 Pyroxenite 31
4.6.3 Syenite 32
4.7 Porcupine Sediments 34

5.0 Alteration 35
5.1 Alteration at Thunder Creek 35
5.1.1 Mafic Volcanics 35
5.1.2 Pyroxenite 36

5.1.3 Rusk Shear Zone 38
5.1.4 Thunder Creek Syenite 38
5.1.5 Thunder Creek Syenite Stock 40
5.2 Hwy-144 41
5.2.1 Mafic Volcanics 41
5.2.2 Pyroxenite 42
5.2.3 Hwy-144 Rusk 43
5.2.4 Syenite 43

6.0 Mineralization 45
6.1 Thunder Creek 45
6.1.1 Sample Strategy 45
6.1.2 Gold Grade vs. Vein Density 46
6.1.3 Petrography 48
6.1.4 Rusk Shear Zone 49
6.2 Hwy-144 Syenite 51

7.0 Geochemistry 53
7.1 Syenite Geochemistry 53
7.2 Pyroxenite Geochemistry 56
7.3 Monitoring Fractionation, Alteration & Mineralization 58
7.4 Mass Balance 61
7.5 Mineral Chemistry 64
7.6 Whole Rock Geochemistry Discussion 65
7.7 Pyrite Mapping 66
7.7.1 TC 695m Disseminated 67
7.7.2 TC 280m Disseminated 67

7.7.3 TC 695m & 660m Vein-Hosted 68
7.7.4 TC 280m Vein Hosted 69
7.7.5 Hwy-144 Disseminated 70
7.7.6 Hwy-144 Fracture Controlled 70
7.7.7 Hwy-144 Vein-Hosted 71
7.8 Pyrite Geochemistry 72
7.8.1 Thunder Creek Pyrite 72
7.8.2 Hwy-144 Pyrite 74
7.9 Trace Element Correlations 80
7.10 Gold Solubility in Pyrite 86
7.11 Pyrite Geochemistry Discussion 88
7.12 Sulfur Isotopes 88
7.13 Sulfur Isotope Discussion 91

8.0 Discussion 93

9.0 Conclusion 103

References 104

List of Figures

Figure 2.1: General geologic map of the Superior Province. 4

Figure 2.2: General geologic map of the Abitibi Subprovince. 5

Figure 2.3: Map displaying the distribution of felsic porphryies in the Abitibi. 7

Figure 3.1: Map of sample localities on the TC 280m level. 11

Figure 3.2: Map of sample localities on the TC 695m level. 12

Figure 3.3: DDH composite cross section of Hwy-144. 13

Figure 3.4: Stratigraphy of drill hole Hwy 11-20. 13

Figure 3.5: Stratigraphy of drill hole Hwy 11-13. 14

Figure 3.6: Stratigraphy of drill hole Hwy 11-12. 14

Figure 3.7: Stratigraphy of drill hole Hwy 10-03. 15

Figure 4.1: Local geology map of Thunder Creek property. 19

Figure 4.2: General cross section of Thunder Creek & Hwy-144. 19

Figure 4.3: Underground photo of mafic volcanics at Thunder Creek. 20

Figure 4.4: Photomicrographs of mafic volcanics. 21

Figure 4.5: Hand sample photo of TC pyroxenite. 22

Figure 4.6: Photomicrograph of TC pyroxenite. 22

Figure 4.7: Underground photos of Rusk Shear Zone. 23

Figure 4.8: Underground photos of Rusk mineralization/alteration. 24

Figure 4.9: Underground photos of TC syenite. 25

Figure 4.10: Photomicrographs of TC syenite. 26

Figure 4.11: Hand sample photo of alteration at the TC stock. 27

Figure 4.12: Photomicrographs of TC stock. 27

Figure 4.13: Image of different vein sets within TC syenite. 28

Figure 4.14: Underground photos of the different vein sets at TC. 29

Figure 4.15: Local geology map of the Hwy-144 property. 29

Figure 4.16: Hand sample photos of Hwy-144 mafic volcanics. 30

Figure 4.17: Photomicrographs of Hwy-144 mafic volcanics. 30

Figure 4.18: Hand sample photos of Hwy-144 pyroxenite. 31

Figure 4.19: Photomicrographs of Hwy-144 pyroxenite. 32

Figure 4.20: Hand sample photos of Hwy-144 syenite. 33

Figure 4.21: Photomicrographs of Hwy-144 syenite. 33

Figure 5.1: Hand sample photos of alteration in mafic volcanics at TC. 35

Figure 5.2: Photomicrographs of alteration within the mafic volcanics. 36

Figure 5.3: Photomicrographs of alteration within the mafic volcanics. 36

Figure 5.4: Hand sample photos of alteration in the TC pyroxenite. 37

Figure 5.5: Photomicrographs of alteration in the TC pyroxenite. 37

Figure 5.6: Photomicrographs of alteration in the TC pyroxenite. 37

Figure 5.7: Hand sample photos of the alteration in the Rusk Zone. 38

Figure 5.8: Photomicrographs of Rusk alteration. 38

Figure 5.9: Hand sample photos of alteration in the TC syenite. 39

Figure 5.10: Tabletop SEM image of alteration in feldspars. 39

Figure 5.11: Tabletop SEM spectra identifying minerals. 40

Figure 5.12: Photomicrographs of alteration in TC stock. 41

Figure 5.13: Photomicrographs of alteration in Hwy-144 volcanics. 41

Figure 5.14: Photomicrographs of alteration in Hwy-144 volcanics. 42

Figure 5.15: Photomicrographs of alteration in Hwy-144 pyroxenite. 42

Figure 5.16: HS and Photomicrograph images of Hwy-144 Rusk alteration. 43

Figure 5.17: Hand sample images of alteration in the Hwy-144 syenite. 44

Figure 5.18: Photomicrograph images of alteration in the Hwy-144 syenite. 44

Figure 6.1: Image comparing vein density versus mineralization. 47

Figure 6.2: Graph showing the correlation between vein density and gold grade. 47

Figure 6.3: Image displaying difference between gold grade and vein sets. 48

Figure 6.4: HS image of mineralization in TC syenite. 49

Figure 6.5: Photomicrograph images of mineralization in TC syenite. 49

Figure 6.6: HS images of Rusk style mineralization at TC. 50

Figure 6.7: Photomicrograph images of Rusk mineralization. 51

Figure 6.8: Photomicrograph images of Rusk mineralization. 51

Figure 6.9: HS images of Hwy-144 mineralization in syenite. 52

Figure 6.10: Photomicrograph images of Hwy-144 syenite mineralization. 53

Figure 7.1: Alkalinity plot of syenite samples from TC and Hwy-144. 55

Figure 7.2: Spider diagram plot of Thunder Creek syenite samples. 55

Figure 7.3: Spider diagram plot of TC, TC stock and Hwy-144 syenite. 56

Figure 7.4: Spider diagram plot of TC syenite, pyroxenite & Rusk. 58

Figure 7.5: Incompatibility plot of TC Mine and TC stock syenite samples. 59

Figure 7.6: Major oxide plot across TC695m syenite body. 60

Figure 7.7: Major oxide plot across Hwy-144 syenite body. 61

Figure 7.8: Mass Balance calculations of Thunder Creek syenite. 63

Figure 7.9: Mass Balance equations comparing TC to Hwy-144. 63

Figure 7.10: Disseminated pyrite mapping (TC695m). 67

Figure 7.11: Disseminated pyrite mapping (TC280m). 68

Figure 7.12: Disseminated pyrite mapping (TC280m). 68

Figure 7.13: Vein-hosted pyrite mapping (TC695m). 68

Figure 7.14: Te levels mapped in TC695m pyrite. 69

Figure 7.15: Vein-hosted pyrite mapping (TC280m). 69

Figure 7.16: Disseminated pyrite mapping (Hwy-144). 70

Figure 7.17: Fracture filling pyrite mapping (Hwy-144). 70

Figure 7.18: Vein-hosted pyrite mapping (Hwy-144). 71

Figure 7.19: Vein-hosted pyrite mapping (Hwy-144). 71

Figure 7.20: Image of gold correlating to inclusion rich core of pyrite. 73

Figure 7.21: Gold values across TC280m vein-hosted pyrite. 74

Figure 7.22: Distribution of gold across vein-hosted TC660m pyrite. 75

Figure 7.23: Distribution of gold across vein-hosted TC660m pyrite. 76

Figure 7.24: Distribution of gold across disseminated Hwy-144 pyrite. 77

Figure 7.25: Distribution of gold across fracture filling Hwy-144 pyrite. 78

Figure 7.26: Dist. of gold across fracture filling Hwy-144 pyrite (mineralized). 78

Figure 7.27: Dist. of gold across vein-hosted Hwy-144 pyrite (mineralized). 79

Figure 7.28: Dist. of gold across vein-hosted Hwy-144 pyrite (unmineralized). 80

Figure 7.29: Trace element correlations within TC pyrite. 81

Figure 7.30: Trace element correlations (Au vs. Cu & Au vs. Ag) TC pyrite. 81

Figure 7.31: Trace element correlations (As vs. Au) TC pyrite. 82

Figure 7.32: Disseminated pyrite Hwy-144 trace element correlations. 83

Figure 7.33: Fracture filling Hwy-144 pyrite trace element correlations. 84

Figure 7.34: Unmineralized fracture filling pyrite tr. element spectra. 85

Figure 7.35: Zoned vein-hosted Hwy-144 pyrite trace element correlations. 85

Figure 7.36: Vein-hosted Hwy-144 pyrite trace element correlations. 86

Figure 7.37: Diagram of gold solubility in Thunder Creek pyrite. 87

Figure 7.38: Diagram of gold solubility in Hwy-144 pyrite. 87

Figure 7.39: Distribution of S isotopes in disseminated TC280m pyrite. 90

Figure 7.40: Distribution of S isotopes in disseminated TC280m pyrite. 90

Figure 7.41: Distribution of S isotopes in disseminated TC695m pyrite. 91

Figure 8.1: Gold solubility with changing temperature. 99

List of Tables

Table 2.1: Outline of the nine stratigraphic units in the Timmins camp. 6

Table 3.1: Standard operating conditions for laser ablation unit. 17

Table 6.1: Gold endowment of different vein sets at Thunder Creek. 46

Table 7.1: Major oxide analyses of representative syenite samples. 53

Table 7.2: Major oxide analyses of representative pyroxenite samples. 57

Table 7.3: Electron Microprobe data from albite grains analyzed. 64

Table 7.4: Electron Microprobe data from K-feldspar grains analyzed. 65

Table 7.5: In-situ Sulfur isotopic analyses of pyrite grains. 89

1.0 INTRODUCTION

Gold mining and mineral exploration in the Timmins Camp began over a hundred years ago in 1912. Since then research by mining companies and research institutions alike, have provided a framework for the current understanding of Archean lode gold (Au) deposits. Extensive exploration in the Timmins camp has uncovered various deposit types: volcanogenic massive sulfide (VMS), banded iron formation (BIF), magmatic nickel (Ni) sulfide, vein-hosted copper and lode gold (Au).

Orogenic gold deposits in the Abitibi share both a structural and geochemical component. A high percentage of intrusion related deposits occur along second order fault structures related to major crustal breaks (Ayer et al., 2005; Bateman & Bierlein, 2008), the structural and geochemical component of both the TC and Hwy-144 properties will be considered. David Rhys has done extensive structural work for Lake Shore Gold Corp and has presentations and reports that will be utilized. Felsic intrusions display a distinct geographic correlation with Archean lode gold deposits (Ayer et al. 2005, MacDonald et al. 2005, Robert & Poulsen, 1997); however a genetic link between intrusions and gold mineralization is still contentious. Felsic intrusives in the Abitibi are compositionally diverse, ranging from: granitic-monzonitic-syenitic. Alkaline intrusions are by far the least abundant, with the majority of intrusions being quartz-feldspar porphyries with a calc alkaline affinity (MacDonald et al., 2005). Alkaline intrusions likely represent a rifting environment, different from subduction-related granitic intrusions. The Thunder Creek, Young-Davidson, Beattie, Douay deposits and the Hwy-144 gold prospect are a few examples of syenite-associated gold deposits in the Abitibi (Robert, 2001). These deposits are different from the traditional shear vein quartz-carbonate-tourmaline deposits, and gold-rich VMS deposits which account for the bulk of gold production in the camp.

Syenite associated deposits have been well documented in the Abitibi; however these intrusions have not always been primary targets for gold mineralization. Within the Ontario portion of the Abitibi Greenstone Belt; gold bearing alkalic suites are located in two geographically separate regions. There is a cluster of alkalic intrusions in the southeastern portion of the belt, located near Kirkland Lake associated with the Cadillac-Larder Lake fault system and there is also the Bristol Township Alkalic Complex (BTAC) located in the southwestern portion of the Abitibi. In between these two localities are suites of primarily granitic intrusives. The Thunder Creek deposit is currently the only economic producer of syenite-hosted gold in the Timmins camp.

Syenite-monzonite composite stock networks are typically elongated parallel to the regional fault system. These multiphase intrusions have two hypothesized associations with gold mineralization: 1) a magmatic-hydrothermal gold system related to the intrusive stock. 2) the small composite stocks provided an ideal brittle host for gold mineralization (Robert, 2001). Gold mineralization within these intrusions is present in disseminated sulphide replacement zones or associated with quartz ± carbonate ± feldspar vein arrays. Mineralization zones are often characterized by one or more of the

following alteration types: iron (Fe) carbonate, potassic (K-spar), sericite and albite (Martin, 2012; Robert, 2001).

Robert (2001) suggested that the Brewery Creek (Yukon), Vunda (Fiji) and the Gold Reward (South Dakota) deposits may represent younger analogs of Archean syenite-hosted deposits. These deposits contain both sulphide replacement and vein-associated ores within larger felsic intrusions. However, younger documented deposits posses a distinctly "reduced" nature compared to oxidized Archean deposits and do not have the spatial relationship with coeval sediments. It is possible that the nonexistent relationship with coeval sediments is due to intrusion emplacement deeper within the crust (Robert, 2001). Similar to the Archean deposits the Cretaceous Brewery Creek deposit is present along a strike-slip fault system in Central Yukon (Diment & Craig, 1998). Sercite and carbonate alteration along with the destruction of mafic phenocrysts are other common characteristics shared with Archean aged syenite-hosted deposits.

.

1.1 THESIS OBJECTIVES

The study of syenite-associated gold at Thunder Creek (TC) and Hwy-144 aims to determine whether the syenite acted as a suitable brittle host, or provided gold mineralization through magmatic-hydrothermal processes. Limited geochemical and petrological study of the TC deposit provides the need for a thorough, regimented sampling process. This will test the hypothesis that a geochemical alteration halo surrounds gold mineralization. Samples were also collected in areas of known mineralization targeting different vein arrays to determine their Au contribution. Other studies (Linnen et al. 2012; Martin, 2012) in the southeastern portion of the Abitibi, along the Cadillac Larder Lake fault system suggest Au concentration is hosted in a potassic alteration zone within the larger intrusion

The study area also contains disseminated sulphide/gold mineralization along with multiple alteration halos, lending to a porphyry style of mineralization. Understanding which component of the system controls the main mineralization phase is a primary goal of this thesis. Using geochemical data across the intrusion and underground mapping of the TC deposit we can better interpret the controls on gold mineralization. Polished section microscopy, electron microprobe analysis, along with sulphur isotopes will allow us to characterize gold mineralization and interpret the origin of mineralizing fluids. The spatial and lithological similarities between the TC deposit and Hwy-144 prospect provide an interesting opportunity to look at exploration potential.

The thesis is designed to answer two questions. What are the main controls on gold mineralization at the Thunder Creek deposit? And, is Hwy-144 an extension of the same mineralizing system? To answer these questions the thesis is broken into three parts: a study of gold controls at the 695m level of the TC deposit, a study of gold controls at the 280m level of the TC deposits, and a study of gold controls on the Hwy-144 gold prospect. At each site geochemical, mineralogical and structural data will be analysed. This will be done thorough whole rock geochemistry, polished section petrography, electron microprobe analysis, S isotopic work and selective sampling of prospective structures and alterations. This sampling strategy is unique to the deposit locality and will provide the first step towards better understanding the controls on gold mineralization.

2.0 REGIONAL GEOLOGY

The Superior Province is one of the largest Archean cratons on Earth (Card, 1990) and is composed of a number of Archean subprovinces that span the majority of Ontario and Quebec (Figure 2.1). The bulk of subprovinces run East-West; however there are a few transposed terranes present in northern Quebec. The province is bound by two orogens on the eastern and western margins. In the west this boundary is defined by the Trans-Hudson, in the east by the Grenville. In the South (Penokean) and Northeast (Labrador Trough) Proterozoic supercrustal rocks have been unconformably thrust onto the craton. With only a few exceptions the vast majority of rocks within the Superior Province are Archean in age. Compositionally the province consists of high-grade gneiss terranes in the North and South, with volcano-plutonic units in between. The presence of xenocrystic zircons similar in age to underlying formations, stratigraphic patterns representing tectonic progression, unconformities and terranes/units largely in logical order suggests an autochthonous formation of the Superior Province (Thurston, 2002).

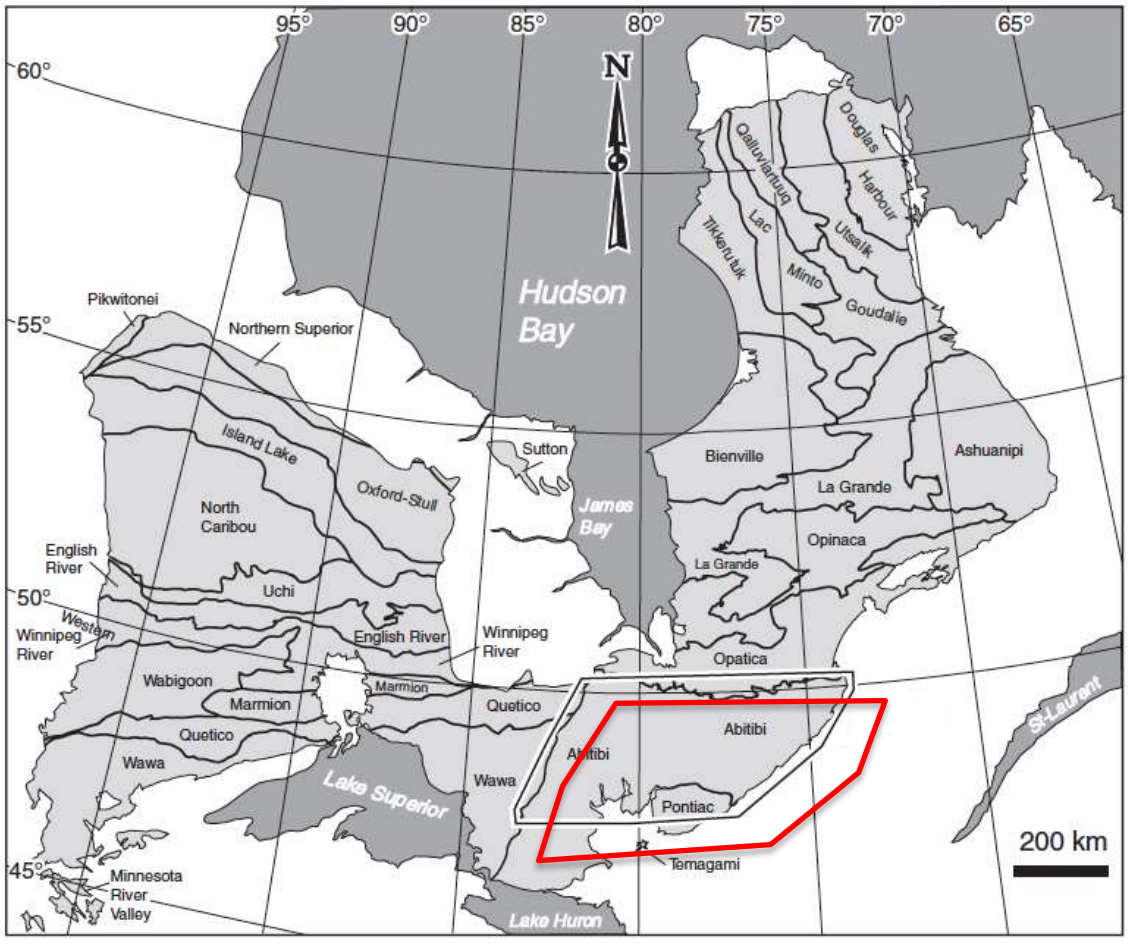

Figure 2.1: The Superior Province (light grey fill) with individual subprovinces labelled. The Abitibi Subprovince is highlighted in red. Modified from Thurston et al., 2008.

2.1 ABITIBI SUBPROVINCE

The Abitibi subprovince is an East to West trending granite greenstone belt within the larger Superior Province. Its' excellent preservation and economic importance make it one of the most extensively studied greenstone belts in the world (Ayer et al., 2005; Bateman & Bierlein, 2007; Card, 1990; Snyder et al., 2008; Thurston et al., 2008). The subprovince is bounded to the west by the Kapuskasing Structural Zone (KPZ) and to the east by the Grenville Tectonic Zone (Snyder et al., 2008)(Figure 2.2). The Opatica subprovince straddles the Abitibi to the North and Pontiac subprovince to the South. The province is composed of 60% granitoid and 40% supracrustal rocks; the supracrustals can be broken down into 80% metavolcanics and 20% metasediments (Card, 1990). The Abitibi can be broken down into four zones outlined in

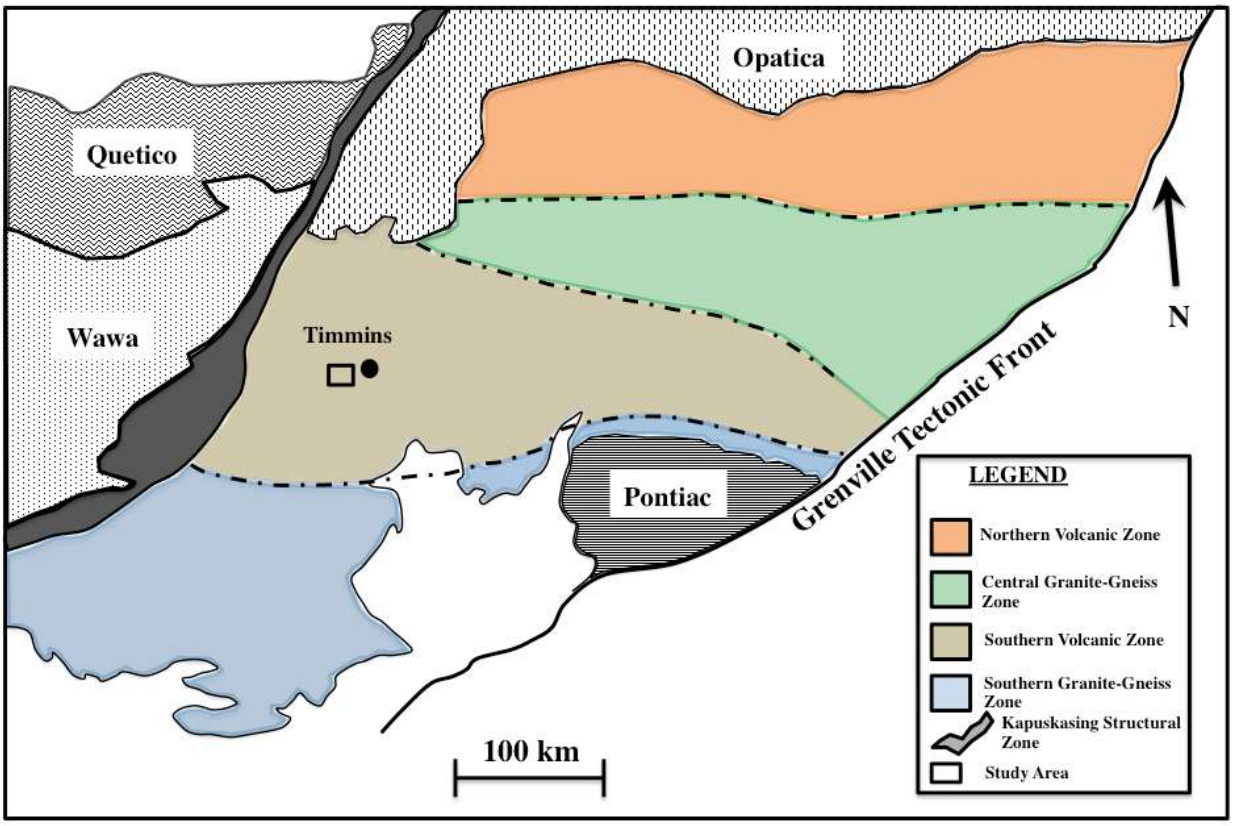

Figure 2.2: Enlarged view of Figure 1, the Abitibi Subprovince is subdivided into four groups. Modified from Ludden & Hubert, 1986.

Figure 2.2, as the Northern Volcanic Zone, Central Granite-Gneiss Zone, Southern Volcanic Zone and Southern Granite-Gneiss Zone. The Northern volcanic zone is composed of evolved basaltic to rhyo-dacitic lavas with a Mg content no higher than 8-9 wt% (Ludden & Hubert, 1986). In the Southern Volcanic Zone tholeiitic and komatiitic lavas are present along with bimodal volcanic complexes. In the North, volcanic centers were above tonalite-granodiorite plutons, while in the south bimodal volcanism occurred in rifts basins between shear zones (Ludden & Hubert, 1986).

2.2 TECTONIC EVOLUTION OF THE TIMMINS CAMP

The Timmins camp sits in the southwest portion of the Abitibi subprovince between two East-West trending regional scale fault structures. Volcanism, sedimentation and plutonism occurred over 90 Ma between 2750-2660 Ma (Ayer et al., 2005). The interpretation of the tectonic evolution of the Timmins camp (Ayer et al., 2005; Bateman et al., 2008; Bateman & Beirlen; 2007; Robert & Poulsen, 1997; Snyder et al., 2008) has resulted in the distinction of eight tectonostratigraphic units (Table 2.1). These units represent the destruction of the supercontinent Vaalbara and the creation of the supercontinent Kenorland (Bateman & Bierlein, 2007). The stratigraphy consists of 6 early mafic-felsic volcano-plutonic units and two late rift basin sedimentary packages. The eight units are described in Table 1.

Table 2.1: Eight stratigraphic units within the Timmins camp, information taken from Thurston et al., 2008.

Unit	Age (Ma)	Thickness (km)	Lithologies
Timiskaming	2676-2670	2-3	Polymictic conglomerate, sandstone, alkaline volcanics
Porcupine	2690-2685	2-3	Turbiditic sediments (argillites, wackes), Krist Fm. volcanics, Qtz-Feldspar porphyries, syenites
Blake River	2704-2696	~16	Mafic-felsic volcanics, minor clastic metasediments
Tisdale	2710-2704	~10-15	Intermediate- felsic flows, mafic volcanics, minor ultramafic, iron formation
Kidd-Munro	2719-2711	~10	Mafic volcanics with localized ultramafic, felsic volcanics and graphitic sediments
Stoughton	2723-2720	12	Tholeiitic basalts with local komatiites and felsic volcanics.
Deloro	2730-2724	~5	Mafic to felsic calc-alkaline volcanic rocks
Pacuad	2750-2735	5	Ultramafic, mafic and felsic volcanic rocks, minor iron formation.

Early mafic to ultramafic volcanism was followed by volcanic shedding and late felsic plutonism, "granite bloom". Post granite bloom late dextral strike-slip movement occurred along the two major breaks in the camp (Porcupine-Destor and Cadillac-Larder Lake fault systems). Gold mineralization is spatially associated to quartz-feldspar and syenite porphyries aligned roughly parallel to the Porcupine-Destor fault system (Figure 2.3). Tectonically, gold mineralization is primarily restricted to deformation events D_2-D_4. D_2 represents thrust imbrication noted by the S_2 foliation associated with ankerite and fuchisite veins (Dome Mine); D_3 is left lateral strike slip movement and en echelon folding resulting in the S_3 foliation (Hollinger Mine); D_4 is produced by right lateral strike slip movement and reverse faulting (Pamour Mine) (Bateman et al., 2008; Bateman & Bierlein, 2007; Snyder et al., 2008).

There has long been an understanding that gold mineralization is spatially related to felsic plutonism in the Abitibi. The Pearl Lake and Paymaster quartz-feldspar porphyries are spatially associated with the Hollinger and Dome mines respectively. Further east in the Kirkland Lake camp syenitic porphyries are associated with the Macassa mine. Felsic plutonism is contemporaneous in age with the deposition of the Porcupine and Timiskaming sediments that formed in late rift basins. The study area hosts syenitic intrusions in the western portion of the Timmins camp, suggesting an alkaline style magmatism/mineralization similar to Kirkland Lake (Figure 2.3).

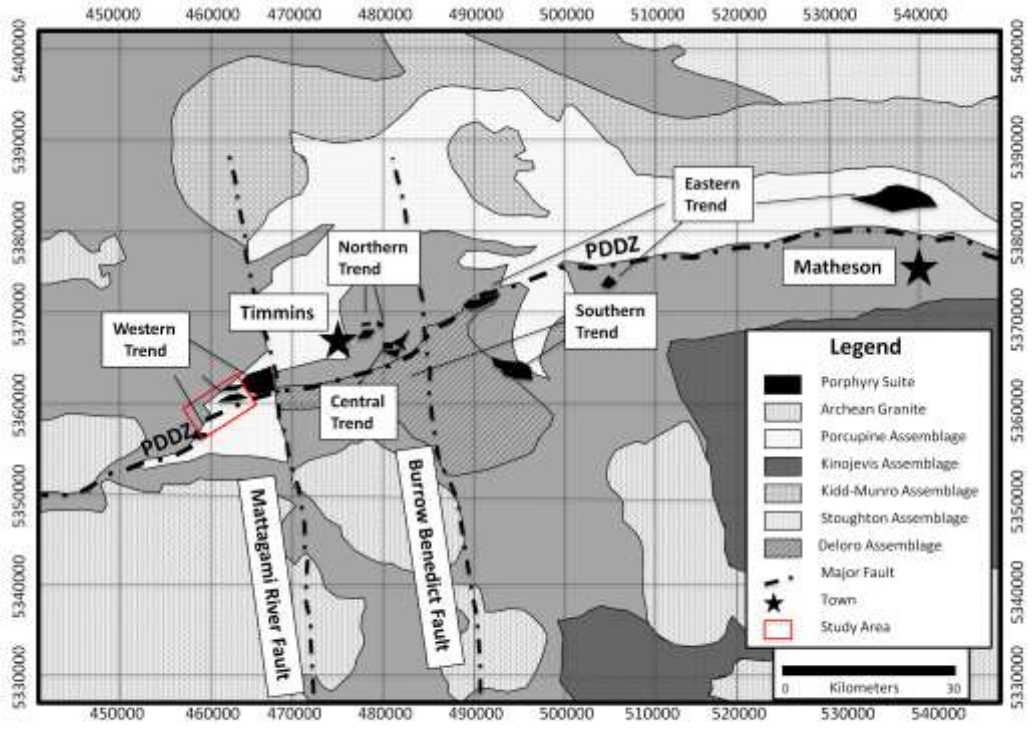

Figure 2.3: Felsic porphyries in the Timmins Camp. Study area highlighted in red. Modified from MacDonald et al., 2005

2.3 METAMORPHISM

Metamorphic grade in the Abitibi ranges from prehnite-pumpellyite to lower amphibolite facies (Ayer et al., 2005). Higher-grade metamorphism is only present in close proximity to isolated shear zones. Metamorphic assemblages present in the greenstone belt are indicative of the following processes: seafloor metamorphism and metasomatism, hydrothermal metasomatism (VMS), burial metamorphism, and contact metamorphism (Card, 1990). Fault structures and shear zones are often associated with aureoles of metasomatic carbonatization, sericitization and silicification. The main metamorphic event occurred post Timiskaming sedimentation. The maximum depth reached during the second metamorphic event was 8-10km with temperatures ranging from 350 to 450°C (Ayer et al., 2005).

Archean gold mineralization is strongly related to large crustal penetrating fault structures. These structures provide both a fluid pathway and emplacement corridor for gold bearing fluids and upper crustal plutonism. Within the Timmins camp there are approximately thirty gold deposits along 20 km of strike, on or slightly off the major break (Bateman & Bierlein, 2007).

These regional structures represent the suture zone formed by collisional plate tectonics. As described above in the tectonic evolution of the Timmins camp, granite emplacement formed along the margin of colliding tectonic plates. There is still discussion regarding whether mantle derived fluids or fluids sourced from listric faults penetrating the supercrustal sequence carried gold mineralization (Bateman & Bierlein, 2007).

3.0 METHODS

A variety of analytical techniques were used to evaluate the controls on gold mineralization at Thunder Creek and Highway-144. The sampling strategy targets both mineralized and non-mineralized samples from both underground and diamond drill holes. The following analytical techniques were used: Spatial imaging software (Photoshop), whole rock geochemistry, Laser Ablation Induced Coupled Mass Spectrometry (LA-ICP-MS), Electron Microprobe Analysis (EMPA), and Secondary Ion Mass Spectrometry (SIMS). Moving from the macro to micro scale we are able to resolve chemical changes that occur in the rock that may be disguised by alteration or limitations on certain analytical equipment. For example, the electron microprobe has a Au detection limit of approximately 200ppm. Creating a trace element Au map may provide no indication of appreciable amounts of gold in that pyrite grain. If we now run a laser ablation transect across the same grain we can get gold values with a lower detection limit of approximately 0.5ppm. We have significantly increased our resolution on the composition of gold in the pyrite grain. A full list of samples collected is available in Appendix B.

3.1 SAMPLING STRATEGY

3.1.1 THUNDER CREEK MINE

At the Thunder Creek deposit, two mine levels separated by approximately 415 meters were sampled to determine if there is any geochemical variation between the upper and lower portion of the porphyry. It has been noted by Lakeshore Gold geologists that the 280m level syenite porphyry is a "darker red" colour with patchy low grade mineralization compared to the 695m level. Three background syenite and two Rusk Shear Zone samples were taken within the shaded area illustrated in Figure 3.1. At the 280m level the mineralized Rusk portion has been stoped out, providing limited access to mineralized samples. The porphyry at the 280m level was not mined because the gold grade is sub-economic. The drift tends southwest-northeast parallel to the mineralization in the rusk. At the 695m level the drift trends

At the 695m level a ~115m transect was mapped and sampled for geochemistry. The sampling begins in the north, beginning in unaltered pyroxenite. Moving southwest the sampling intersects altered pyroxenite, Rusk Shear Zone, syenite porphryry and mafic volcanics respectively. Twenty-two geochemical samples were taken across the east wall illustrated in Figure 3.2. Each geochemical sample taken has a corresponding thin section to verify the mineralogical and textural significance of the geochemistry.

In addition to geochemical sampling, mineralization specific sampling was undertaken to constrain the timing and controls on gold mineralization. Approximately eighty samples were taken at various levels (280, 660m, 695m, 730m and 765m) of the Thunder Creek deposit. The sampling takes into account the different vein sets described in the Chapter 3. V_1, V_2, V_3 and background syenite were all sampled to try

and determine the average gold grade for each mineralizing events. Results of this sampling program are outlined in the Mineralization Chapter.

3.1.2 TC 05-21-EXT

The diamond drill hole TC05-21-EXT was chosen because it intersects the Thunder Creek stock, which locally outcrops at surface. A location map for the Thunder Creek stock is available in Chapter 3. The stock was chosen because it is sufficiently far away from the shear zone/mineralization and the syenite still possesses primary biotite and blue amphibole phenocrysts. The degree of alteration varies in the drill hole making it a perfect locality to study the progression of alteration. Eight samples were assayed for major and minor trace element geochemistry and nine thin sections were made.

3.1.3 HWY-144

At the Hwy-144 gold prospect four drill holes were used to derive a composite cross section through the geologic package. The holes Hwy 11-12, Hwy 11-13, Hwy 11-20 and Hwy 10-03 were chosen based on their location and relatively strong gold grades. A total of ninety-two geochemical samples were taken, focusing on the syenite porphryry, but also encompassing hanging wall mafic volcanics, pyroxenites and footwall sediments. Outlined in Figure 3.3, is the location of the drill holes and a composite cross section created to visualize the stratigraphy. Hwy-144 was chosen because of its' resemblance to the Thunder Creek deposit. Current drilling has not outlined a gold deposit of the same scale as TC. One of the primary objectives of this project is to understand the similarities and differences between TC and Hwy-144 to improve the current exploration strategy.

The sampling strategy looks to assess the presence of gold mineralization based on geochemistry/alteration. The targets of the sampling procedure are outlined below(Figure 3.4-3.7):

- Sample systematically throughout the syenite in each drill hole to assess for the presence of carbonate, sericite, hematite and potassic alteration.
- Take multiple samples of the mafic volcanics, pyroxenite and sediments to accurately characterize the rock types and alteration.
- Sample tightly on each side of known mineralized intercepts to assess the differences between mineralized and non-mineralized rocks.
- Avoid vein material to preserve the integrity of the representative geochemical sample.

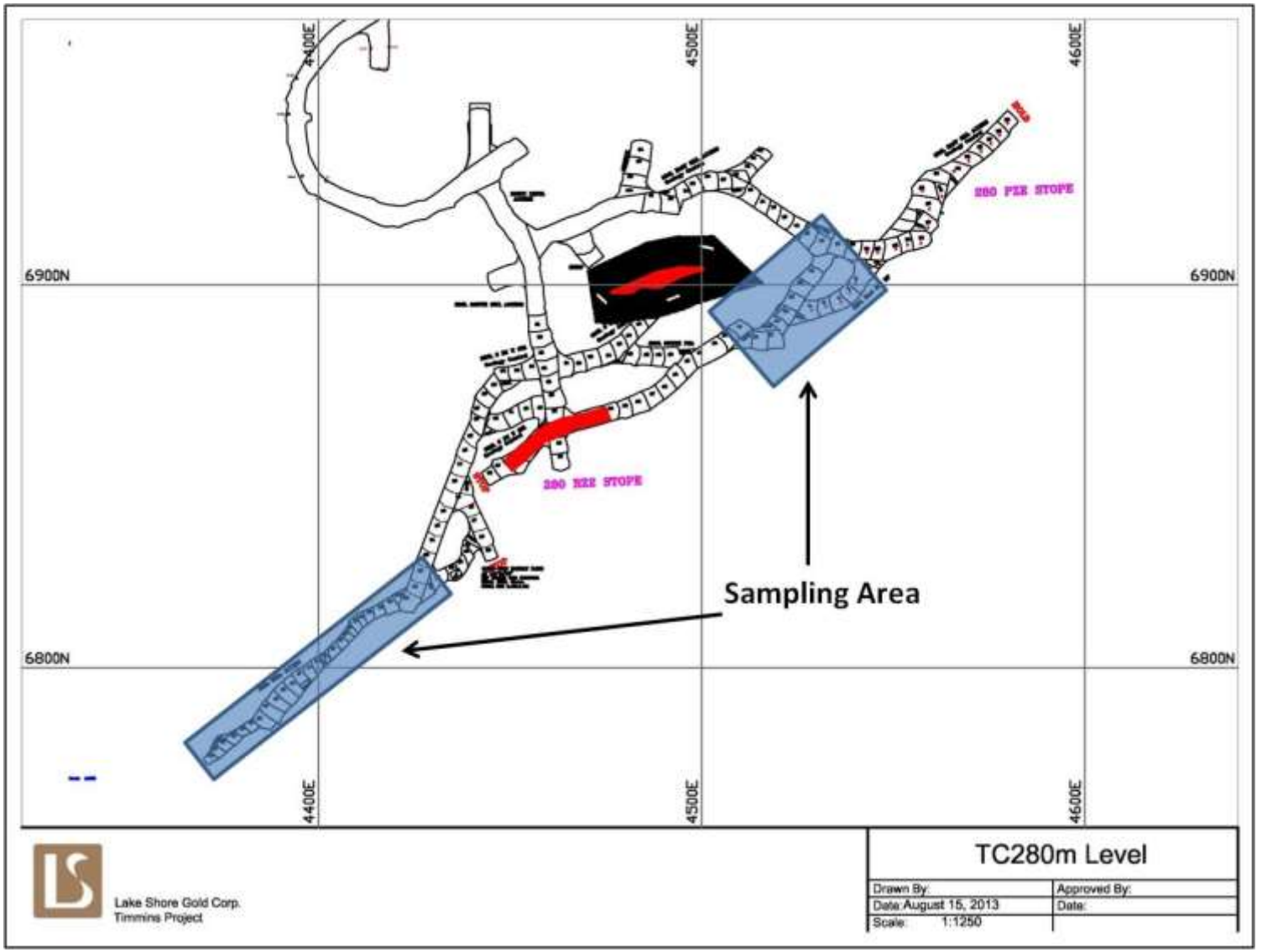

Figure 3.1: 280m level plan of the Thunder Creek deposit. Geochemical samples of the syenite and Rusk zone were taken from the areas shaded in blue.

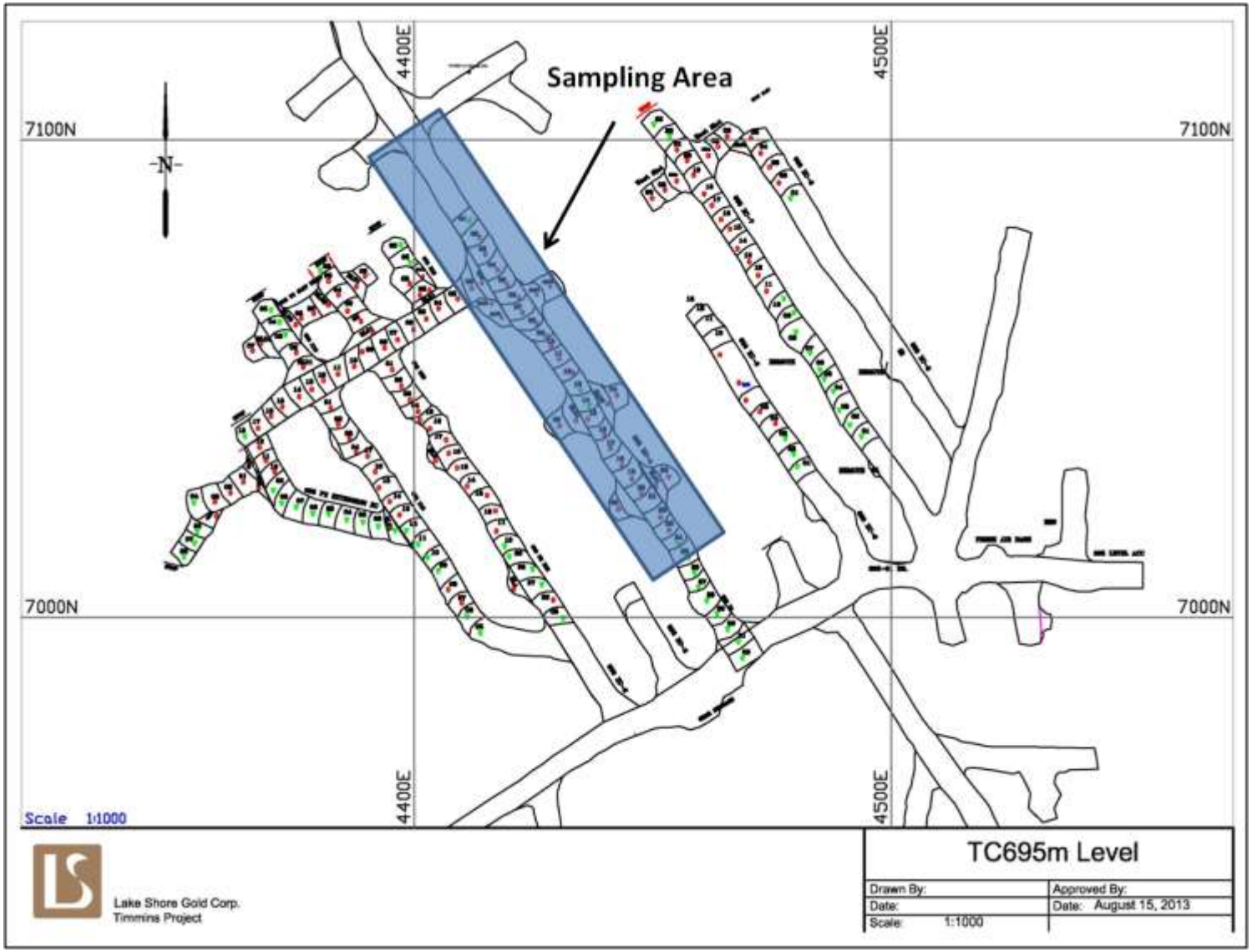

Figure 3.2: TC 695m level plan. Geochemical samples were taken from the east wall of crosscut four shaded in blue.

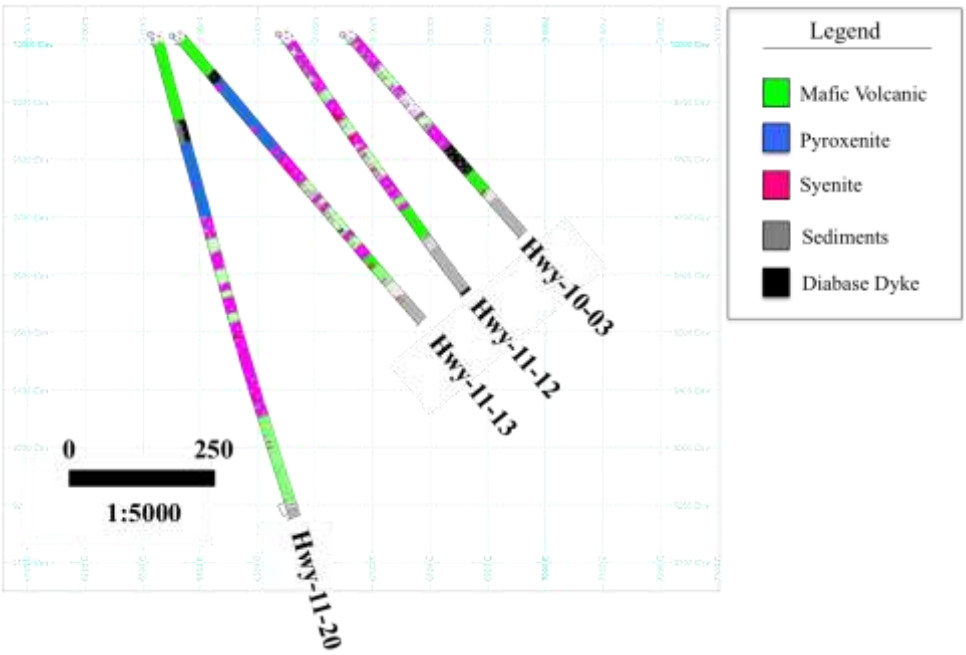

Figure 3.3: Hwy-144 composite cross section created by combining the four drill holes labeled above.

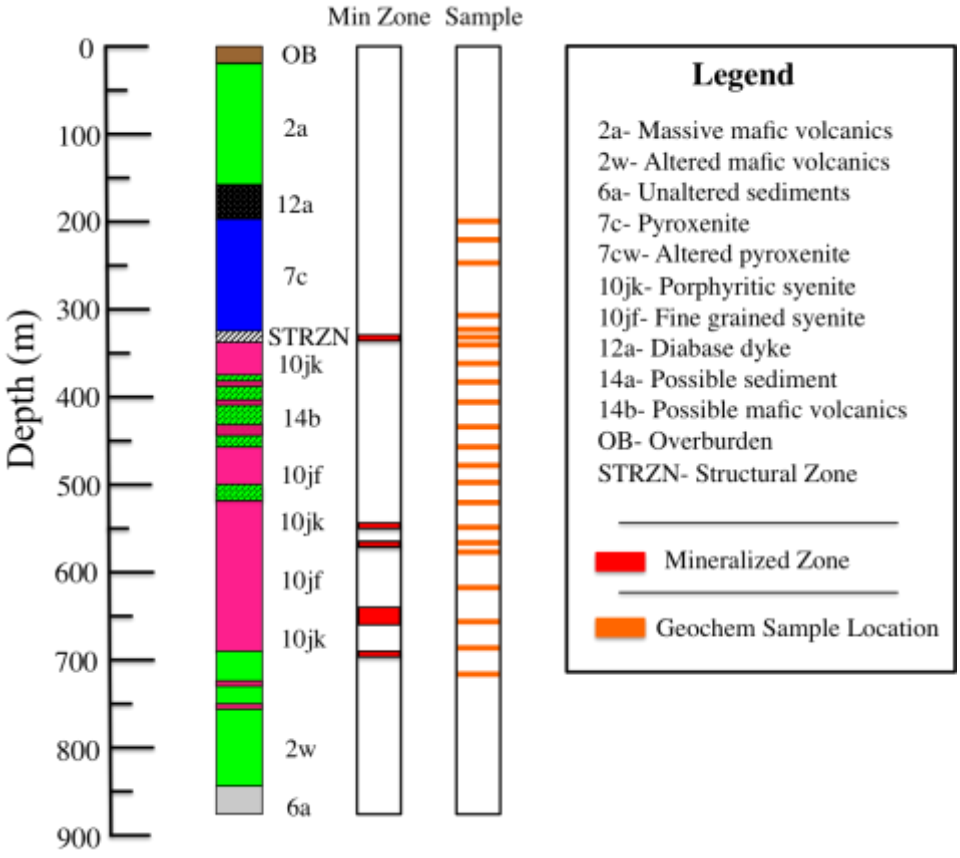

Figure 3.4: DDH Hwy 11-20 with sample locations and mineralized zones annotated.

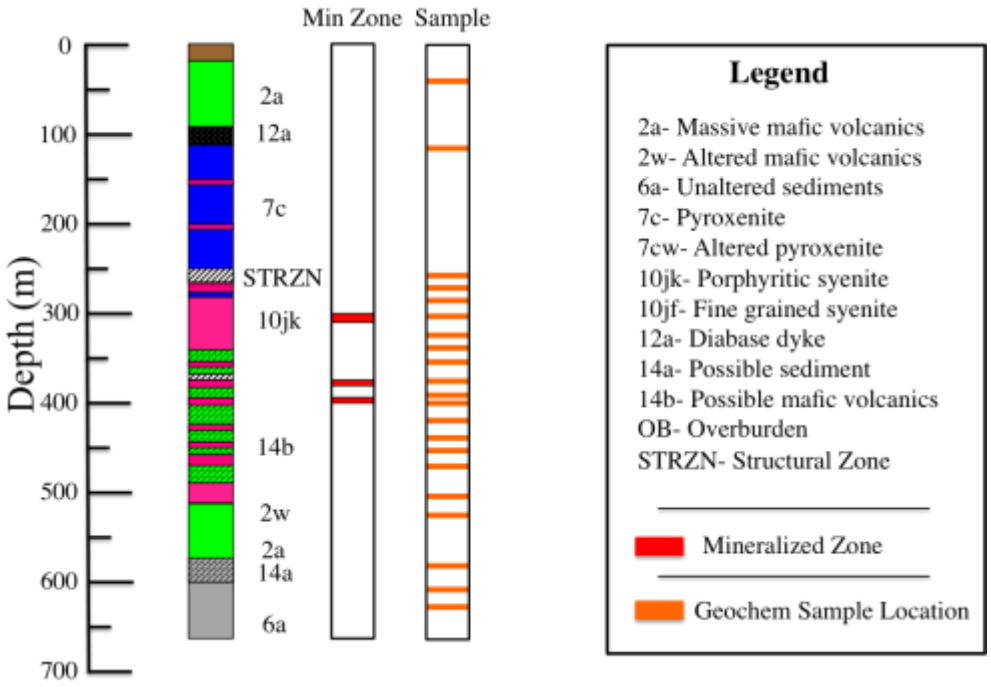

Figure 3.5: DDH Hwy 11-13 with sample locations and mineralized zones annotated.

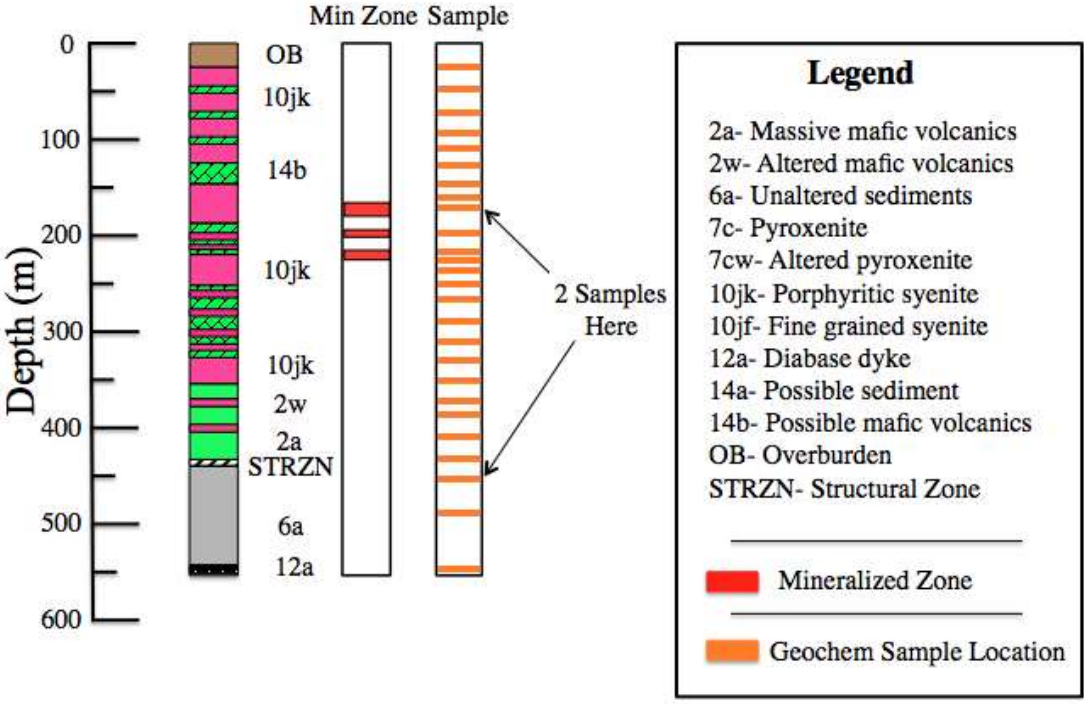

Figure 3.6: DDH Hwy 11-12 with sample locations and mineralized zones annotated.

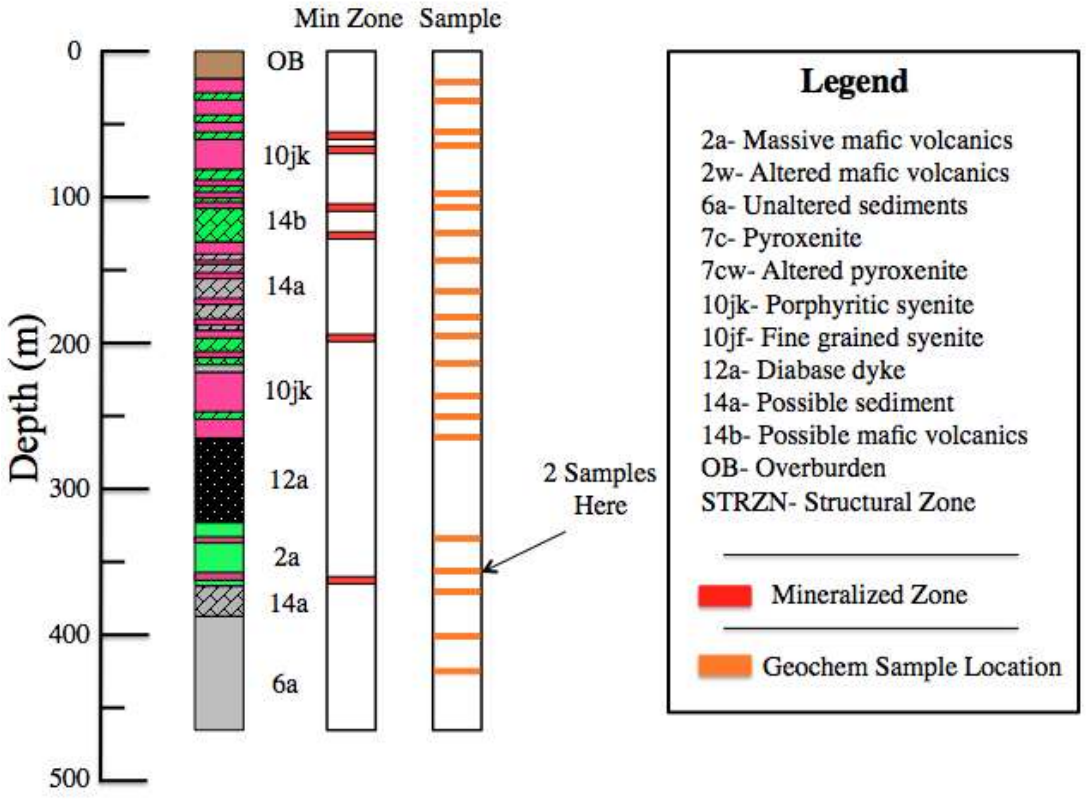

Figure 3.7: DDH Hwy 10-03 with sample locations and mineralized zones annotated.

3.1.4 VEIN DENSITY CALCULATIONS

Vein density calculations were performed at the 695m level of Thunder Creek Deposit. The calculations were done to try and correlate gold grade versus vein density. Gold grade was determined through continuous chip sampling across the wall of the drift. Photographs were taken underground across the drift and the chosen sections were stitched together in Corel Photo-Draw X3®. Next, the chip sampling results were analyzed to isolate increments of relatively uniform gold grade. Intervals were chosen based on low, moderate and high gold assays. Stitched photo sections from each of the intervals described above were imported into Adobe Photoshop CS4®. The total pixels of the stitched sections were recorded. Next using the 'Magic Wand' tool each vein was traced and the pixels from each vein were added together. The total number of vein pixels was calculated. Dividing the total number of pixels in the photograph by the total number of vein pixels calculates the surface area of vein material. The surface area was inferred to roughly represent the three-dimensional volume of vein material (vein density).

3.2 WHOLE ROCK GEOCHEMISTRY

Major and trace element geochemistry was performed on ninety-two samples from the Hwy-144, twenty-two samples from a transect done on the 695m level of the

Thunder Creek deposit, five samples from Thunder Creek 280m and eight samples from the Thunder Creek stock (DDH TC-05-EXT). A total of sixty major and trace elements were analysed. Major element geochemical data was obtained by Induced Coupled Plasma Atomic Emission Spectroscopy (ICP-AES). The sample is mixed with lithium metaborate and fused in a furnace at 1000°C, cooled and then mixed with 4% Nitric acid/2% Hydrochloric acid and then analysed by ICP-AES. Trace element geochemistry was obtained by ICP-MS (inductively coupled plasma-mass spectroscopy). Samples were mixed with a lithium metaborate flux and fused in a furnace at 1000°C to ensure that all minerals were broken during sintering and could be dissolved. Afterwards the samples were cooled, mixed with 4% HNO_3/ 2% HCl_3 and then analysed by ICP-MS. Total sulfur was calculated using a leuco sulfur analyser. The sample was heated to 1350°C in a furnace while a stream of oxygen is passed through the sample. IR detection of the sulfur dioxide released provides the total sulphur amount. Base metals were determined by a four acid digestion followed by ICP-AES.It is assumed that the base metal content in refractory phases is negligible. Finally, gold was analysed AAS (atomic absorption spectroscopy). The sample was prepared by fire assay fusion, formed into a precious metal bead (lead oxide, borax, sodium carbonate, silica, and other reagents) digested by dilute nitric and then hydrochloric acid, and then analysed. If the sample is above 10 g/t, the sample is measured using the gravimetric method. The sample is prepared similarly using fire assay fusion, mixed with similar reagents to the method above, procured as a lead button, the lead is removed, the sample is washed in dilute nitric acid, and the sample is weighed.

3.3 LASER ABLATION INDUCTIVELY COUPLED PLASMA MASS SPECTROMETRY (LA-ICP-MS)

Trace element concentrations were measured in pyrite grains from the Thunder Creek deposit and Hwy-144 exploration target. Disseminated and vein-hosted pyrite grains were analyzed from both the 280m and 695m level of the mine. Disseminated, vein-hosted and fracturing filling pyrite from DDH Hwy 11-13, Hwy 11-12, Hwy 11-20 and Hwy 10-03 were analyzed. All samples analyzed had been previously trace element mapped with the electron microprobe at the University of Western Ontario. LA-ICP-MS was conducted at the University of Windsor, Great Lakes Institute for Environmental Research. The samples were ablated using a Quantronix Integra C® fs laser operating at a fundamental wavelength of 785nm (Saheen et al., 2008). It is a multipass and regenerative titanium sapphire (Ti:sapphire) laser ablation system based on the Chirped Pulse Amplification (CPA) technique (Saheen et al., 2008). The operating conditions for the LA operating system are outlined in Table 3.1 below. Ablated material is transported from the stage via argon gas through a 4mm internal diameter polyethylene tube. The material is then analyzed by a ThermoElectron X7-II® ICP-MS. ICP-MS analyses were calibrated using a NST610 standard from the National Institute of Standards and Technology. The average concentration of Fe in each pyrite

was determined using the electron microprobe and then used as an internal standard. The NIST 610 consists of a silicate glass as opposed to sulphide standard which would reduce matrix effects when calculating the concentration of trace elements in pyrite. The data was processed at the University of Western Ontario using the program Plasma Lab Ver 2.5.5. Pyrite grains were analyzed for the following list of elements: Al, Si, Ca, Ti, Fe, Co, Ni, Cu, Zn, As, Se, Mo, Te, Ag, Cd, Sn, Sb, Te, W, Re, Au, Pb, and Bi. Hg was left out because there was not a National Instrument Standard available. The lower detection limit was calculated as three times the standard deviation of the gas background. The excel macro multiplies the gas background by three and then divides it by the sensitivy. Sensitivty is calculated by dividing the concentration of the NIST 610 standard by a known concentration of a given element. Matrix effects need to be considered when picking a appropriate known standard to calibrate against. Sylvester, 2008 determined that the matrix effects created from using a silicate glass standard (NIST 610) while analysing sulfides can be reduced by using internal standardization. Using an internal Fe standard Sylvester accuracies of ~5% for Cu, Zn, Ag and Pt; 10% for Au; 16% for Co and 25% for Ni. Even though we used a different mass spectrometer than the one used by Sylvester, we believe that by following the same procedures reduces the matrix effect. The results of our LA-ICP-MS study allow us to observe the larger variations in trace element abundances rather than focusing on the precise concentration.

Table 3.1: Standard operating conditions for laser ablation unit.

	Sample	Standard
Rep Rate (Hz)	100	100
Pin Hole Diameter (mm)	2.5	2.5
Energy (μj)	27	27
Stage Speed (μm/s)	5	5

3.4 ELECTRON MICROPROBE ANALYSES

Electron microprobe analyses were collected both for mineral analyses and to generate WDS trace element maps. Probe data was collected with a Jeol JXA-8530f field emission electron microbe at the University of Western Ontario, London Ontario. Mineral analyses were performed on feldspars and pyrite.

Pyrite maps were generated for the following elements: S, K, Ca, Ti, V, Fe, Co, Ni, Cu, Zn, As, Ag, Te, Au, and Pb. All the maps were done with a wavelength spectrometer (WDS) except for K, Ca, Ti and V which were generated with an energy dispersive spectrometer (EDS). The maps were run at the following conditions: Accelerating voltage 20 kV, 1.0 nA, and a dwell time of 10 seconds.

3.5 SECONDARY ION MASS SPECTROMETRY (SIMS)

Insitu sulfur isotopes were collected using a Cameca IMS 4f Secondary Ion Mass Spectrometer at Memorial University in St. Johns Newfoundland. Insitu analyses were done to determine if there is an isotopic difference in Co and Ni zoning is present at Hwy-144. Determining the isotopic composition of both mineralized and non-mineralized pyrites was also a critical objective. The insitu method provides the opportunity to determine spatially the change in S isotopic composition across individual pyrite grains. A total of fourteen samples from both Thunder Creek and Hwy-144 were analyzed. Vein-hosted, fracture filling and disseminated pyrite grains were sampled from each location to determine if there is a different isotopic signature between different generations of pyrite. Pyrite samples were previously WDS trace element mapped and laser ablated for trace element concentration variation. All samples were sputter coated with 300Å of Au to mitigate charging. ^{34}S determinations were performed by bombarding the sample with an ion microbeam of 600-800 pA of Cs^+. The beam was pulled through a potential of 10 keV and focused into a 5-15 μm diameter spot. To remove foreign material from the analyzed surface, each spot was pre-sputtered with a 25μm square raster for 180s. Negatively charged ions are then accelerated into the mass spectrometer at a potential of 4.5 keV. Overall reproducibility is generally better than ±0.5 per mill.

4.0 LOCAL GEOLOGY

4.1 THUNDER CREEK

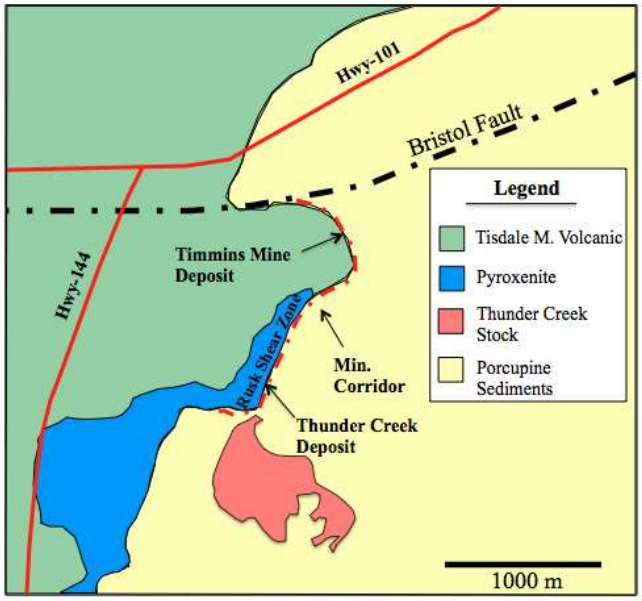

Figure 4.1: Local Geology of the Thunder Creek and Timmins Mine deposits. The sinuous mineralization zone has been outlined in red (Modified from Rhys, 2012)

The Timmins West mine is the furthest west gold producer in the Timmins Camp. The mine is located approximately 18 kilometers outside of Timmins Ontario just off of Hwy-101. The mine is owned and operated by Lake Shore Gold Corporation where gold is currently being extracted from both the Timmins Mine deposit and the Thunder Creek deposit. Both deposits are accessed from a single shaft and represent gold mineralization focused along a sinuous folded deformation corridor (Figure 4.1). The Timmins Mine deposit is hosted in ultramafic to mafic rocks. These rocks are cross cut by quartz-tourmaline veining hosting gold, pyrite and arsenopyrite (Rhys, 2010). The focus of this project is the Thunder Creek deposit, located along a North Easterly trending shear zone

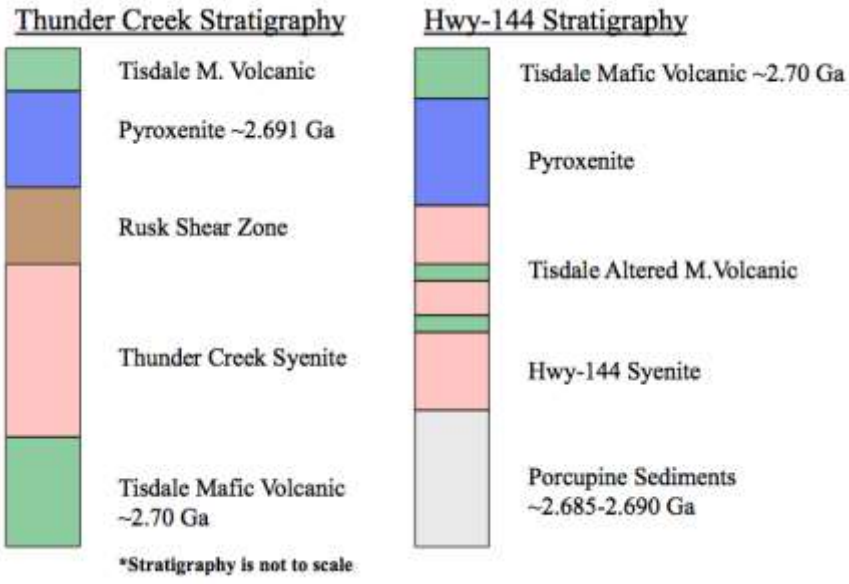

Figure 4.2: Cross Section of the two study areas.

where South Easterly facing Tisdale aged mafic volcanics in the hanging wall are in

fault contact with South Easterly facing Porcupine sediments in the footwall. The Bristol Township Alaklic Complex (BTAC) defined by Beakhouse (2011) is emplaced along the shear zone. The BTAC consists of a hanging wall pyroxenite that is increasing carbonatized and deformed towards the Rusk Zone. The Rusk Shear Zone is adjacent to the pyroxenite. The Rusk Shear Zone is a strongly carbonatized/sericitized multiprotolith shear zone that has been mylonitized (J.Samson per commun). This zone is often strongly mineralized. Adjacent to the shear zone is a felsic intrusion of monzonitic composition, locally termed the syenite porphyry. The porphyry is the footwall unit within the BTAC. The porphyry is also mineralized, commonly characterized by increasing sulphides and vein density. Beakhouse (2011) hypothesized that both the ultramafic and felsic components of the complex were related, "based on i) spatial proximity, ii) broadly similar field relationships, iii) local gradational contacts and iv) shared broad compositional characteristics (e.g., shared exotic mineralogy, alkalic character, HFSE enrichment)". The AIC intrudes along an unconformable contact between the Tisdale aged mafic volcanics and Porcupine aged sediments.

4.1.1 Mafic Volcanics

Tholeiitic mafic volcanic rocks are present in the footwall to the syenite. The volcanic rocks are dark green to black and fine-grained. At the intrusive contact the volcanic rocks are strongly foliated with moderate ankerite and carbonate alteration (Figure 4.3). In zones of stronger deformation, pyrite mineralization increases to ~1-3% and the zones are moderately mineralized (1-3 g/t). The foliation at the 695m level is parallel to the Rusk Shear zone and deformation dissipates ~0.5-2m from the contact. Moving away from the contact, the mafic volcanic rocks are weakly epidote altered. Pillow textures are often present in the weakly altered volcanic rocks.

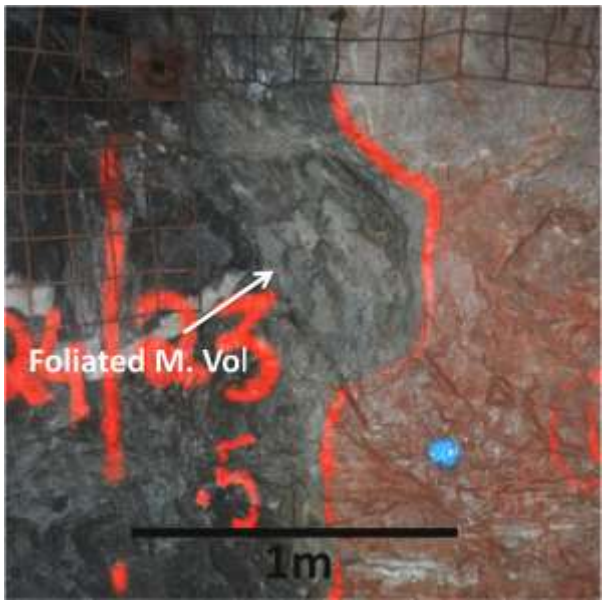

Figure 4.3: Sheared and strongly altered contact between syenite and mafic volcanics at Thunder Creek. The deformed zone hosts strong carbonate and sericite alteration.

In thin section the mafic volcanic unit is fine-grained composed predominantly of amphibole with minor chlorite, biotite, garnet, and plagioclase in decreasing order. A completely unaltered volcanic assemblage was not present. The least altered unit has been described below. Amphiboles are fine-grained and interlocking. Biotite grains are subhedral and green in PPL, with an average size of 250µm. Garnet grains represent the largest phase at a width of 500µm. Garnet grains are embayed and irregular (Figure 4.4). Plagioclase is very fine-grained (50-100 µm), anhedral, with twinning often not present. Progressive alteration during metamorphism has altered the majority of the plagioclase in the volcanics.

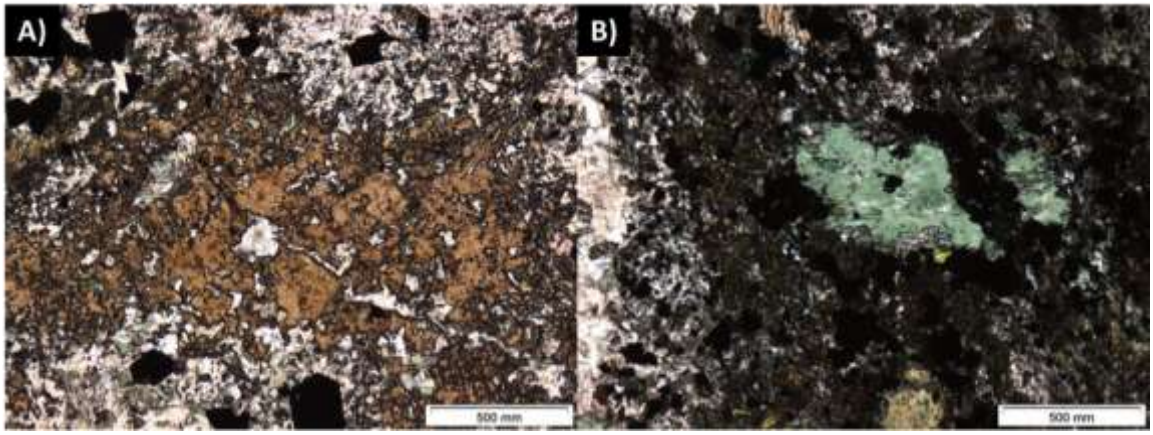

Figure 4.4: A) PPL image of embayed garnet phenocryst in altered volcanic sample. B) Green biotite phenocryst in least altered volcanic sample

4.1.2 Pyroxenite

The pyroxenite unit lies in the hanging wall to the Rusk Shear zone and syenite intrusion. The unit is relatively undeformed, however carbonate alteration is present in even the most unaltered samples. Previous work by Barron (1991) interpreted the pyroxenite mineralogy, specifically the andradite garnets, to represent a fenite alteration halo, with the Rusk Shear zone representing a carbohydrothermal carbonatite. The average mineralogy based on hand sample examination is amphibole, magnetite, and biotite ± apatite ± garnet in decreasing order. Small discrete layers of garnet-rich (garnetiferous), biotite-rich (lamprophyric), and apatite-rich zones are present over 1-50 cm intervals. Grain size varies from fine to coarse grained. Magnetite, garnet and biotite often manifest as coarse (0.5-1cm) phenocrysts. Texturally, the pyroxenite ranges from fine-grained and equigranular (Figure 4.5) to porphyritic. In general, garnet bearing ultramafic rocks are interpreted to be mantle-derived forming under high pressure. In this circumstance the pyrope and spessartine garnet compositions would be expected. At Thunder Creek and Hwy-144 the garnets are andradite in composition and their origin is contentious. Andradite garnets can form in low-pressure hydrothermal

environments in response to boiling (Jamtviet et al., 1995). The tectonic environment for Thunder Creek is believed to be a low-pressure rift setting.

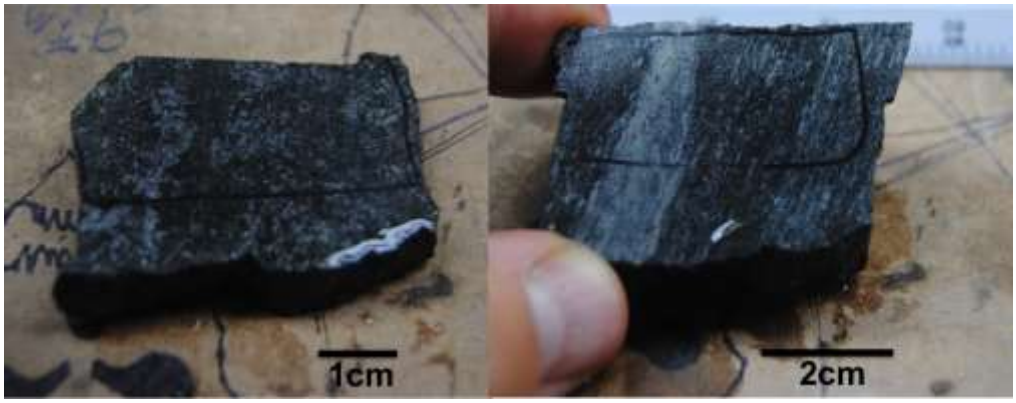

Figure 4.5: Hand samples of Thunder Creek pyroxenite. On the left is an example of 'least altered' pyroxenite while the sample on the right represents a deformed altered pyroxenite.

Both amphibole and biotite are fine-grained ranging from 0.2-0.6 mm. The minerals are subhedral and form interlocking textures composing the majority of the least altered protolith. Magnetite is disseminated throughout the unit, primarily fine-grained but occasionally coarse-grained over small intervals (10cm). Magnetite often displays primary exsolution of ilmenite (Figure 4.6). Apatite forms pink tabular grains in hand sample. In thin section, apatite is fine grained with an average length of 0.5mm on the long axis (Figure 4.6). Apatite is a minor disseminated phase within the rock. Garnet is the largest phase (0.4cm to 1cm). Garnet grains are often fractured and irregular.

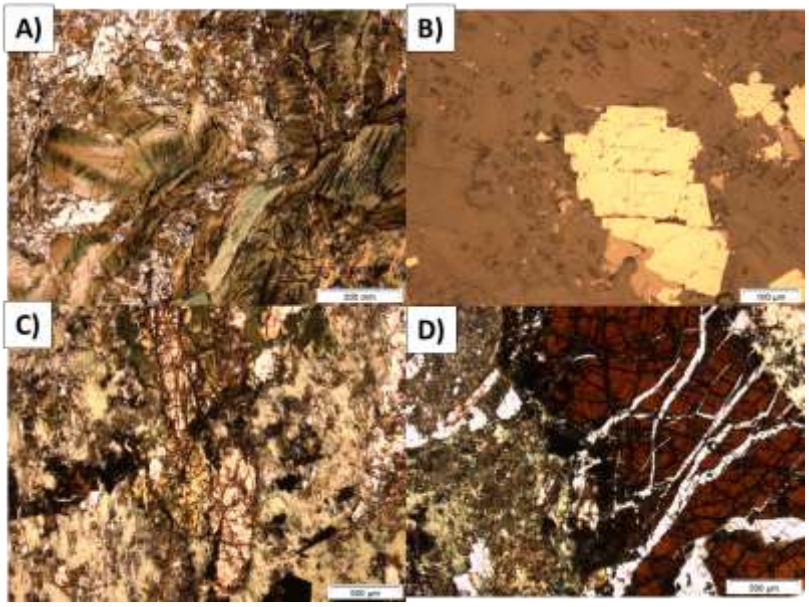

Figure 4.6: Thin section micrographs of pyroxenite minerals. A) PPL image of nterlocking amphibole and biotite. B) Magnetite with exsolution(reflected light). C) Tabular apatite grains (PPL). D) Coarse garnet phenocrysts(PPL).

4.1.3 The Rusk Shear Zone

The Thunder Creek (TC) gold deposit is proximal to the Porcupine Destor Fault Zone (PDFZ) and is specifically associated with the "Rusk" shear zone. The Rusk shear zone is located at the contact between ultramafic (pyroxenite) and felsic (syenite) units, which is contemporaneous with the Timmins Porphyry suite (2.691-2.688 Ga; Barrie 1992). Rhys (2011) characterizes the deformation corridor as a multi-protolith mylonite with intense ductile deformation (Figure 4.7). He suggests that intense shearing has tectonically transposed individual protoliths, which now have skewed gradational contacts. The mylonite foliation is steeply dipping to the northwest at an orientation of 234/61, representing the regional foliation of S_3-S_4 (Rhys, 2011). Later crenulation and folding has been interpreted by Rhys as D_5. D_5 deformation is overprinted by extensional quartz veinlets (Figure 4.7), often associated with increased sulphides and gold mineralization (Figure 4.8). The shear zone sits along a re-activated fault structure. At depth, the Rusk shear zone periodically pinches and swells. At approximately the 700m level, a second small splay diverges away from the main zone. This divergent limb of the Rusk Zone is hosted within the larger pyroxenite body to the north and has been called the "Kilt Zone". In thin section, there are almost no primary textures or minerals preserved to allude to the protolith. Disseminated fine to medium magnetite and close proximity to weakly altered pyroxenite suggests that the Rusk represents a strongly deformed and altered pyroxenite. The alteration and mineral assemblage of the Rusk Zone will be discussed in detail in the Geochemistry Chapter.

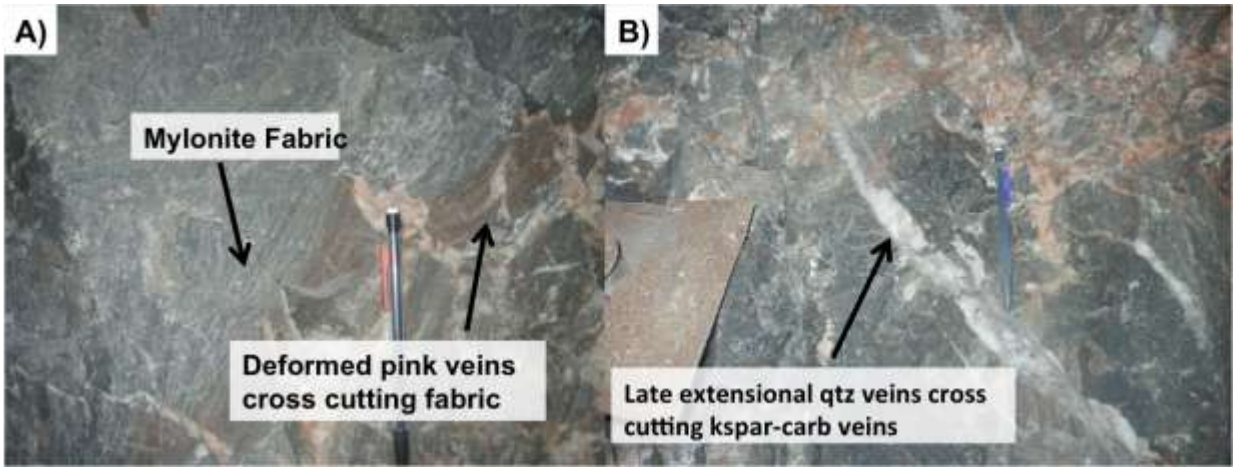

Figure 4.7: Thunder Creek 695m level Rusk Zone photos. Photograph A) highlights the mylonite fabric that defines the Rusk. Photograph B) Late quartz veins cross cut the Rusk fabric.

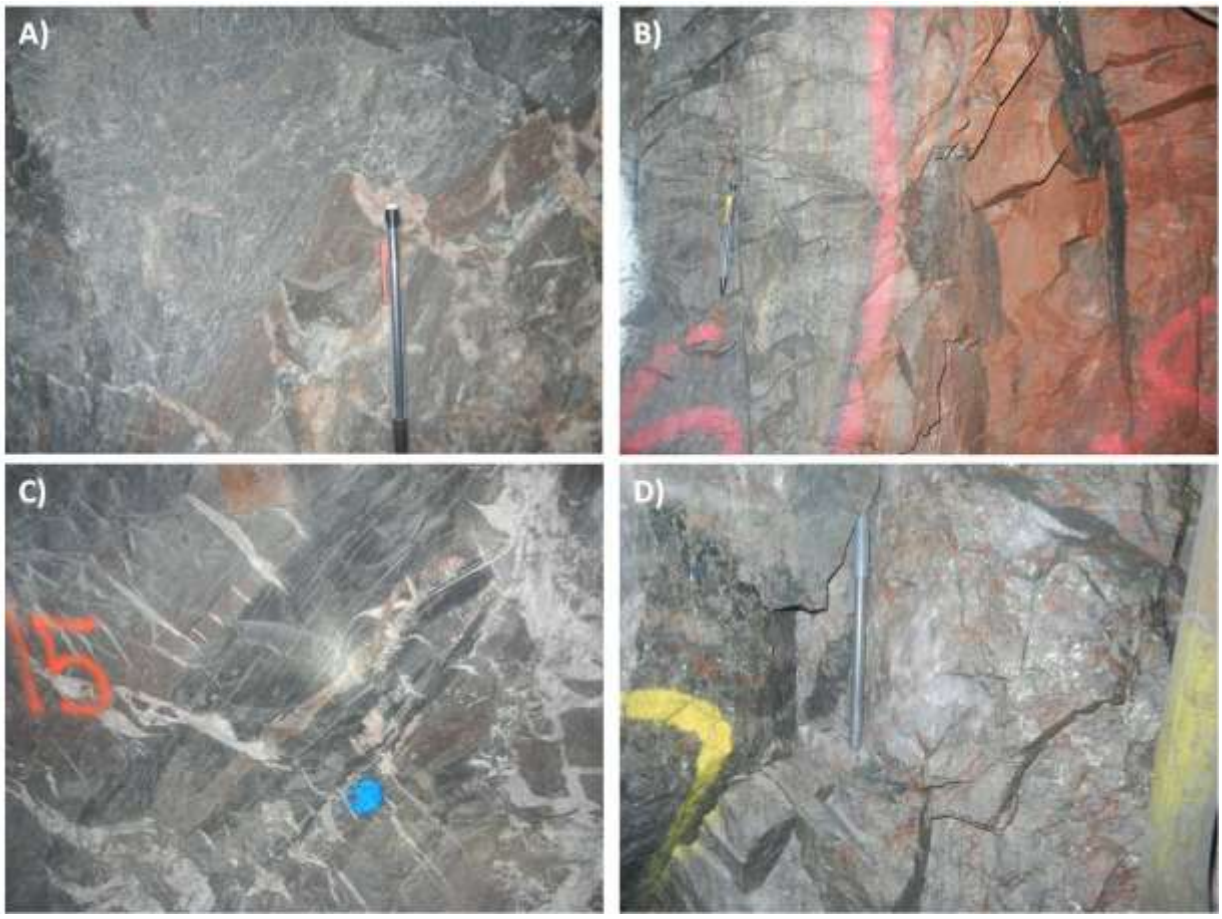

Figure 4.8: Photograph A) Larger photo of Figure 4.4.1 A). B) the Rusk Shear Zone steeply dipping to the northwest at the contact with a syenite dyke. C) Late extensional quartz veins cross cutting the Rusk Shear zone. Photograph D) is an example of strongly altered (bleached) and strongly mineralized Rusk Shear Zone.

4.1.4 Transitional Lithologies

Within the Bristol Township Alkalic Complex, there are multiple dykes, dykelets and lithologic units that appear to be an intermediary between the pyroxneite and syenite end members. The field data is confirmed by geochemical data that indicates there is a continuous evolution between the mafic and felsic end members. Underground samples and drill core logs detail "monzonites" that are moderately magnetic with a mafic matrix. This "monzonitic pyroxenite" has shared characteristics with both units. Also, strongly hematized and deformed pyroxenite units have a minor feldspar component. Incompatible trace element data of both end member units reveals that they have similar trace element trends along a spider diagram plot including Nb and Ti subduction signatures.

4.2 Thunder Creek Syenite (Mine)

The syenite at TC is medium grained, equigranular and relatively homogeneous. The rock is consistently a salmon pink colour in the lower portion of the mine, but is a darker red colour when present as dykes or at the top of the mine (Figure 4.9). The red colour is interpreted primarily as an increase in hematite alteration, with K_2O values are

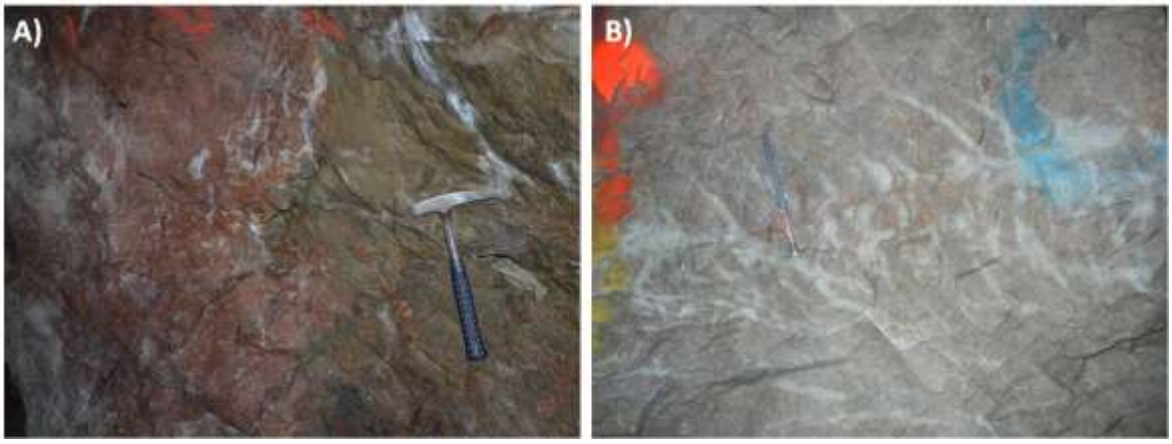

Figure 4.9: Underground photos of A) the 280m level and B) the 695m level of Thunder creek. Note the change in colour of the porphyry between the two levels. B) En echelon quartz vein array present at the 695m level.

remaining constant within the intrusion. The primary magmatic mineral assemblage within the syenite is K-feldspar, albite with minor quartz in decreasing order. K-feldspar forms the largest grains with an average grain size of 0.5mm. K-feldspar grains often display Carlsbad twins and occasionally display microcline twinning (Figure 4.10). Albite grains are sub to anhedral with an average size of 0.2mm. Quartz grains are fine-grained (0.1-0.3mm) and anhedral. Within the deposit no primary mafic minerals have been observed. The TC deposit appears to be vertically zoned, determined by a clear colour change between the top and bottom of the intrusion (Figure 4.9). The syenite is not foliated and displays only brittle deformation characterized by different vein arrays and fracture planes. There are also two dominant slip planes within the intrusion that cross cut all vein arrays. The orientations of the slip planes are 055/40 dipping to the north and 131/40 dipping to the south. The lack of intense deformation compared to the surrounding mafic volcanics and sediments suggests that the intrusion was emplaced relatively late (Beakhouse, 2011).

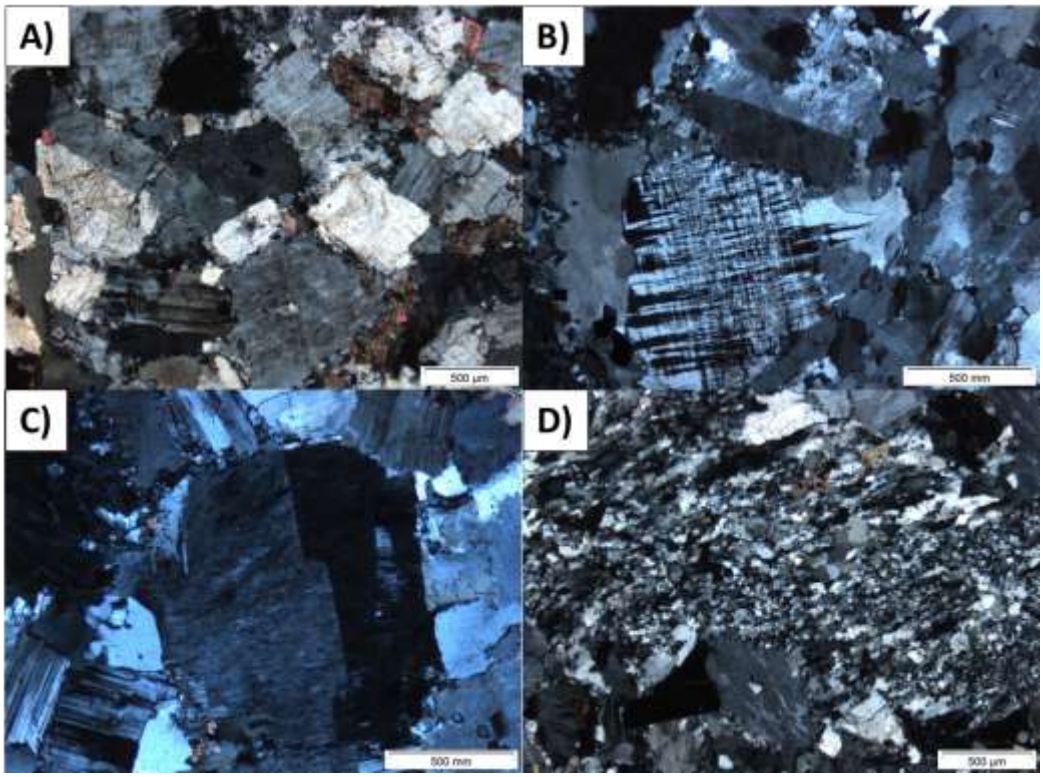

Figure 4.10: Photomicrograph images of the Thunder Creek syenite. A) XPL image of syenite groundmass. B) XPL image of medium grained microcline. C) XPL image of Carlsbad feldspar twin with enclosed plagioclase. D) XPL image of fine grained deformed quartz domain.

4.2.1 TC280m Level

At the 280m level, the syenite is a deep red colour with moderate hematization. The intrusion is present as small dykes (fingers) stemming from the larger intrusive body at depth, and no contiguous syenite body is present at this level and individual fingers are approximately 5-10m thick. Compared to the syenite at depth, veining has decreased and there is a lower sulphide content (~Trace-1%). Coarse pyrite is generally disseminated but also present along vein margins. Extensional flat quartz veins (V_2) are cross cut by later subvertical quartz veins (V_3).

4.2.2 TC695m Level

At the 695m level, the syenite body has increased to a continuous width of ~55m. The unit is relatively homogeneous in colour (salmon pink), fine to medium grained and equigranular. Four vein arrays are present at this level (discussed below). Sulfide content has increased to 1-3% and locally up to 8%. Coarse disseminated pyrite is often corroded.

4.3 Thunder Creek Syenite Stock

The Thunder Creek stock outcrops at surface slightly to the south of where the Thunder Creek deposit is interpreted to outcrop (Figure 4.1). The stock has been drilled and is not mineralized and locally unaltered. The syenite ranges from purple to light pink in colour. The colour change corresponds to the destruction of primary mafic minerals (biotite, amphibole) and addition of feldspar (Figure 4.11). The unit is medium grained and generally equigranular. The Thunder Creek stock represents the best example of a 'least altered' syenite in the area. The main mineral assemblage is K-feldspar, albite, quartz, blue amphibole, biotite, and titanite in decreasing order.

Figure 4.11: Progressive alteration of the Thunder Creek stock. Moving from unaltered (left) to strongly altered (right).

The main mineral assemblage is K-feldspar, albite, quartz, blue amphibole, biotite, and titanite in decreasing order. K-feldspar and albite are the largest grains (0.4-1.5mm) making up the majority of the groundmass. K-feldspar grains are commonly zoned (Figure 11). Quartz grains are anhedral and fine-grained, accounting for ~10% modal rock volume. Blue and green amphibole are disseminated throughout the sample (Figure 4.12). Amphiboles are poikilitic, subhedral and 0.1-0.4 mm in size. Associated with the amphibole is fine-grained titanite. Titanite is euhedral and 50-300μm. Similar to amphibole, biotite is a minor fine-grained phase disseminated throughout the rock.

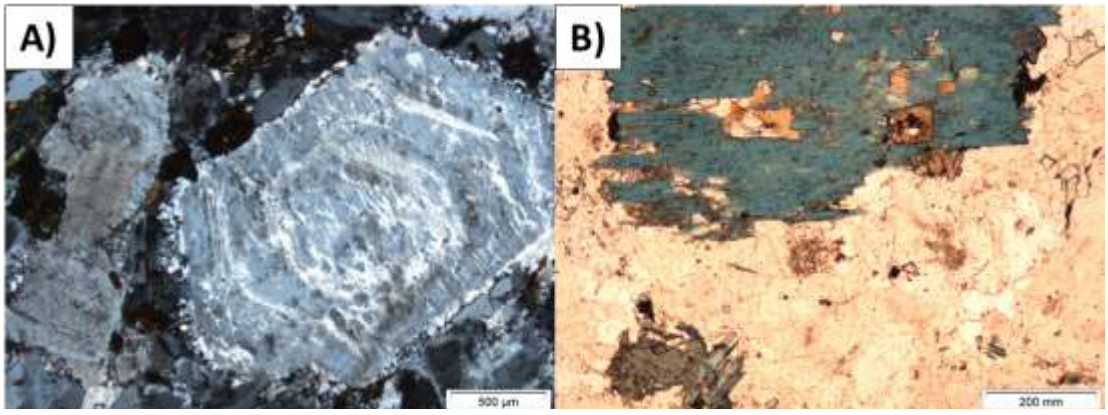

Figure 4.12: A) XPL image of medium grained zoned feldspar grain. B) PPL image of fine-grained, poikilitic, blue amphibole.

4.4 Structure

Multiple structural assessments of both the Timmins and Thunder Creek deposits have been conducted from 2008-2012 (Rhys, 2010 & 2012). Structural information from each of these deposits has been correlated to larger camp wide deformation events. Within the Timmins Camp D_1 and D_2 represent pre-Timiskaming folding events (Bateman et al., 2008; Rhys, 2010). D_2 was a widespread extensive fold and thrust regime resulting in the Porcupine Syncline and Hollinger Anticline (Rhys, 2010). Gold mineralization in the Thunder Creek area is related to syn-metamorphic D_3 and D_4 events. Textural elements of the D_3 and D_4 events are preserved west-northwest trending shear zones and foliations. These textural elements truncate earlier D_2 folds (Rhys, 2010). Both the Rusk (Thunder Creek) and Holmer Shear (Timmins Mine) formed during D_3 deformational events. The folding of the Rusk Shear zone and other deformation zones in the camp represents a D_4 tectonic event and is likely post mineralization (Dave Rhys, pers commun). During syn-metamorphic deformation, steep stretching occurred visible in the elongation of pillows, clasts and mineral aggregates (Rhys, 2010). The stretching L_4 lineation plunges steeply to the northwest, parallel to the Rusk Shear Zone. During deformation, the syenite pluton adjacent to the Rusk Shear Zone accommodated strain. The multiple vein arrays within the Thunder Creek syenite are believed to be the result of strain partitioning in the Rusk Shear Zone (Rhys, 2011).

4.5 Vein Types

The abundance of quartz veining within the Thunder Creek syenite suggests that the rheological competence of the syenite was a good host for fluids compared to adjacent lithologies. The pyroxenite also hosts late quartz veins but they are not strongly mineralized. Three stages of veins cross cut the intrusion; V_1 veins form a set of deformed and diffuse quartz stockwork veins that do not have clear timing relationships established with the two other vein types, V_2 veins define a flat extensional quartz-carbonate system, V_{2b} veins form a set of translucent quartz veinlets generally parallel to V_2 veins that occasionally contain medium grained Py, and V_3 veins are steeply dipping subvertical quartz veins that cross cut V_2 (Figure 4.13).

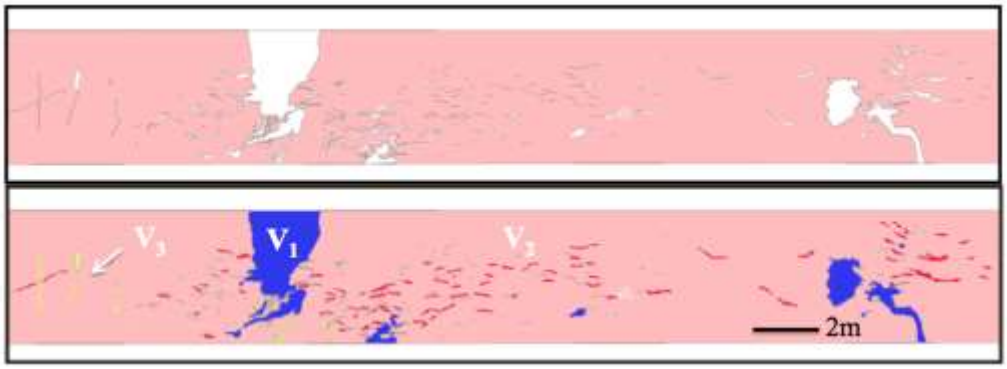

Figure 4.13: Above is a diagram of the TC695m level. Early V_1 veins are in blue, V_2 veins in red and late V_3 veins in yellow.

V_1 veins are deformed suggesting they formed early compared to their V_2 and V_3 vein counterparts. V_1 veins are early and were deformed during regional stress while V_2 and V_3 veins intruded later post ductile deformation. In the Yilgarn complex stockwork like vein arrays are developed adjacent to shear zones and the intersection of shear zones (Cox et al., 1991). V_1 veins are primarily quartz with minor pyrite and galena. Sulfides are present both along the margin and within the core of the vein. V_2 veins are flat to shallowly dipping (~0-15 degrees) quartz veins with minor amounts of pyrite, molybdenite, galena and scheelite. Sulphides occupy on average 1-2% of the vein and are preferentially found on the vein margins. Veins are on average 1-2cm thick, with a range from 0.5cm to 25 cm. V_3 veins are a set of subvertical (~80 degrees) dipping veins consisting of primarily quartz with minor carbonate. There is a trace amount of medium grained pyrite associated with this vein set. The abundance of V_3 veins is much lower than V_1 or V_2. The veins are on average 1 cm thick, with a range of 1-15cm.

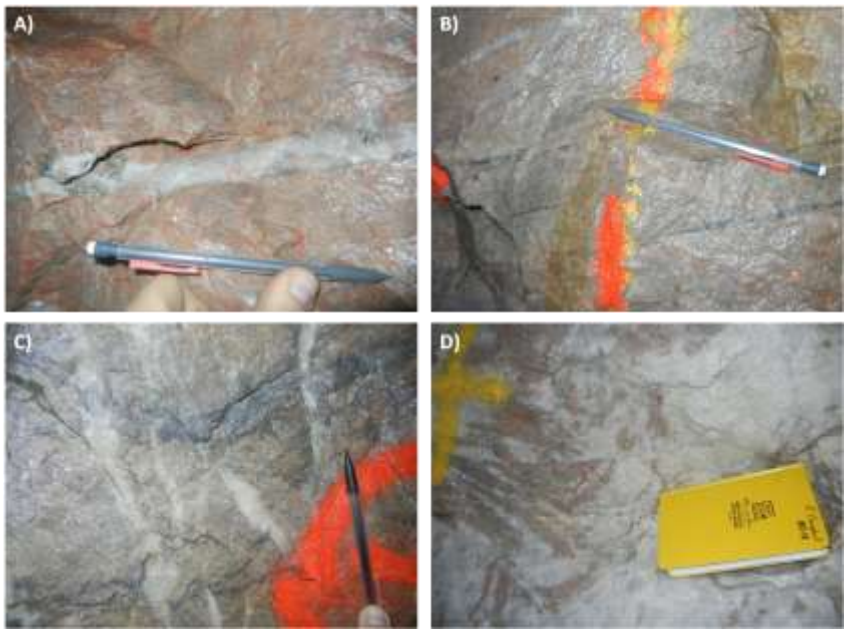

Figure 4.14: Different vein arrays typical of the Thunder Creek Deposit. A) V_2 veins. B) V_{2b} veins. C) V_3 veins. D) V_1 veins.

4.6 Hwy-144 Exploration Target

The Hwy-144 exploration target is located about 0.5-1.5 km's west southwest of the Thunder Creek Deposit (Figure 4.15). Both TC and Hwy-144 are hosted by the same rock assemblages. At Hwy-144, the stratigraphy consists of mafic volcanic rocks in the hangingwall, alkaline intrusive complex, and sediments in the footwall. Deformation at the contact between the pyroxenite and syenite is markedly weaker compared to Thunder Creek, with only slight hints of "Rusk" style deformation. The syenite pluton at Hwy-144 is not as continuous as at Thunder Creek and the syenite has

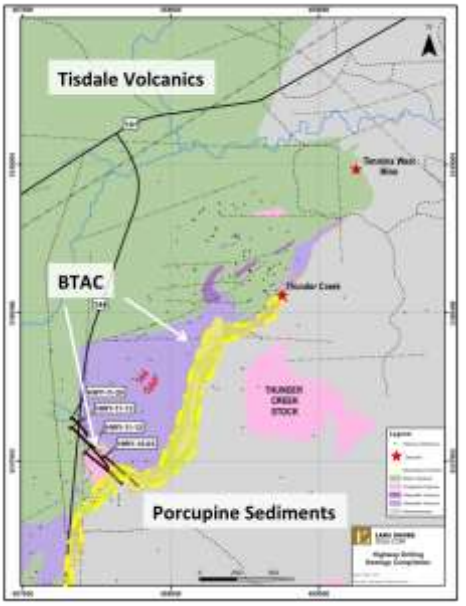

Figure 4.15: Map of TC and the north end of the Hwy-144 property. Drill holes sampled are highlighted along with an idealized mineralization corridor (yellow)(Modified from Lake Shore Gold Corp).

incorporated mafic volcanic slivers during emplacement and is not one homogenous body.

4.6.1 Mafic Volcanics

Mafic volcanic rocks at Hwy-144 are visibly and geochemically similar to those described above at Thunder Creek. The rocks are weakly epidote altered often display pillow selvages. The volcanic rocks are fine-grained and black to light green in colour (Figure 4.16). Both disseminated and fracture-filling pyrite are present in localized intervals (0.5-5m). Pyrite is generally fine to medium grained and locally increases to 30%. Areas of abundant pyrite in the syenite or Rusk Zone are often mineralized, in the mafic volcanic rocks they are not.

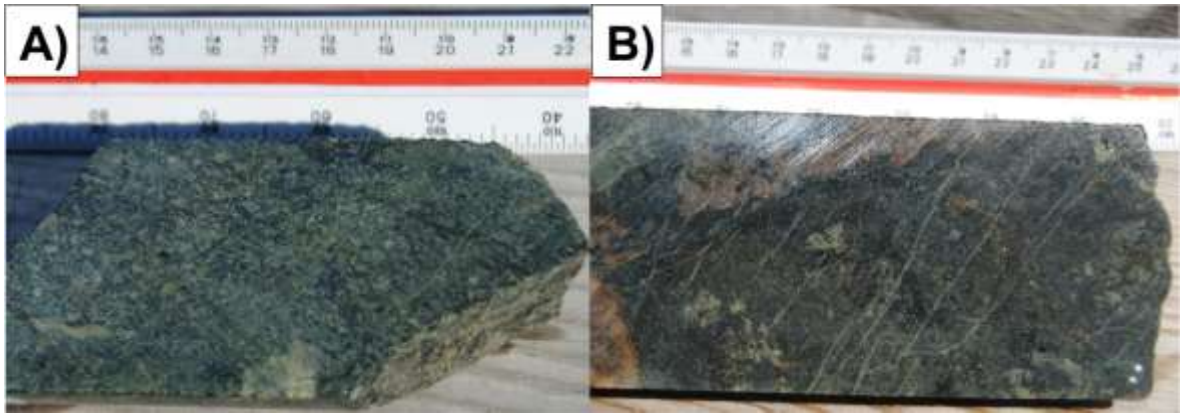

Figure 4.16: Hwy-144 representative mafic volcanic samples. A) Least altered dark green homogenous sample. B) Altered volcanic with light green epidote clusters and later pink K-spar veinlets cross cutting the sample.

In think section the least altered volcanic samples contain epidote, plagioclase and chlorite in decreasing order. All mineral phases are extremely fine grained (10-60μm). Epidote grains cluster in localized domains, outside of epdiote domains chlorite increases (Figure 4.17). Plagioclase is interstitial to epidote grains and quite irregular. The prevalence of twinning in the feldspars decreases with alteration.

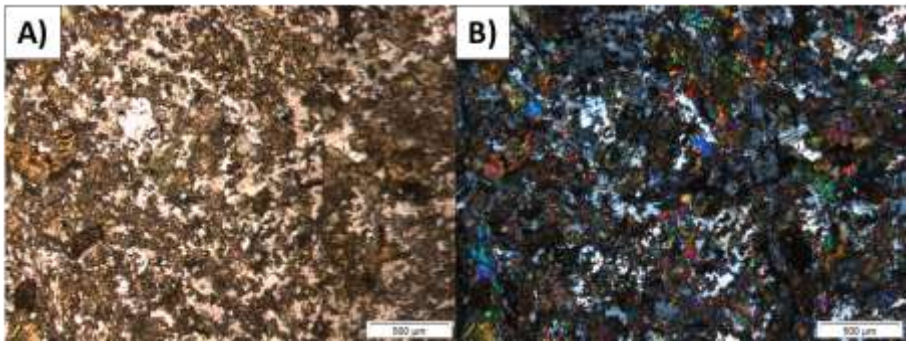

Figure 4.17: Photomicrographs of the Hwy-144 least altered mafic volcanic. A (PPL) & B(XPL) image of the mafic volcanic groundmass. The groundmass comprises primarily of epdiote, plagioclase and chlorite.

4.6.2 Pyroxenite

The pyroxenite is dark blue to dark green in colour and medium grained. Localized intervals (10-50 cm) contain coarse garnet, biotite and magnetite. These intervals often contain an abundance of one phase (eg. garnet) and minor amounts of the other two (Figure 4.18). The unit is relatively massive with occasional felsic dykes cross cutting. Carbonate alteration is pervasive, however the bleaching seen at Thunder Creek in the Rusk Shear Zone is not seen at Hwy-144. When bleaching is present, it occurs over small intervals (10cm-1.0m), while the Rusk Shear Zone can be multiple meters thick.

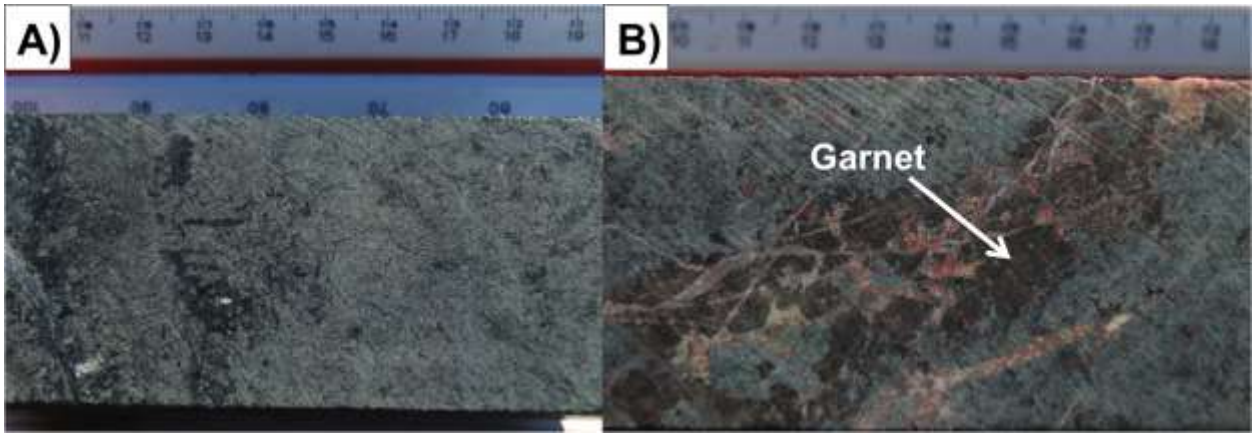

Figure 4.18: Hwy-144 pyroxenite samples. A) Least altered pyroxenite with biotite books (black). B) Altered pyroxenite with garnet band and increased feldspar alteration.

In thin section, the pyroxenite is mainly fine to medium grained, with domains of coarse-grained (biotite, garnet and magnetite) phases. Least altered samples at Hwy-144 contain primary pyroxene grains, which suggests the unit is less altered than the pyroxenite at the Thunder Creek mine. The primary mineral assemblage is pyroxene, biotite, magnetite ± apatite ± garnet. Pyroxene grains range from 0.1 to 1.1mm, are subhedral, and when large poikilitic (Figure 4.19). 95% of the pyroxene grains are clinopyroxene with 5% orthopyroxene. Biotite is mainly fine grained (150-300μm) and subhedral, occasionally coarse biotite clots form over small (10-50cm) intervals. Magnetite is mainly fine grained, fractured and disseminated throughout the pyroxenite. Apatite is equant to tabular in shape, fine grained (100-300μm), and subhedral. Garnet forms medium to coarse grained (1.5mm-1.5cm) fractured and poikilitic phenocrysts (Figure 4.18).

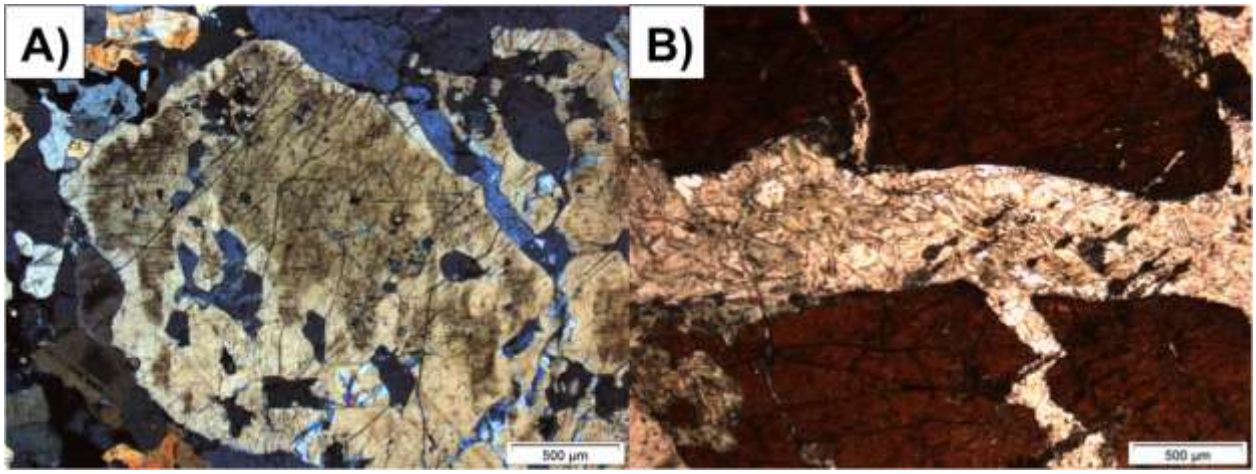

Figure 4.19: Photomicrographs of Hwy-144 pyroxenite. A) XPL image of coarse, poikilitic clinopyroxene grain. B) PPL image of fractured andradite garnet grain.

4.6.3 Syenite

The syenite intrusion is a polyphase, equigranular to porphryitic syenite that has been locally altered by iron (Fe) carbonate, K-feldspar and hematite (Figure 4.20). Colour changes in the syenite vary based on the dominant alteration assemblage present. The syenite varies from pink to dark red in colour. Porphyritic phases of the syenite contain up to 1.5cm feldspar phenocrysts often containing hematite along fractures staining the rock red. Coarse feldspar phenocrysts are commonly zoned and often displaced by post crystallization deformation. The primary mineral assemblage is K-feldspar, albite and quartz in decreasing order. Only one slide contained an example of a primary clinopyroxene replaced by amphibole (Figure 4.21). The mineral assemblage is similar to Thunder Creek, however the albite and quartz content is lower with more K-feldspar present. K-feldspar forms fine to medium grains in the groundmass and coarse subhedral phenocrysts in the porphyritic unit. K-spar grains display primary magmatic textures like microcline/carlsbad twinning and oscillatory zoning (Figure 4.21). Albite grains are fine to medium grained and subhedral. Quartz is fine-grained and anhedral.

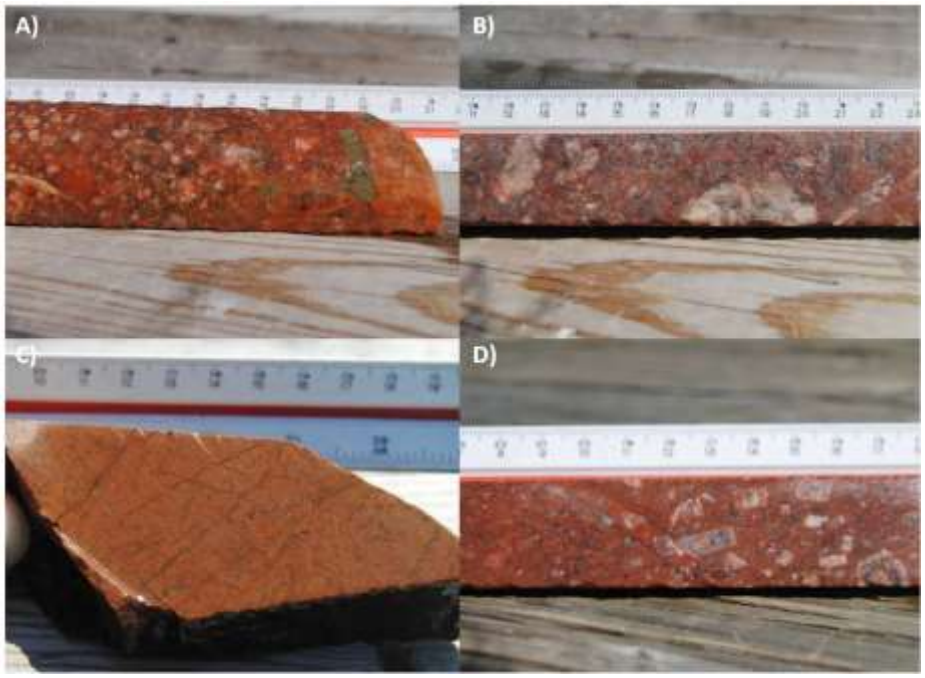

Figure 4.20: Phases of the Hwy-144 syenite. A) Dark red hematized syenite with coarse disseminated pyrite. B) Porphyritic syenite with hematite alteration along feldspar fractures. C) Fine-grained equigranular syenite. D) Zoned feldspar phenocrysts within the syenite.

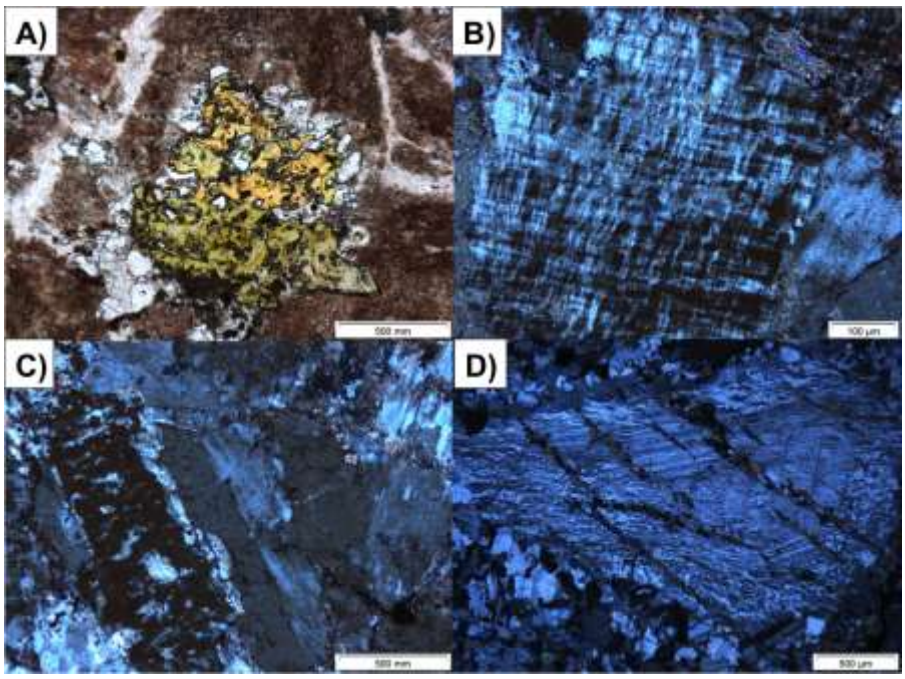

Figure 4.21: Photomicrographs of the Hwy-144 syenite. A) PPL image of primary clinopyroxene replaced by amphibole. B) XPL image of microcline twinning. C) XPL image of Carlsbad twinning. D) Primary growth zoning in K-feldspar phenocryst deformed by subsequent deformation.

4.7 Porcupine Sediments

The base of the Hwy-144 stratigraphic column consists of poorly sorted, fine-grained greywackes. The sediments are blue-grey in colour with preferential fracture planes. The general mineralogy is: sericite, carbonate, quartz, chlorite, and feldspar. The sediments are generally relatively undeformed but near contacts and strain zones they have a schistose fabric.

5.0 ALTERATION

To accurately describe progressive alteration three sampling locations were selected (Thunder Creek Mine, Thunder Creek Stock and Hwy-144). Alteration was mainly determined through petrographic and SEM analyses, but is complimented with major and trace element geochemistry in Chapter 6. Full thin section descriptions are available in Appendix D.

5.1 Alteration at Thunder Creek

5.1.1 Mafic Volcanics

The mafic volcanic unit is strongly altered at the footwall contact with the syenite. The tectonic contact is strongly foliated, with carbonate and sericite alteration. Samples were taken at the contact and incrementally (eg. 3 samples taken at 1m intervals from the contact) outwards to record the degree of alteration. Figure 5.1 demonstrates the visual change between the altered contact and a sample outside of the alteration zone.

Figure 5.1: Hand sample photographs of alteration in Thunder Creek mafic volcanics. On the left is an altered volcanic sample. The right is a least altered sample. The sample on the left has visible iron carbonate staining (brown).

In thin section, all primary magmatic minerals have been replaced by carbonate, magnetite, chlorite, muscovite and feldspar in decreasing order of abundance. Carbonate alteration is pervasive, present in the groundmass and late cross cutting veinlets. Using a portable tabletop SEM both calcite and ankerite were present. Calcite is more prevalent, however the term carbonate alteration going forward denotes both species. Carbonate grains are subhedral and 80-300μm across. Magnetite is fine-grained and present in two distinct forms. The first type consists of patchy disseminated magnetite occupying up to 25% of the rock. The second type consists of a

foliated and crenulated magnetite that defined by the deformation fabric (Figure 5.2). Muscovite forms tight interlocking lathes that occupy isolated domains within the rock (Figure 5.3). Feldspar is fine-grained and disseminated.

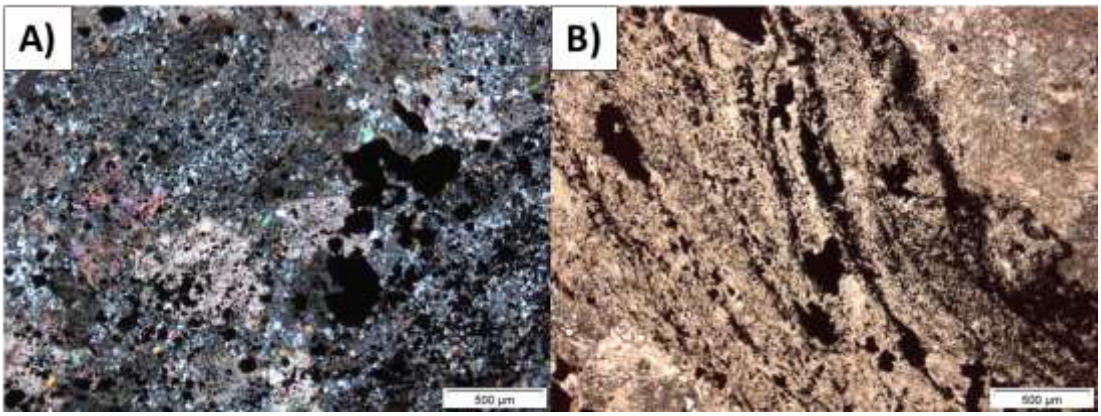

Figure 5.2: A) XPL image of pervasive carbonate alteration. B) PPL image of fine grained foliated magnetite grains.

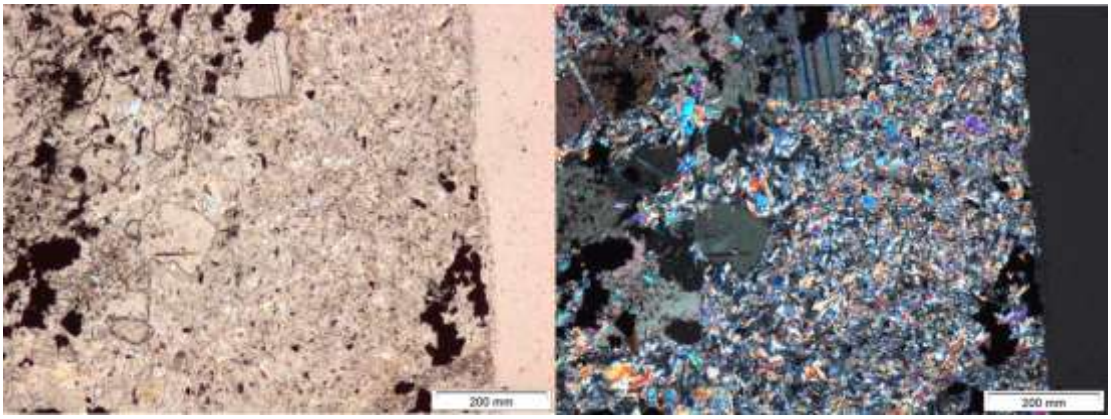

Figure 5.3: PPL (left) and XPL (right) image of isolated muscovite altered domain.

5.1.2 Pyroxenite

The pyroxenite at the Thunder Creek deposit is increasingly more deformed and altered closer to the contact (Rusk Shear Zone) with the syenite. The deformation becomes visually evident underground approximately 12m from the shear zone/syenite contact. Least altered pyroxenite samples at TC are more altered than samples at Hwy-144, but still record increasing alteration. In hand sample, alteration is present as increased carbonate and K-feldspar content (Figure 5.4). Deformation increases with alteration, present as late quartz veins that cross cut the altered pyroxenite. Alteration progresses from an amphibole, biotite and magnetite assemblage gradationally changing to a biotite/chlorite and magnetite assemblage (Figure 5.5). As alteration progresses even further (~8m from contact) the rock is composed of only carbonate, magnetite and minor feldspar (Figure 5.6). The biotite is fine-grained, subhedral and often foliated.

Carbonate alteration is pervasive and fine grained. Similar to the mafic volcanics, both the calcite and ankerite carbonate species are present. Medium grained carbonate veinlets cross cut the groundmass. Magnetite intensity increases with carbonate alteration. Magnetite is mainly fine to medium grained and disseminated throughout the rock.

Figure 5.4: Hand sample images of the Thunder Creek pyroxenite becoming increasingly altered moving right.

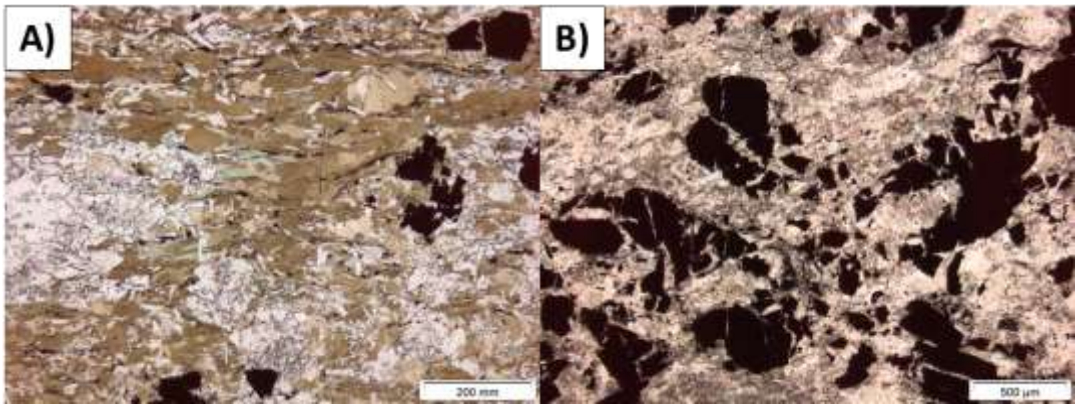

Figure 5.5: A) PPL image of fine-grained biotite and chlorite. B) PPL image of disseminated magnetite.

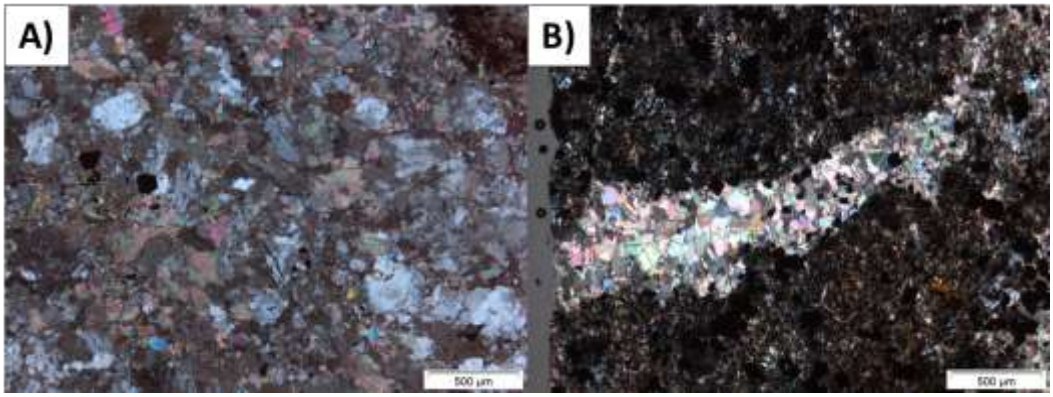

Figure 5.6: A) Fine-grained carbonate and feldspar groundmass. B) Late carbonate veinlet cross cutting altered mafic protolith.

5.1.3 Rusk Shear Zone

The Rusk Shear zone represents a predominantly strongly altered pyroxenite at the contact with the Thunder Creek syenite. The rocks are bleached and locally mylonitized (Figure 5.7). The dominant alteration mineral is calcite with lesser ankerite cross cut by late quartz and K-feldspar veins. In thin section, the rock is fine-grained and locally up to 70% carbonate. Locally grain size reduction causes the rock to become very fine grained (10-300μm). Grain size reduction and deformation are visible in subgrains forming along coarser quartz grains in vein material (Figure 5.8).

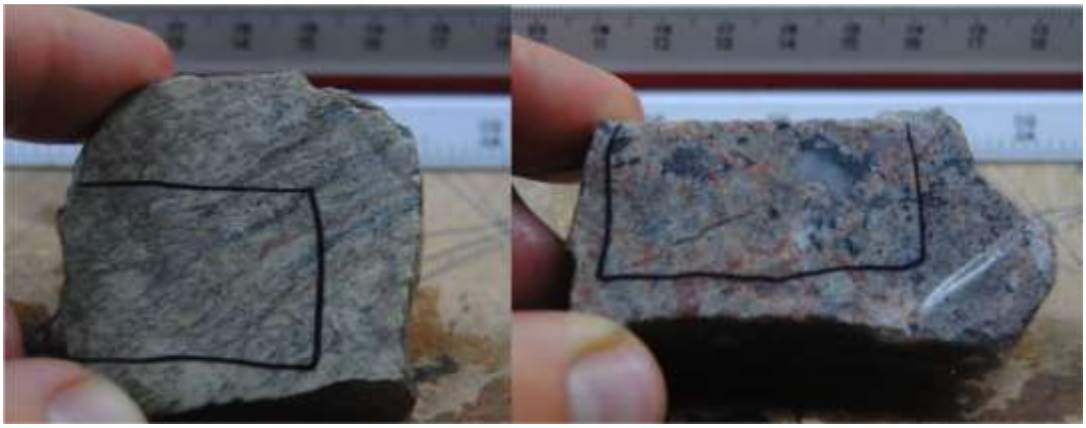

Figure 5.4: Hand sample photos of the Rusk Shear zone. The photo on the left displays the Rusk foliation, while the photo on the right shows the late quartz flooding.

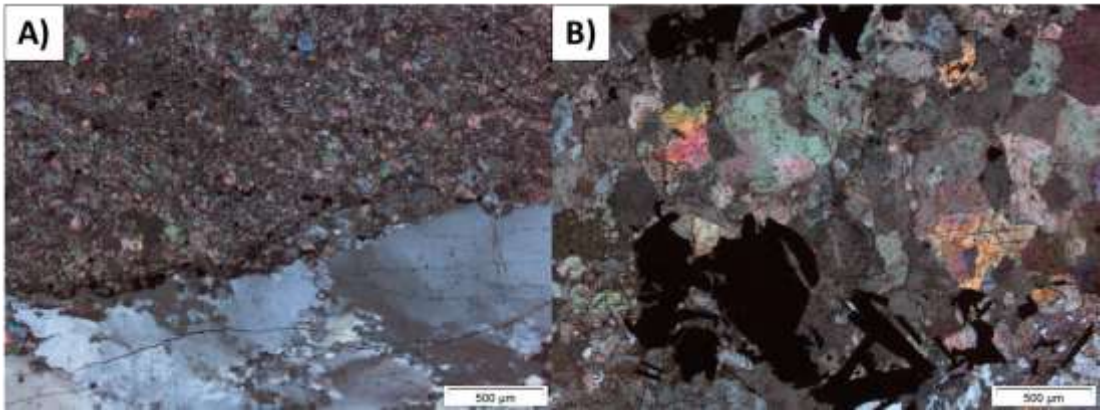

Figure 5.5: Photomicrographs of Rusk material. A) XPL image of very fine-grained carbonate groundmass with late deformed quartz vein. B) XPL image of coarser carbonate grains with needle like magnetite grains.

5.1.4 Thunder Creek Syenite

At the Thunder Creek deposit the syenite is visibly altered, but the whole rock geochemical composition has not changed substantially. Very little calcite/ankerite, sericite and hematite alteration are present in the most mineralized portion of the

intrusion. Disseminated pyrite is present throughout the syenite indicating pervasive fluid flow has altered the rock. Also, the destruction of mafic phenocrysts in the least altered Thunder Creek Stock indicates the rock has been altered. The most visibly altered portions of the intrusion are syenite dykes and the upper levels of the intrusion (TC 280m) (Figure 5.9). In hand sample, hematitic and potassic alteration overprint the rock. K-feldspar grains often display Carlsbad and Microcline twinning. Late barite is associated with late K-feldspar rims overgrowing albite cores (Figure 5.10 & 5.11). Barite compositions range from Ba-rich (barite) to Sr-rich (celestine).

Figure 5.6: Hand sample photographs of TC 695m syenite dyke (left) and TC 280m background syenite sample with dark red colour.

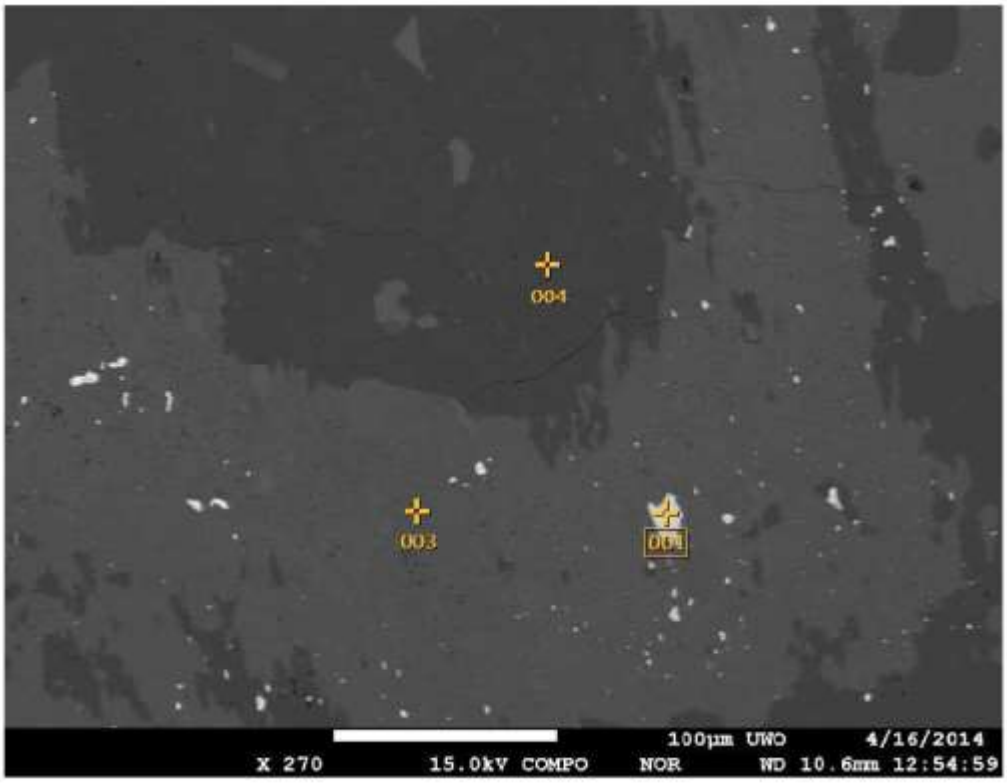

Figure 5.7: Backscatter image of secondary K-spar/barite overprinting albite core. Albite is point 004, Orthoclase point 003 and Barite 001.

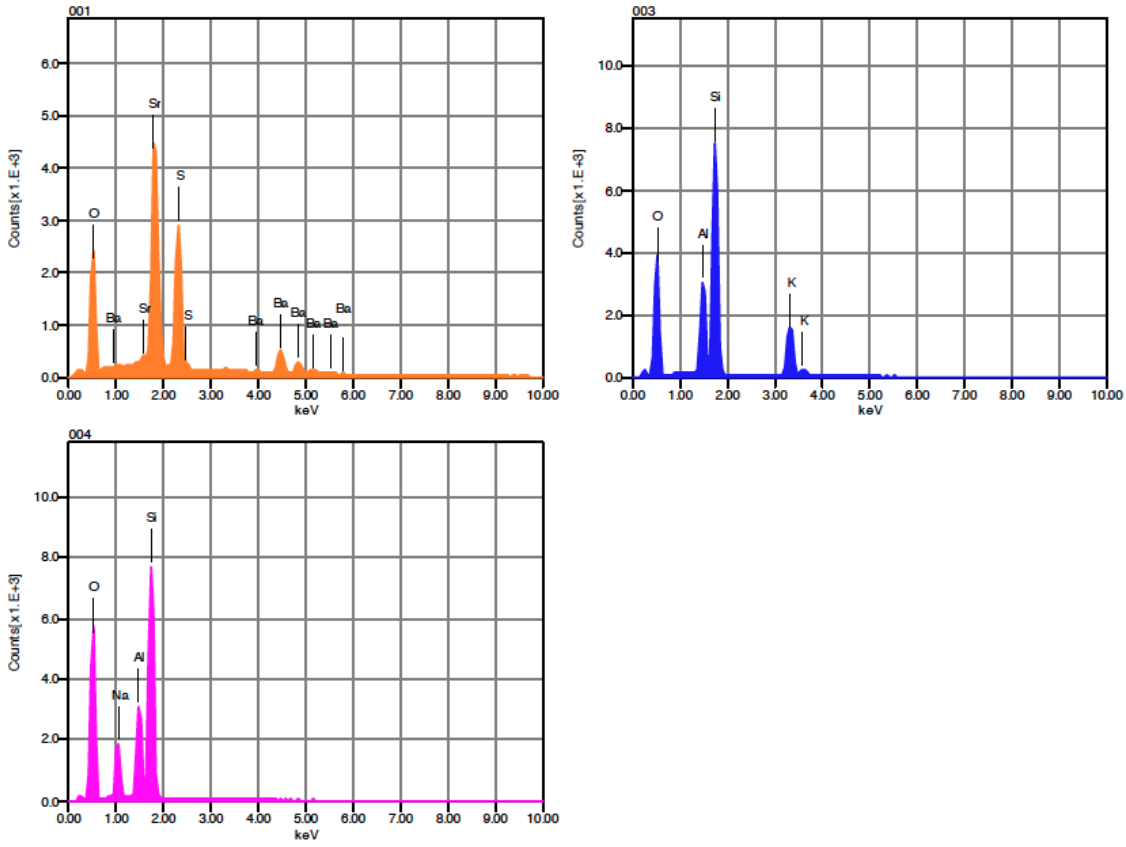

Figure 5.8: EDS spot analysis of feldspar replacement texture at Thunder Creek. Spot 001 (orange) represents barite in a K-spar rim (spot 003/blue spectra). Spot 004 (pink) represents the albite core.

5.1.5 Thunder Creek Syenite Stock

The Thunder Creek stock host examples of the least altered syenite located. However, drill core through the stock also records the earliest stages of alteration. The colour of unaltered to weakly altered syenite changes from a dark purple to pink colour (Figure 4.11). In thin section, the transition from purple to pink involves complete destruction of the mafic mineral phases (biotite, blue amphibole and titanite). Accompanying the destruction of mafic phases is the increase of quartz, K-spar, carbonate and rutile. Rutile forms pseudomorphs after titanite highlighting the alteration (Figure 5.12). Albite records late feldspar alteration, with K-spar rims forming around albite cores. Fine-grained sericite alteration also overprints albite grains (Figure 5.12).

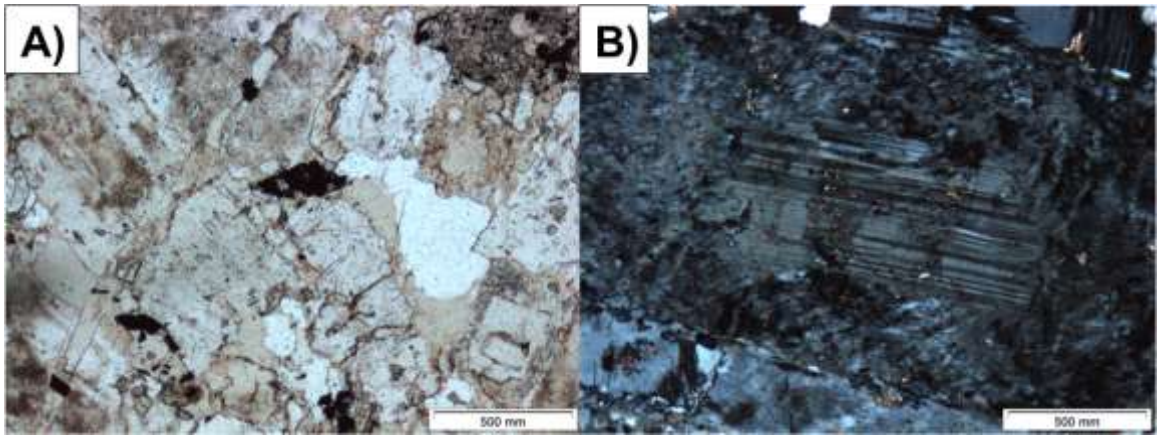

Figure 5.9: Photomicrographs of the alteration at the Thunder Creek stock. A) Rutile forms a pseudomorph of titanite. B) Fine-grained sericite overprints albite grain.

5.2 Hwy-144

5.2.1 MAFIC VOLCANICS

Mafic volcanic samples from Hwy-144 are weakly altered. The weakly altered mineral assemblage in the mafic volcanic rocks is typical of greenschist metamorphic assemblages present in other areas of the Timmins Camp. With increasing calcite and ankerite alteration, epidote and chlorite disappear and carbonate, albite and magnetite account for 90% modal rock volume. Carbonate forms fine grains (20-100μm) often in clusters (Figure 5.13). Magnetite forms fine grains that are preferentially aligned along foliation planes within the rock. The foliation is syn-metamorphic, preferentially in the albite-rich regions with no cross cutting relationships visible in carbonate clusters (Figure 5.14).

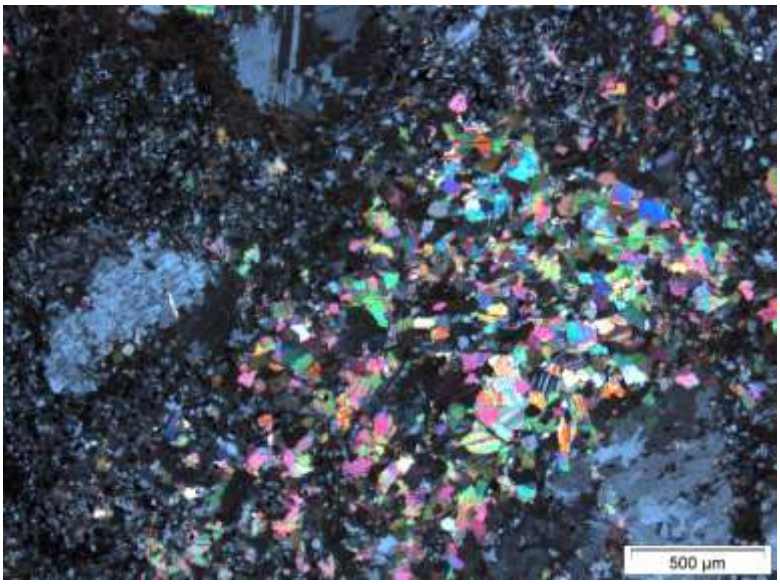

Figure 5.10 XPL photomicrograph of carbonate cluster in an altered mafic volcanic sample.

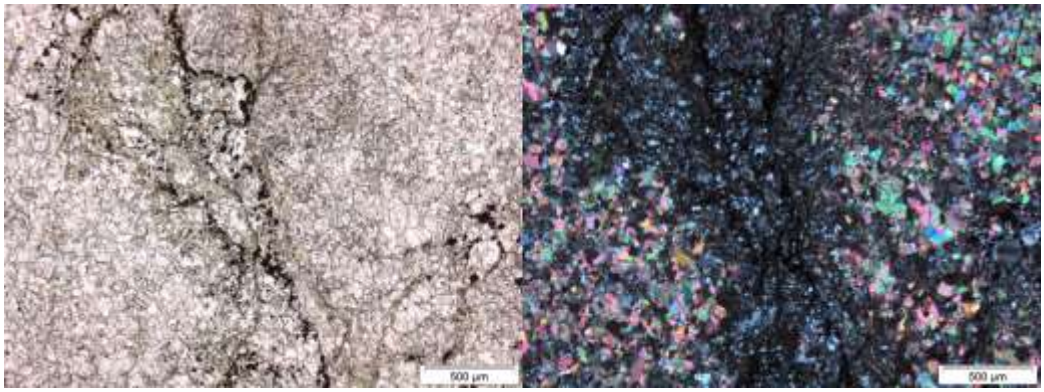

Figure 5.11: PPL (left) and XPL (right) of fine-grained magnetite focused along a foliation plane within a albite-rich domain.

5.2.2 Pyroxenite

The suite of pyroxenite samples from the Hwy-144 zone represents a full assemblage from weakly altered clinopyroxenite to moderately altered pyroxenite (Figure 5.15). The main alteration minerals are: carbonate, K-feldspar, amphibole and chlorite. Carbonate forms fine-grained (200-400μm) veinlets that cross cut the pyroxenite body. Carbonate alteration is locally pervasive with carbonate-rich domains within the groundmass. Similar to carbonate, late K-spar veinlets cross cut the altered pyroxenite. K-spar grains are mottled and fine to medium grained (200-1200μm). Chlorite grains are present in the interstitial space between coarser pyroxene crystals. With increasing chlorite abundance there is a decrease in pyroxene content. Chlorite is fine-grained (40-300μm) and anhedral.

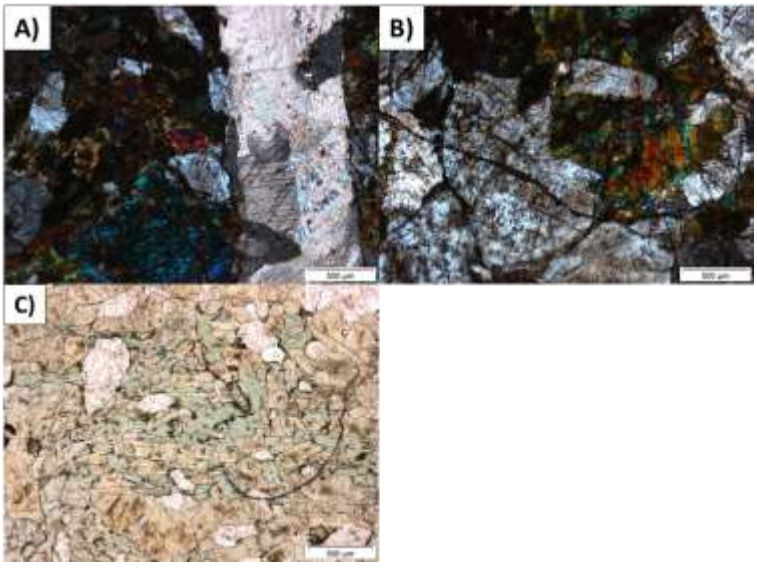

Figure 5.15: Photomicrographs of pyroxenite alteration at the Hwy-144 zone. A) XPL image of late carbonate veinlet. B) XPL image of late K-feldspar veinlet. C) PPL image of fine-grained interstitial chlorite surrounded by clinopyroxene.

5.2.3 Hwy-144 Rusk

Only one example of "Rusk" style alteration was found in the four studied drill holes of the Hwy-144 zone. Similar to Thunder Creek the Rusk style alteration forms at the contact between pyroxenite and syenite units. In hand sample the rock is bleached and strongly foliated (Figure 5.16). The mineral assemblage is carbonate (calcite + ankerite), quartz and magnetite in decreasing order. This mineral assemblage is similar to that seen at Thunder Creek. The rock has completely replaced the pyroxenite protolith with an extremely fine-grained (10-40μm) carbonate groundmass. Late fine to medium grained quartz veins cross cut the groundmass. The quartz veins are quite deformed with subgrains development present (Figure 5.16). Fine-grained, subhedral, poikilitic magnetite is disseminated throughout the groundmass.

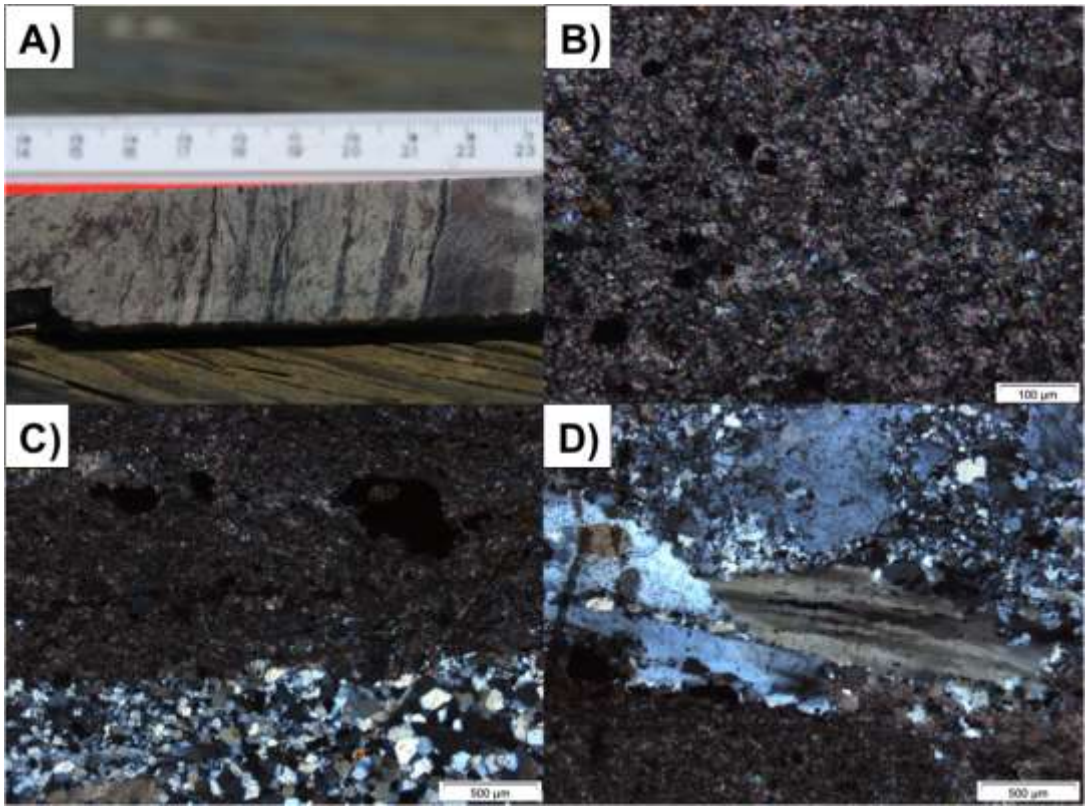

Figure 5.16: A) Hand sample photograph of Rusk style deformation. B) XPL image of fine-grained carbonate groundmass. C) XPL image of fine-grained quartz vein cross cutting groundmass. D) XPL image of sub-grain formation within larger quartz grain.

5.2.4 SYENITE

Syenite samples from the Hwy 144 zone are significantly more altered compared to their Thunder Creek counterparts. Only one sample contained mafic phenocrysts, where as most exhibit strong potassic, hematitic or carbonate alteration. In hand sample many of the Hwy-144 samples are red in colour, similar to Thunder Creek at the 280m

level (Figure 5.17). The main alteration assemblage is hematite, K-spar, and carbonate with minor sericite. In thin section hematite alteration is present along thin fractures within feldspar crystals. Hematite alteration varies, but can be pervasive (Figure 5.18). Similar to Thunder Creek, feldspar replacement textures are abundant within the syenite. Albite cores are commonly followed by K-spar rims. The modal plagioclase/albite content at Hwy-144 is much lower than Thunder Creek, suggesting that pervasive potassic alteration occurred. Carbonate alteration is fine-grained and generally localized to small domains. Sericite is not a major phase in the Hwy 144 syenite but has been noted in a few samples. Sericite is fine-grained and is often associated with carbonate.

Figure 5.17: Two hand sample photographs of the dark red altered syenite. The photo on the right side contains a carbonate altered bleached zone in the right corner.

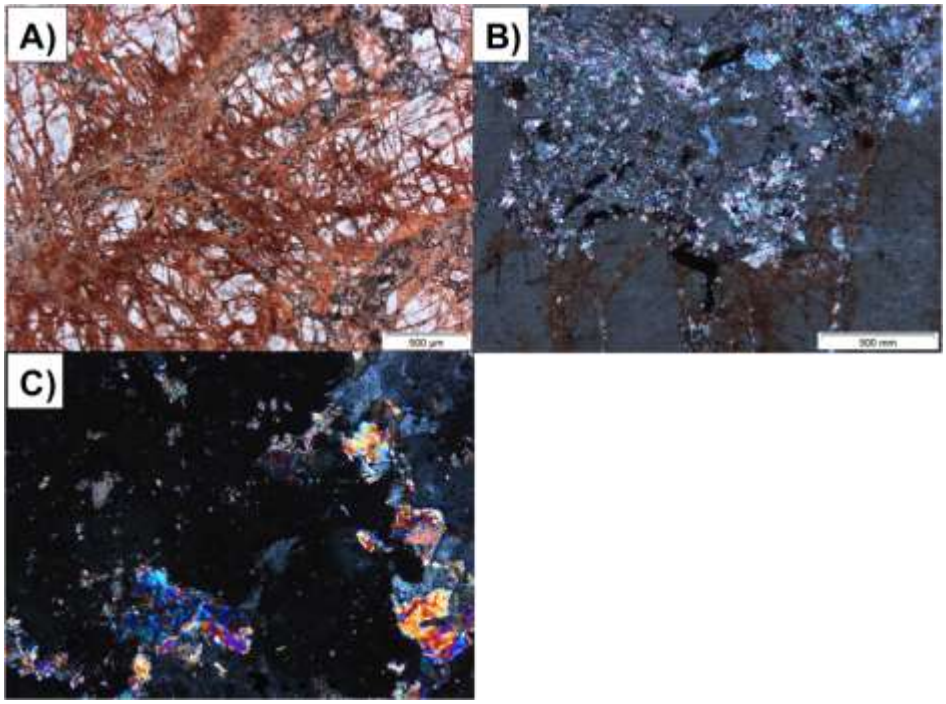

Figure 5.18: A) PPL image of pervasive fine-grained hematite alteration. B) Xpl image of fine-grained carbonate rich domain. C) XPL image of sericite rich domain.

6.0 MINERALIZATION

Gold mineralization was studied at three locations: the Rusk Shear zone, Thunder Creek syenite, and Hwy-144 syenite. Gold mineralization is occasionally present in the pyroxenite that are splays off the Rusk up to 25m away from the Rusk/syenite contact (pers commun, J. Samson). They are occasionally ore grade, but pinch and swell sporadically making it difficult to mine. The focus of the study was the two syenite-hosted styles of mineralization, however, the close spatial relationship between the Rusk and TC syenite suggests comparisons should be made between these two styles of mineralization as well. In order to fully characterize gold mineralization the following techniques were used: strategic sampling, vein density calculations, petrographic microscopy, table top SEM analysis, WDS microprobe mapping and LA-ICP-MS pyrite geochemistry. These analyses move from the macro to microscopic scale to provide a full interpretation of the controls on gold mineralization. Microprobe mapping and laser ablation will be touched on in this chapter but the results of these methods are discussed in detail in the Geochemistry chapter.

6.1 Thunder Creek

6.1.1 Sampling Strategy

During routine core logging, it was noticed by Lake Shore Gold Corp geologists that strong gold assays are often associated with areas of increased veining within the syenite. With that in mind a sampling program was developed for the Thunder Creek mine utilizing several different mine levels (TC280m, TC660m, TC695m, TC730m). Within the syenite four different sampling zones were targeted: background syenite, V_1 quartz veins, V_2 extensional quartz veins, and V_3 subvertical quartz veins. A full description of each vein type is presented in Chapter 4. Approximately 80 samples were taken and the results are displayed in Table 6.1. Vein samples were analyzed for gold via fire assay by Lake Shore Gold's in-house lab in Timmins, Ontario. Background syenite samples were analyzed for gold via fire assay by ALS Global in Vancouver, British Columbia.

Table 6.1: The table below highlights the results of a mineralization specific sampling program.

	Background Syenite	V_1 Veins	V_2 Veins	V_3 Veins
Number of Samples	25	15	29	12
Min. Grade (g/t)	0.08	0.27	0.13	0.08
Max. Grade (g/t)	6.11	433	941	8.64
Avg. Gold Grade (g/t)	0.94	3.77	10.89	1.16

***A cut off grade of 30 g/t was used**

The results of the sampling program indicate that the two early stages of veining provide economic gold grade mineralization. The variability between minimum and maximum gold grades in V_1 & V_2 veins highlights the nuggety nature of gold in the veins. The background syenite with disseminated pyrite is significantly enriched in Au relative to an average unmineralized syenite. Background syenite samples contain approximately 0.5-3.0% disseminated medium to coarse grained pyrite. There is no visible difference between a sample with 0.8 g/t and the 6.11 g/t. V_3 veins are not nearly as abundant as V_1 or V_2. This late vein array is weakly mineralized compared to the two earlier vein generations, suggesting that gold mineralization is in the dying stages during their formation. Considering vein density varies from approximately 1-20% it is the superimposition of these events that provides an economic gold grade.

6.1.2 Gold Grade vs. Vein Density

The results of the strategic sampling program prompted further examination of vein density versus gold grade. A series of photographs were taken of the east face of the 695m level Thunder Creek syenite. These photos were stitched together and intervals of consistent vein density were selected for study. Chip sampling was systematically (1 sample per meter) performed across the east wall of the syenite and provided the average gold grade data. Once an interval of consistent vein density was chosen the average gold grade was calculated using chip sample data. The vein density was calculated using Adobe Photoshop®. Stitched sections were imported into the program and the total photo pixels were calculated. Next, the vein material was traced with the magic wand tool and the total vein pixels were calculated. The vein area was calculated and inferred as a good approximation for vein density. Figure 6.1 demonstrates the changing gold grade in association with increasing vein density.

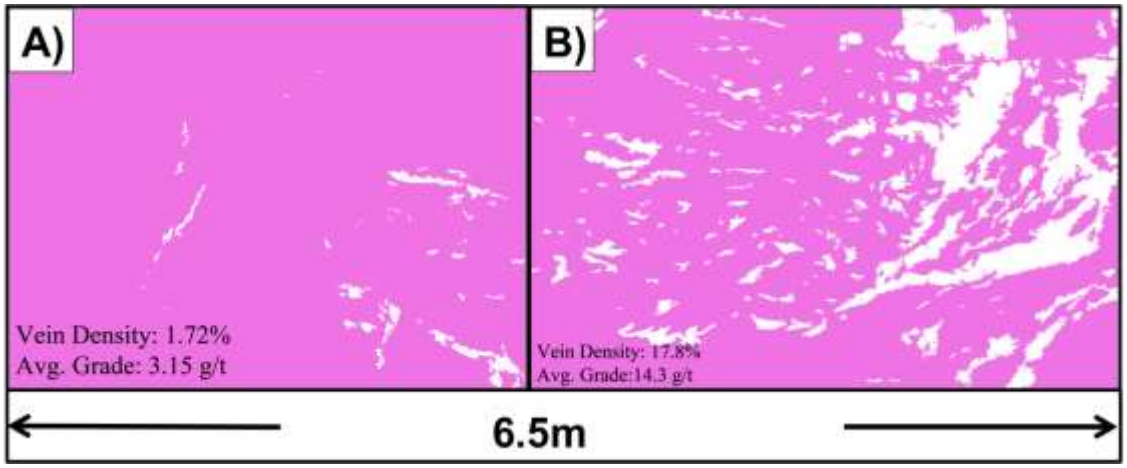

Figure 6.1: Vein density changes considerably between the two consecutive panels A & B. A&B are defined by a change in vein density. Gold grade is proportional to increasing vein density.

Ten intervals were chosen on the east face of the TC695m level cross cut four. A plot of gold grade versus vein density was created to determine whether these variables are related (Figure 6.2). There is a positive trend with a regression line of 0.617. There is not a perfectly linear correlation between vein density and gold grade, however the samples with the highest vein density correspond to the highest gold grade and the samples with the lowest vein density have the lowest gold grade. A separate comparison was made that illustrates different gold grades based on the predominant vein array in the sampled region. Two regions were compared: one with predominantly V_2 veins and the other with V_3 veins (Figure 6.3). The vein density between the two areas is similar so the difference in gold grade should be directly related to the vein type.

The results correlate well with the strategic sampling done on vein material. Areas with predominantly V_2 veins have a higher average gold grade compared to zones of predominantly V_3 veins.

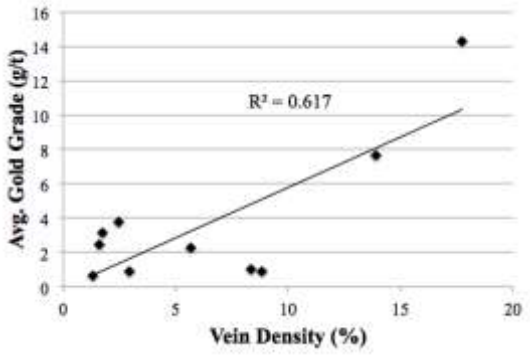

Figure 6.2: Plot of vein density versus gold grade.

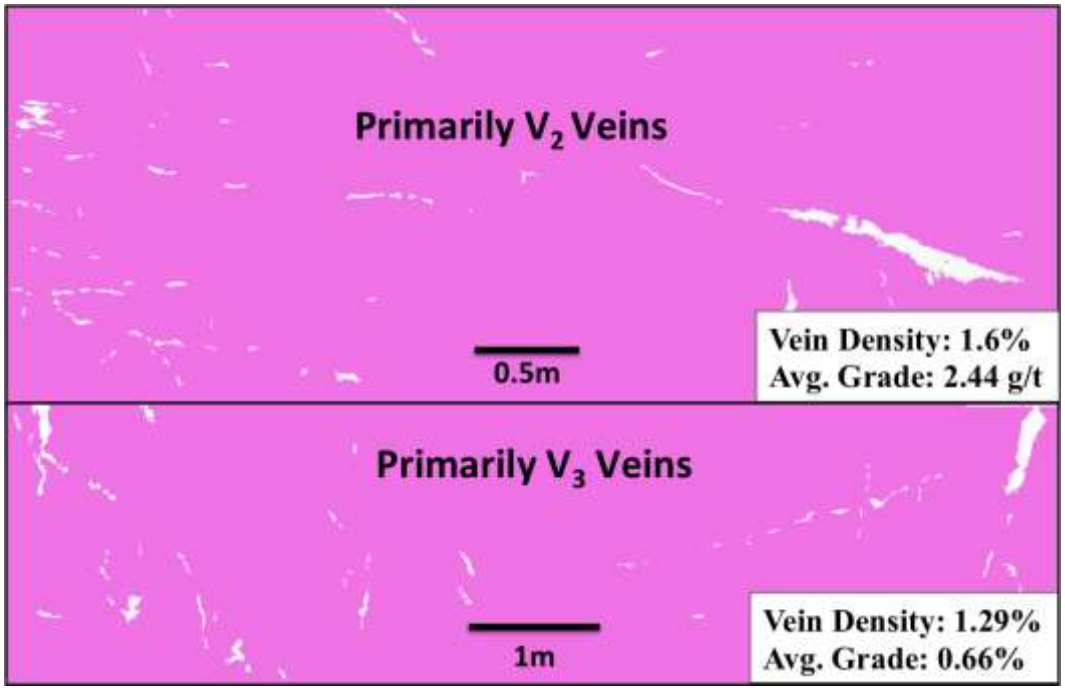

Figure 6.3: Comparison of V2 to V3 veins with a similar vein density.

6.1.3 PETROGRAPHY

Pyrite is present in two generations within the Thunder Creek syenite. Disseminated pyrite is corroded and generally fine to medium grained (0.1-0.8 cm). Inclusions in disseminated pyrite are K-feldspar, quartz, albite, magnetite and rutile. Vein-hosted pyrite is primarily medium to coarse-grained (0.5-1.8 cm) present in V_1, V_2 and V_3 veins. Vein-hosted pyrite is usually subhedral and generally silicate-inclusion free. In thin section, barren vein-hosted pyrite commonly contains chalcopyrite and galena as inclusions. In hand sample, V_1 veins have pyrite associated with galena and molybdenite. V_2 veins have pyrite associated with scheelite, galena and molybdenite. V_3 veins contain only pyrite.

Hand sample, petrographic and EDS analyses were conducted on mineralized samples from Thunder Creek. Gold mineralization is spatially related to pyrite, typically present as inclusions or along fractures. Galena and sphalerite are common sulfides locally near, but not in the same, gold-rich pyrite grains. In hand sample, mineralization is most commonly associated with veining + pyrite, but areas of coarse disseminated pyrite are also prospective (Figure 6.4). At Thunder Creek gold is spatially related to silicification of the syenite.

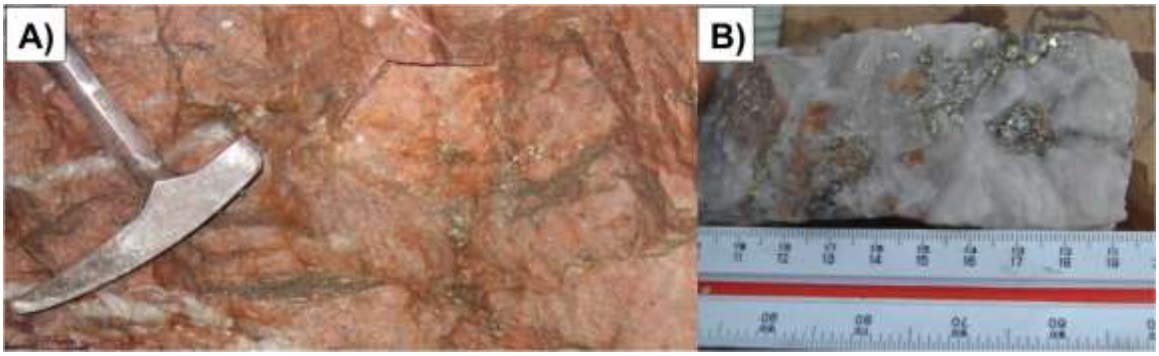

Figure 6.4: Hand sample photographs from the TC deposit. A) Coarse disseminated pyrite within the syenite. B) Medium to coarse vein-hosted pyrite.

In thin section gold mineralization is primarily present within fractured, V_2 vein-hosted pyrite grains (Figure 6.5). Minor amounts of gold are present as free gold in V_1 and V_2 quartz veins. Gold forms small (10-20μm) anhedral grains primarily as inclusions in pyrite. Gold also forms along fractures in pyrite associated with quartz and ankerite. Gold is generally not associated with any other sulfide mineral. K-feldspar, barite, quartz, and ankerite are commonly located near gold grains as inclusions in pyrite or as the vein material hosting the pyrite.

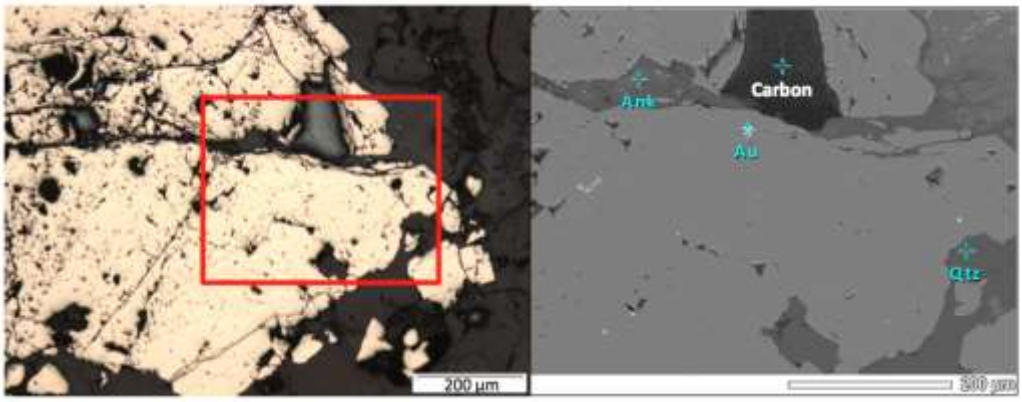

Figure 6.5: Reflected light and SEM images of gold mineralization in vein-hosted pyrite from the Thunder Creek deposit. The red box highlights the area studied with the SEM.

6.1.4 Rusk Shear Zone

The Rusk Shear zone hosts the richest mineralization present, and is a significant portion of gold mineralization extracted from the Thunder Creek deposit. Gold is associated with medium grained disseminated pyrite, and late quartz/K-feldspar vein-hosted pyrite that cross cut the strongly foliated and carbonatized shear zone. The veins are deformed, and likely are similar in timing to V_1 veins in the syenite. Both disseminated and vein-hosted pyrite are medium-grained and fractured. Quartz veins

that host the pyrite display pressure shadows and subgrain boundary development. Both styles of pyrite are anhedral and contain carbonate and quartz inclusions. Pyrite crystallization occurred after the major shearing event, but is synchronous with late vein quartz deformation. Gold mineralization is hosted in a thin (0.5-3m) deformation zone that is higher grade compared to syenite-hosted mineralization. Similar to syenite style mineralization gold is directly proportional to pyrite intensity. In hand sample, the unit is strongly bleached with syenite dyklets incorporated into the shear zone (Figure 6.6).

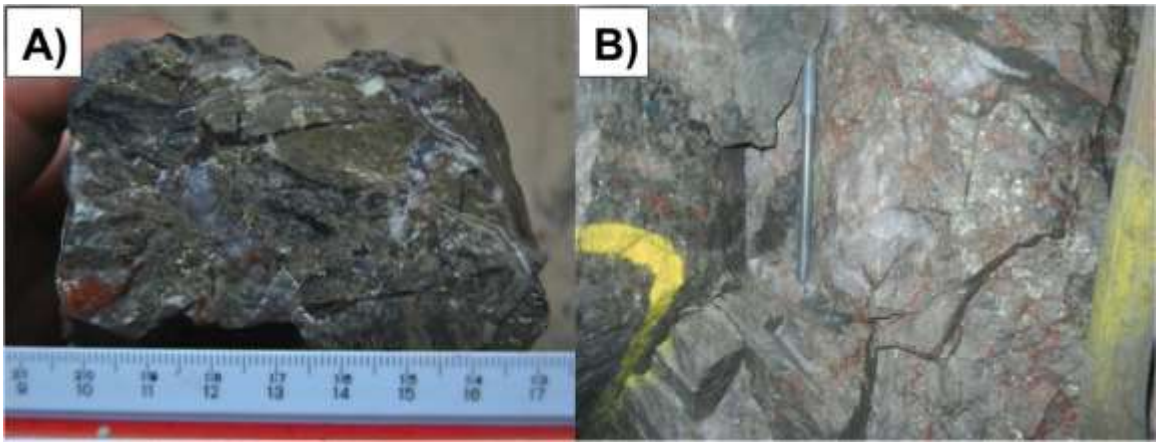

Figure 6.6: Rusk style mineralization. A) Late quartz veins cross cut bleached host rock. B) Intense pyritization associated with quartz veining and thin pink syenite dykelets.

In thin section gold is almost exclusively present as inclusions within pyrite grains. A small percentage of gold is present in fractures or the silicate/carbonate vein material. Gold present along fractures is often associated with quartz and K-feldspar. Gold forms small anhedral blebs approximately 5-40μm in diameter (Figure 6.7). Gold is not associated with any other sulphide other than pyrite. Quartz and ankerite are common minerals within the veins that host gold bearing pyrite. K-spar, quartz, rutile, and monazite are often other inclusions proximal to gold grains in pyrite (Figure 6.7 & 6.8). Rutile inclusions are often anhedral and also present on pyrite grain margins.

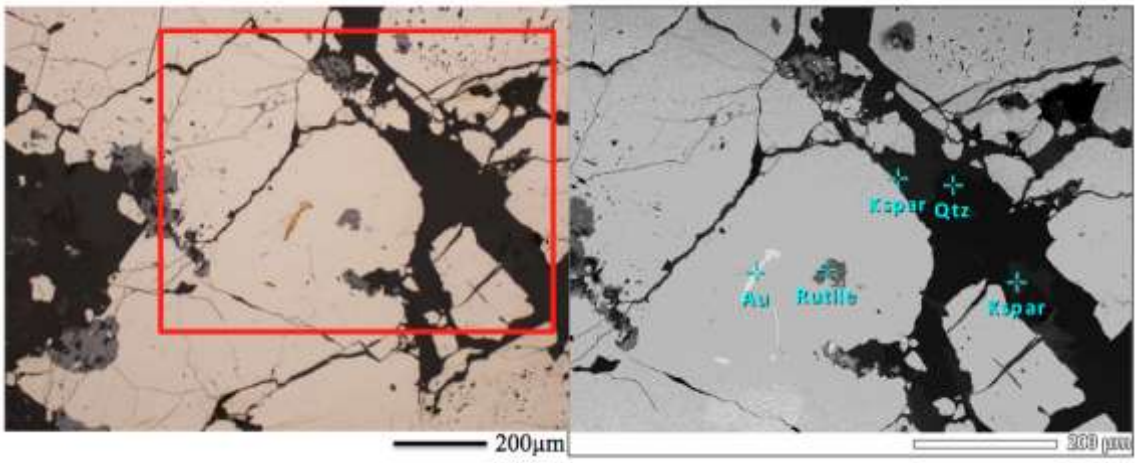

Figure 6.7: Reflected light (left) and tabletop SEM image (right) of gold in Rusk style mineralization. The red inset designates the perimeter of the backscatter image. Minerals were determined through EDS spectroscopy.

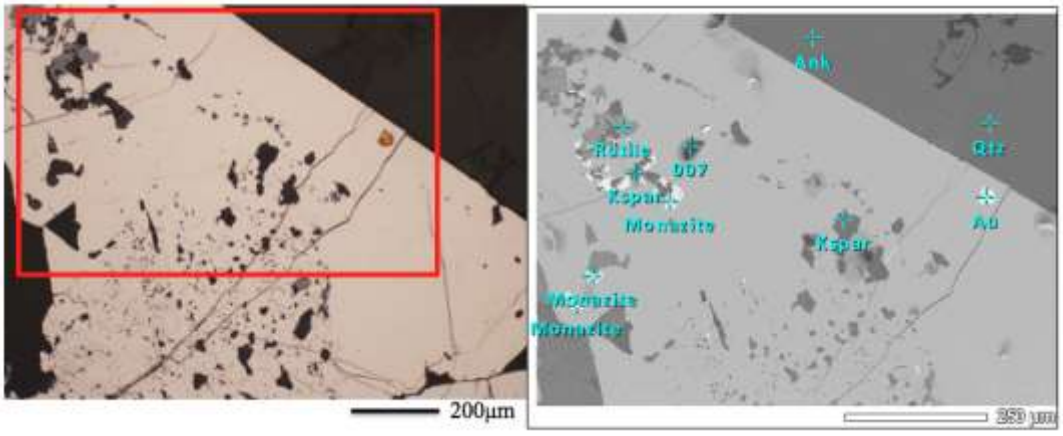

Figure 6.8: Second image of Rusk style mineralization. Reflected light (left) and tabletop SEM (right) image of gold and associated minerals. Minerals were determined through EDS spectroscopy.

6.2 Hwy-144 Syenite

Gold mineralization at Hwy-144 shares many similarities with Thunder Creek. Both systems host mineralization in a felsic pluton, are associated with quartz veins, and are associated with medium-grained disseminated and vein-hosted pyrite. While they share many similar features, Hwy-144 contains its' own unique attributes. Pyrite at Hwy-144 is generally more euhedral and does not usually have the same ratty and corroded textures that are present in disseminated pyrite from Thunder Creek. At Hwy-144 the intrusion is polyphase, equigranular to porphyritic, often strongly altered (potassic, hematitic, carbonate), and is not adjacent to a visible Rusk Shear zone. In hand sample mineralized intervals contain medium- to coarse-grained pyrite and thin 0.5-3.0cm quartz veins (Figure 6.9). The possibility of disseminated mineralization was tested by sampling background syenite with pyrite and no vein material. Syenite samples with no

pyrite and no vein material often fall below the 0.005ppm detection limit using fire assay. Samples with disseminated pyrite assay between 0.006-1.57ppm Au. Disseminated pyrite is often fine grained (0.1-0.5cm), euhedral, occasionally with albite, quartz and rutile inclusions. Vein-hosted pyrite is medium to coarse grained (0.3-1.2 cm), sub to euhedral, and occasionally contains carbonate, quartz and feldspar inclusions. Hwy-144 generally contains less poikilitic pyrite, and inclusions where present are often carbonate. Thunder Creek disseminated pyrite contains abundant inclusions, but they are rarely carbonate.

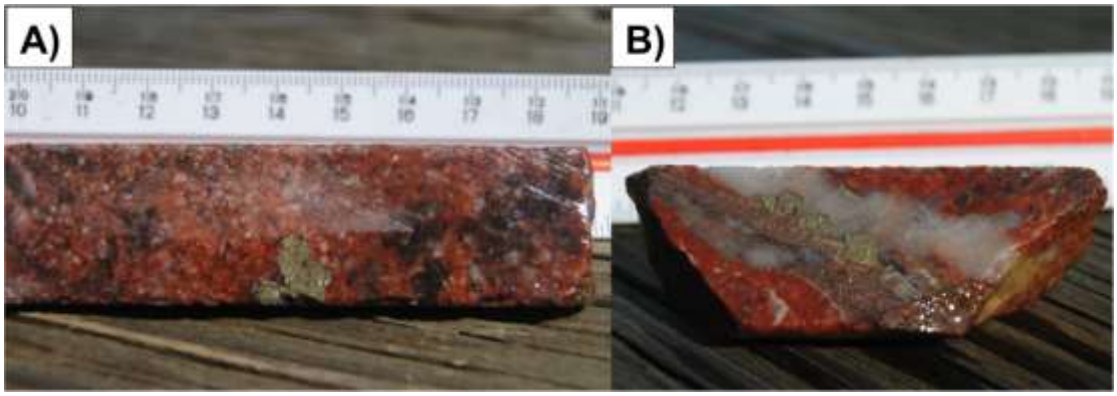

Figure 6.9: Hand sample photographs of Hwy-144 mineralization. A) Coarse grained disseminated pyrite. B) Medium to coarse-grained vein-hosted pyrite.

In thin section gold grains were only found within vein-hosted pyrite samples. Gold grains are small (10-40μm) anhedral grains primarily present as inclusions but also form along fractures within pyrite grains. Gold grains are commonly associated with pyrite hosted in quartz-ankerite vein material. Barite has been located in the vein material near gold grains (Figure 6.10). Mineralized samples contain pyrite with inclusions of K-feldspar, albite, quartz, magnetite, and rutile. Other sulfides such as galena and chalcopyrite are present in pyrite grains but are not often spatially near gold grains.

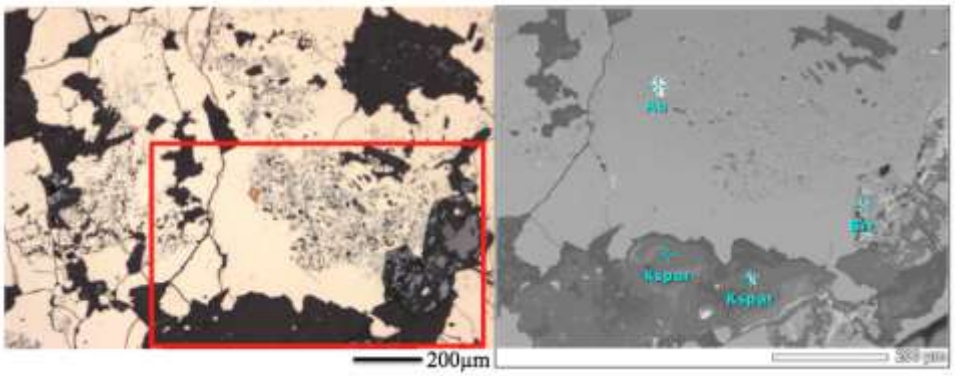

Figure 6.10: Reflected light and SEM image of gold mineralization in vein-hosted pyrite from the Hwy-144 area.

7.0 Geochemistry

Whole rock geochemistry was conducted at three localities targeting the Thunder Creek Stock, Thunder Creek Mine and Hwy-144 zones. Each major lithological unit was sampled, targeting unaltered through altered. The purpose of the sampling was to correlate and extrapolate mineralization trends along geochemical trends. All geochemical data was analyzed by ALS Global Ltd's lab in Vancouver, British Columbia, Canada. All raw data from the geochemical analyses is available in Appendix D. Whole rock geochemistry was used to characterize alteration and calculate mass balance equations. A review of the analytical techniques used to acquire whole rock geochemistry is presented in the Methods chapter.

7.1 Syenite Geochemistry

Representative major element geochemistry of syenite samples from Thunder Creek and Hwy-144 are shown in Table 7.1. The least altered samples were determined visually and petrographically. In hand sample, the Thunder Creek least altered samples have little to no carbonate or hematite alteration, along with primary biotite, blue amphibole and titanite grains. Pyrite abundance increases with both carbonate and feldspathic alteration. At Hwy-144, the least altered samples have minimal carbonate, hematite and potassic alteration with no sulfides. In thin section, least altered samples display primary magmatic textures and feldspars lack the mottled appearance characteristic of hydrothermal alteration (Allen et al., 1996). In general syenite samples range from 55-70 wt% SiO_2, 0.49-7.35 wt% CaO, 2.27-8.52 wt% Na_2O, 3.5-9.5 wt% K_2O, 0.12-1.4 wt% BaO and 0.08-1.62 wt% S.

Table 7.1: Demonstrates representative major element geochemistry of syenite samples at Thunder Creek and Hwy-144.

	Thunder Creek Stock (Least Altered)	Thunder Creek Mine (280m)	Thunder Creek Mine (695m)	Hwy-144 (Least Altered)	Hwy-144 (Strongly Altered)
SiO_2	66.5	69.2	70.2	61.6	63.8
Al_2O_3	14.9	14.25	15.85	15.6	15
Fe_2O_3	2.05	1.46	1.24	2.23	3.22
CaO	1.8	2.57	0.5	2.48	1.96
MgO	0.69	0.15	0.19	0.69	0.63

Na_2O	5.29	5.51	5.67	5.74	3.67
K_2O	6.18	4.6	6.02	5.66	8.19
TiO_2	0.21	0.08	0.09	0.29	0.24
MnO	0.05	0.02	0.02	0.05	0.08
P_2O_5	0.16	0.03	0.01	0.12	0.07
SrO	0.13	0.04	0.12	0.24	0.06
BaO	0.27	0.1	0.23	0.32	0.15
C	0.38	0.59	0.18	1.01	0.85
S	0.08	0.56	0.55	0.1	0.07
LOI	1.72	2.49	1.35	4	3.09

All samples measured in wt.%

Ca values vary substantially within the data set, values are lowest in the most strongly mineralized portion of the mine (Table 1, TC 695m). Again looking at Table 7.1, the most strongly mineralized samples (TC 280m and TC 695m) have the highest SiO_2 values. The barium content of the rock is directly proportional to the barite content of the rock. Table 7.1 demonstrates with increasing feldspathic alteration at Hwy-144 the BaO content does not change substantially. Using the discrimination diagram of Miyashiro (1978), syenite samples at each locality were subdivided into alkaline and subalkaline (Figure 7.1). The majority of the samples plot in the alkaline portion of the diagram. Both Na and K are mobile during hydrothermal alteration. Using both visual and petrographic characteristics, it is determined that variable Na_2O and K_2O values likely represent alteration rather than igneous fractionation or a separate igneous source. REE spider diagrams were created to evaluate the inherent immobile composition of the Thunder Creek syenite. Figure 7.2 shows that the syenites are elevated in light REE's and depleted in heavy REE's. Each of the three syenites plots along a similar REE profile with varying degrees of enrichment/depletion. To test the cogenetic nature between the Hwy-144 syenite and Thunder Creek syenite a similar REE diagram to Figure 7.2 was created (Figure 7.3). The Thunder Creek stock (purple) represents a least altered syenite. Hwy-144 (pink) shows REE enrichment relative to the unaltered protolith while the Thunder Creek mine is depleted relative to the unaltered stock.

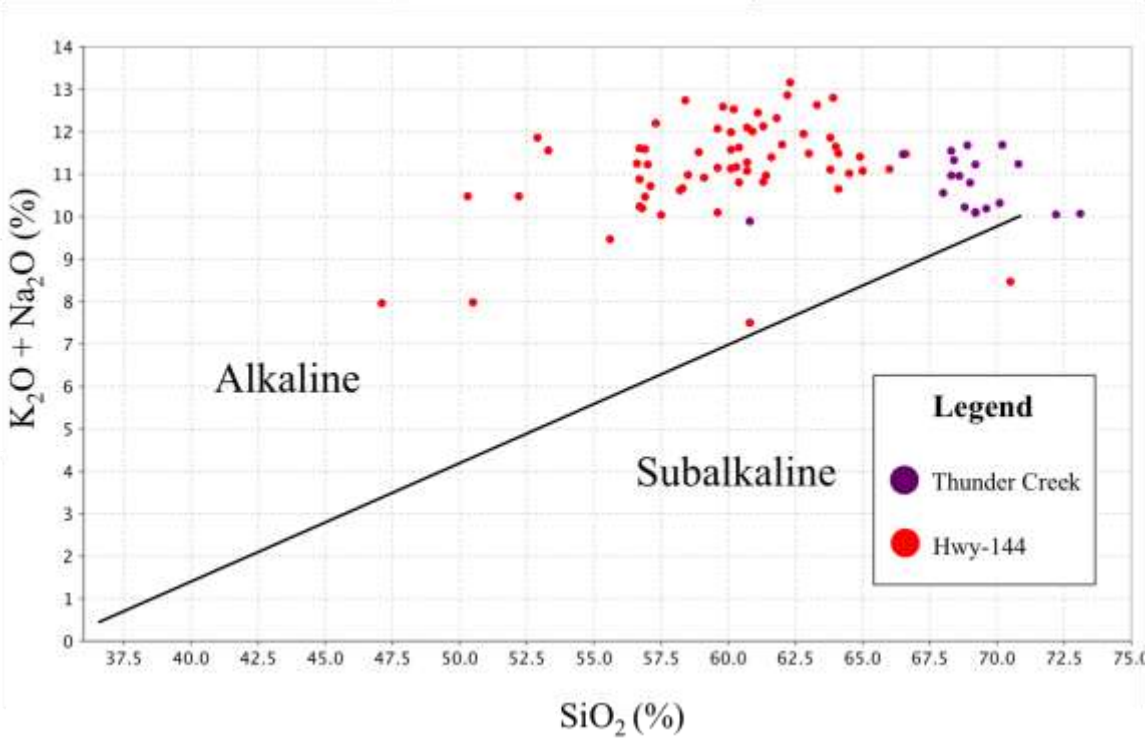

Figure 7.1: Plot of alkalinity of Thunder Creek and Hwy-144 syenite samples based on Miyashiro (1978).

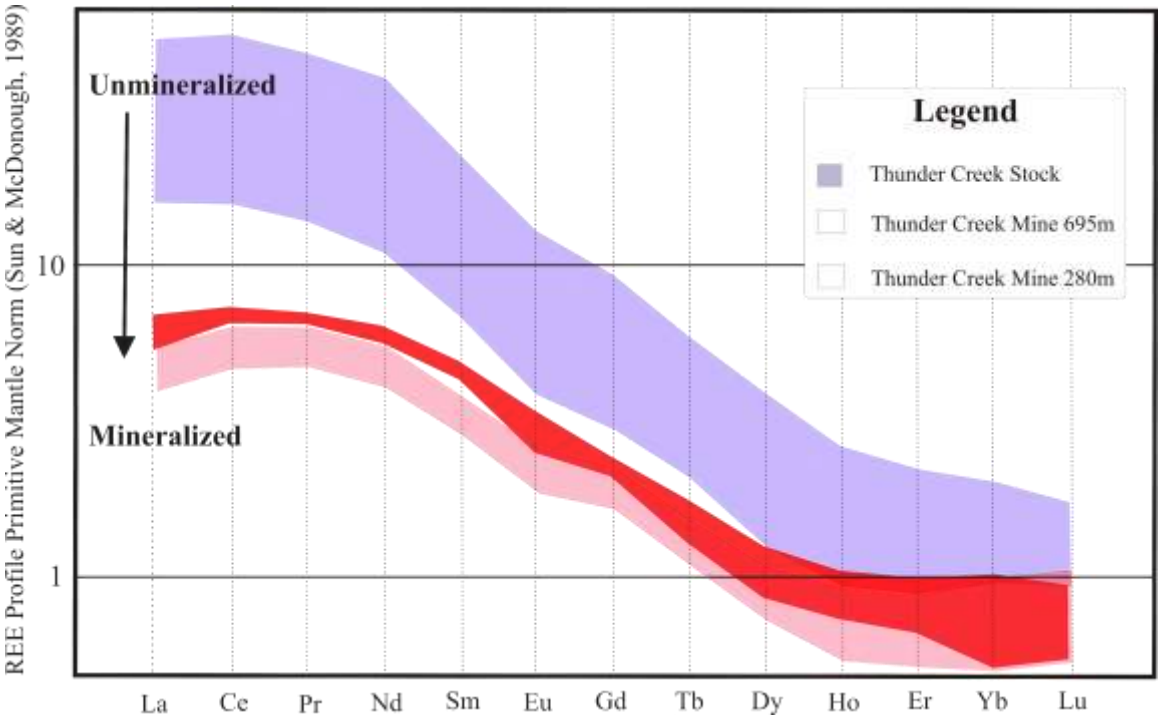

Figure 7.2: REE spider diagram of the Thunder Creek syenite.

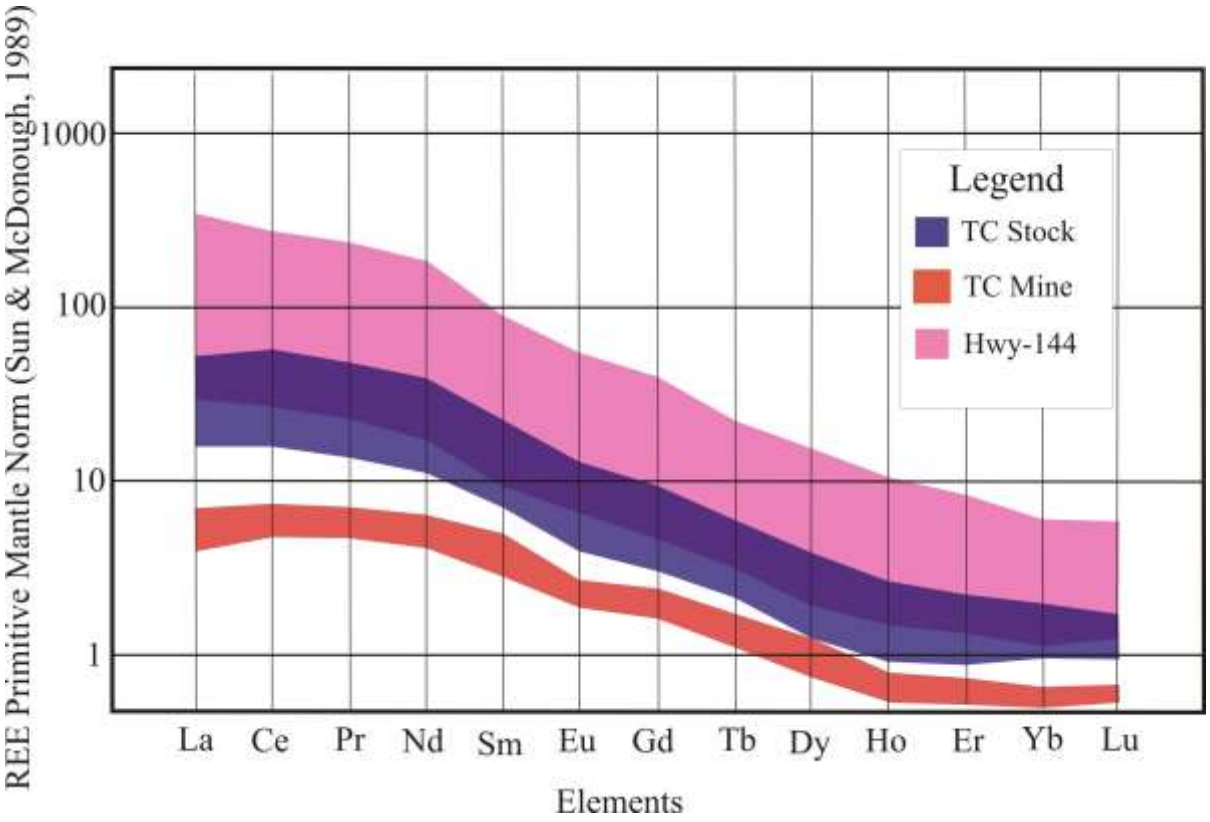

Figure 7.3: REE spider plot of the Hwy-144, Thunder Creek mine and Thunder Creek stock syenite samples.

7.2 Pyroxenite Geochemistry

The pyroxenite samples were taken from both underground (TC 695m) and drill core (Hwy-144). At the mine the pyroxenite is moderately altered, with no primary pyroxene grains present. The pyroxenite becomes increasingly more altered towards the Rusk Shear zone. With increasing alteration the rock becomes bleached and the CaO content increases significantly (Table 7.2). Petrologically, Hwy-144 hosts the least altered pyroxenite samples containing primary clinopyroxene grains.

Table 7.2: Representative major element geochemistry of least altered and altered pyroxenite samples from Thunder Creek and Hwy-144.

	TC 695m Moderately Altered	TC 695m Altered	Hwy-144 Least Altered	Hwy-144 Altered
SiO_2	38.6	31.5	43.7	36
Al_2O_3	9.79	8.39	4.59	8.74
Fe_2O_3	16.4	10.95	11.85	8.94
CaO	7.51	19.4	24.5	15.4
MgO	12.45	3.45	10.45	4.49
Na_2O	<0.01	3.72	0.51	4.37
K_2O	3.76	1.56	0.02	0.94
Cr_2O_3	0.01	<0.01	0.03	<0.01
TiO_2	2.06	2.07	1.26	1.04
MnO	0.21	0.26	0.23	0.19
P_2O_5	0.03	0.77	2.68	1.21
SrO	0.09	0.3	0.23	0.32
BaO	0.21	0.21	<0.01	0.27
C	1.62	5.19	0.1	4.53
S	0.12	0.15	0.06	0.15
LOI	9.04	18.8	1.59	16.85

All samples measured in wt.%

Major element geochemistry demonstrates the reduction of Si/Fe/Mg and input of Ca, Na and LOI during alteration. Compatible/immobile elements such at Ti stay fairly constant during alteration. The REE profile of the pyroxenite remains uniform moving from unaltered to altered. The final rock classification diagram attempts to determine the protolith of the Rusk shear zone (Figure 7.4). The shear zone has been interpreted as "multi-protolith", although it is believed to be primarily deformed pyroxenite. Using a REE spider diagram normalized to primitive mantle, the Thunder Creek pyroxenite,

Rusk shear zone and Thunder Creek syenite are compared (Figure 7.4). The diagram helps illustrate the co-genetic nature of the Bristol Township Alkalic Complex as a whole, interpreted by (Beakhouse, 2011). The one visual outlier in the Rusk shear zone may represent a sliver of mafic volcanic or sediment incorporated into the shear zone. Contrary to fractional crystallization processes, the syenite is strongly depleted in incompatible elements compared to pyroxenite.

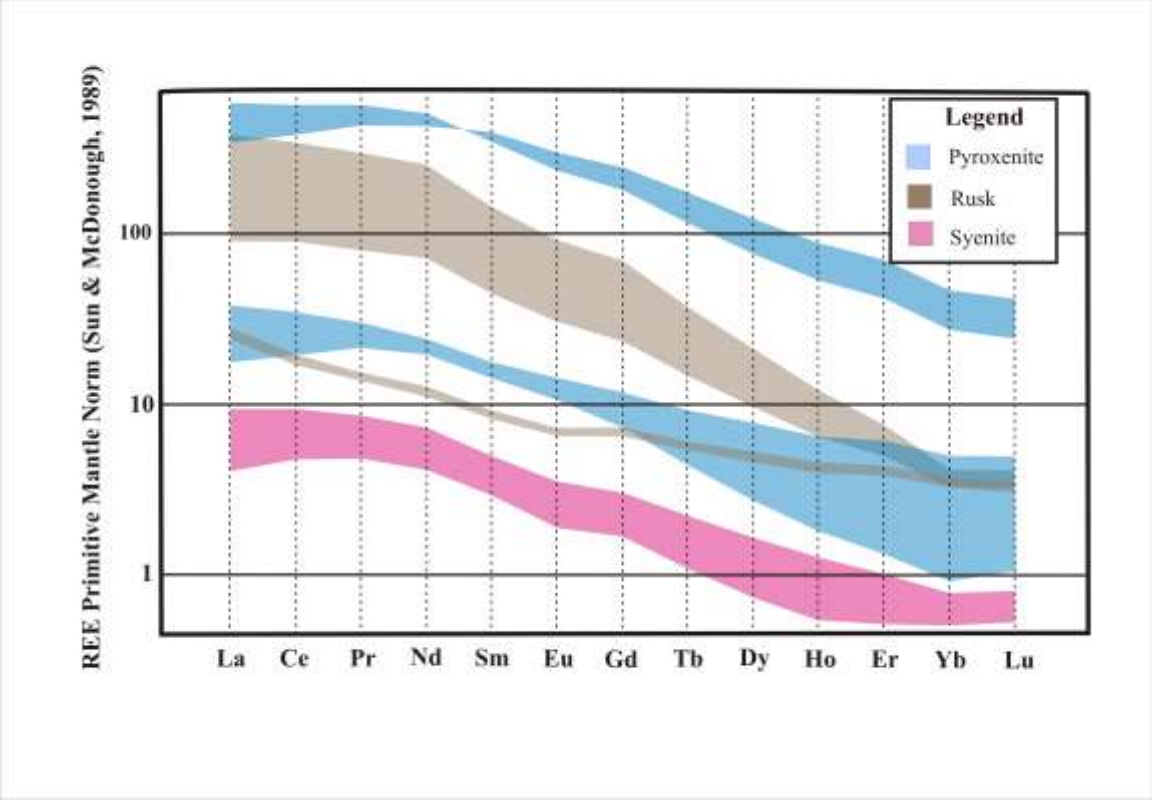

Figure 7.4: REE spider diagram comparing the Thunder Creek pyroxenite, Rusk Zone and syenite.

7.3 Monitoring Fractionation, Alteration & Mineralization

The Thunder Creek zone can be subdivided into three groups: the Thunder Creek stock, Thunder Creek mine 280m and Thunder Creek mine 695m. These three sites were used to examine the geochemical composition change between unaltered vs. altered, and unmineralized vs. mineralized samples. The Thunder Creek stock represents relatively fresh syenite that contains on average below the 0.005ppm detection limit for gold. The upper portion of the mine (TC280m) represents thin syenite fingers that contain sub economic mineralization with moderate alteration. Finally the lower portion of the syenite (TC695m) has only been affected by feldspathic alteration, and its composition appears to be close to the primary magmatic composition. This zone of the syenite is also strongly mineralized. Hwy-114

represents a zone of varying alteration ranging from moderate to intense and contains low to moderate mineralization.

Geochemical data can be used to understand hydrothermal alteration and igneous fractionation (Cathelineau, 1986; Grant, 1986; Gresens, 1967; Kerrich & Fyfe, 1981; MacLean & Barrett, 1993; Stanley & Russell, 1989). The first step in evaluation whether the data reflects magmatic or hydrothermal systems is to locate a set of immobile and incompatible elements. MacLean & Barrett (1993) suggested using bivariate plots to determine incompatibly. The two incompatible elements should be strongly correlative with an r factor equal to 0.9-0.99, ideally intercepting the origin. Through petrographic analyses it was determined that the least altered samples are from the Thunder Creek satellite stock. In thin section these samples have primary mafic minerals such as blue amphibole and biotite. This locality also shows the progressive evolution from a dark purple to pinkish syenite. The sample area is also sufficiently far enough away from mineralization and the Thunder Creek Mine. Moving from this unaltered zone towards the mine we can document the changes geochemically. Bivariate plots were created to test the hypothesis of igneous fractionation and hydrothermal alteration (Figure 7.5). Figure 7.5 uses an incompatible/immobile plot of Nb-Dy to document the alteration change between sites. Moving southwest toward the most-altered Hwy-144 syenite, element mobility appears to be pervasive. At Hwy-144 bivariate plots using incompatible elements do not provide a strong correlation with an R factor near 0.9. The only elements that strongly correlate are the REE, therefore it is difficult to determine whether these elements behaved incompatibly or partitioned at a constant rate into the same mineral phase.

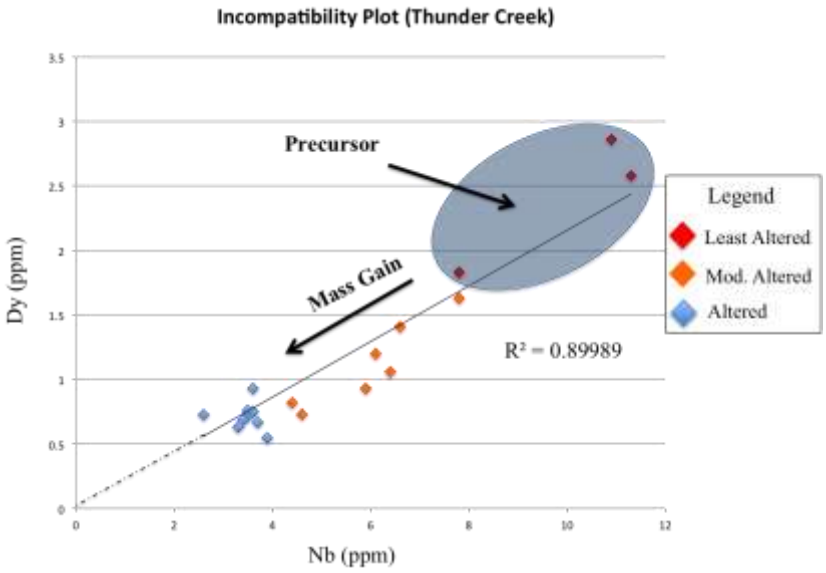

Figure 7.5: Incompatibility plot monitoring the alteration moving from the unaltered Thunder Creek stock towards the Thunder Creek mine.

Major oxide phases K_2O, Na_2O and CaO were used to monitor potassic, carbonate and albite alteration at both Thunder Creek and Hwy-144. Because the degree of alteration was difficult to quantify in hand sample, geochemistry was used to monitor the style and intensity of alteration. To compare the two areas, the oxides mentioned above were monitored moving across the syenite pluton. Figure 7.6, demonstrates that Thunder Creek is geochemically homogenous and only weakly altered. K_2O values do not vary between the periphery and central portions of the intrusion (Figure 7.6). Carbonate alteration is noted at the contact with the Rusk Shear zone but is not present elsewhere in the intrusion. Moving to Hwy-144, DDH Hwy 11-13 displays significant variability throughout the intrusion. K_2O values vary between 3.0-9.5wt%, CaO varies between 1.8-4.5wt% and is generally three times higher than Thunder Creek.

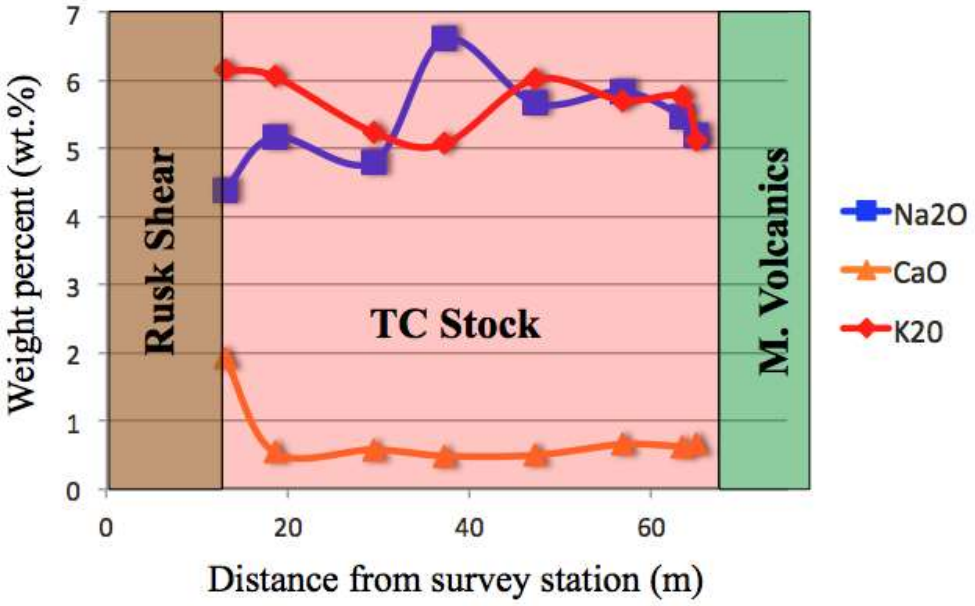

Figure 7.6: Major oxide geochemistry across the Thunder Creek syenite at the 695m level.

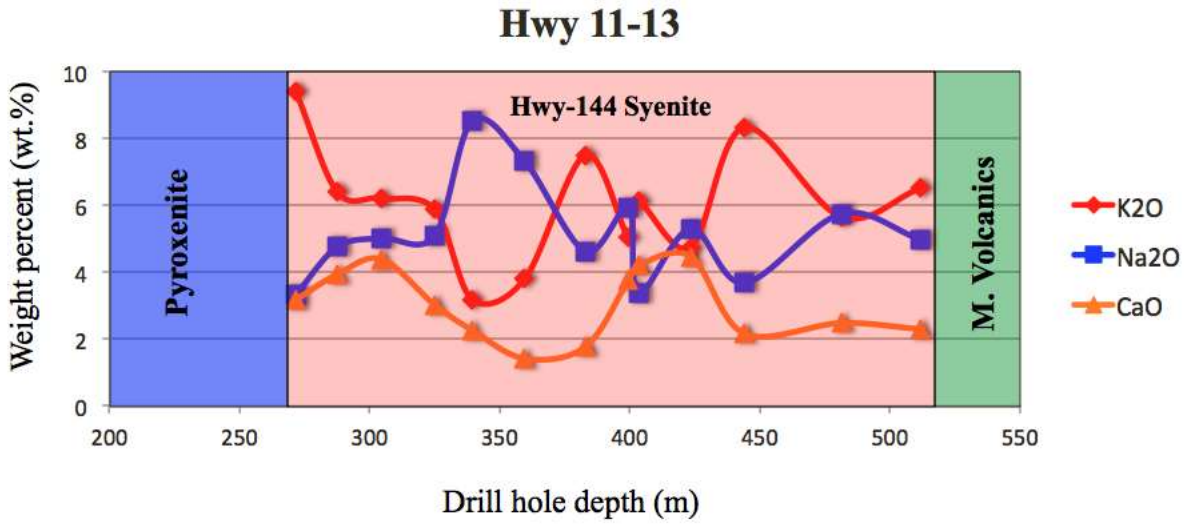

Figure 7.7: Major oxide geochemistry across the DDH Hwy 11-13 syenite.

7.4 Mass Balance

Mass balance calculations have been used to quantify the enrichment and depletion of major and trace elements during alteration (Grant, 1986; Gresens, 1967; Kerrich & Fyfe, 1981; López-Moro, 2012; Maclean & Barrett, 1993). To perform these calculations a 'least altered' and 'altered' sample were determined. Samples were picked visually from drill core and then verified through petrographic microscopy. The density of each sample was calculated to help compare normative major and trace element geochemistry. Rock density calculations were done on the reject powders from whole rock geochemistry. The calculations were performed at the University of Western Ontario, in the Chemical Engineering lab. A Mettler Toledo AB265-S/FACT analytical balance was used to calculate the weight, accurate to four significant digits. The samples were then placed into the Micromeritics Accupyc II 1340 gas pycnometer. The machine is calibrated against a known standard, which then measures the volume of the sample accurate to three significant digits. The sample is measured three times, providing an average volume and standard deviation between samples.

Two samples were taken from four locations: Thunder Creek Stock, Thunder Creek Mine 280m, Thunder Creek Mine 695m, and Hwy-144. Mass balance calculations were done using the Gresens, 1967 method. Volume factors were calculated for the following incompatible elements: Al, Ti, Cs, REE's, Th, Hf, Nb, Nd, Yb and Zr. Suitable volume factors were chosen on incompatible element clusters using reasonable volume changes (i.e. 0.7> & <1.3). In our sample suite Al and Zr were the most reasonable incompatible elements used based on the volume factors calculated from the Gresens method. Samples from the Thunder Creek stock and Thunder Creek mine were

initially compared (Figure 7.8) because they are proximal and likely cogenetic. It is difficult to make the same assumption between Hwy-144 and the Thunder Creek stock, which are separated by ~1km. Instead a representative least altered Hwy-144 sample was compared to an altered Hwy-144 sample. Then the alteration at Thunder Creek is compared to the alteration at Hwy-144 (Figure 7.9). The Thunder Creek samples display similar mass balance trends that only vary in the intensity of enrichment or depletion. The majority of elements plotted for mass balance increase or decrease proportionally to the amount of alteration indicated by previous petrographic work. At Thunder Creek the resulting alteration associated with mineralization is characterized by silicification with a systematic decrease in major oxides like Al_2O_3, Na_2O, K_2O, FeO, MgO, CaO (except TC 280m), and P. However this alteration sequence is associated with an increase in S and Au. Base metals like Cu and Bi are associated with gold mineralization. Other notable gold indicators like As, Zn and the base metals Co, Ni are depleted during the gold-bearing alteration phase. The Hwy-144 mass balance calculations were compared to Thunder Creek to evaluate if the alteration processes were the same or different. Both the alteration recorded at Hwy-144 and Thunder Creek result in gold mineralization, so this comparison provides an opportunity to compare mineralization styles. There are clear differences between the alteration styles at the two locations. At Thunder Creek silicification occurred, whereas at Hwy-144 there is silca loss along with carbonate and potassic alteration (Figure 7.9. In both areas sulfur is added to the system. Thunder Creek gold mineralization is associated with S, Bi, and Cu. By contrast at Hwy-144, the gold mineralization is associated with an increase in As, Ni, Pb, and Zn. The large increase in Pb and minor increases in other base metals may be a result of element mobility during alteration. The source of these elements could be the altered slices of mafic volcanic within the syenite.

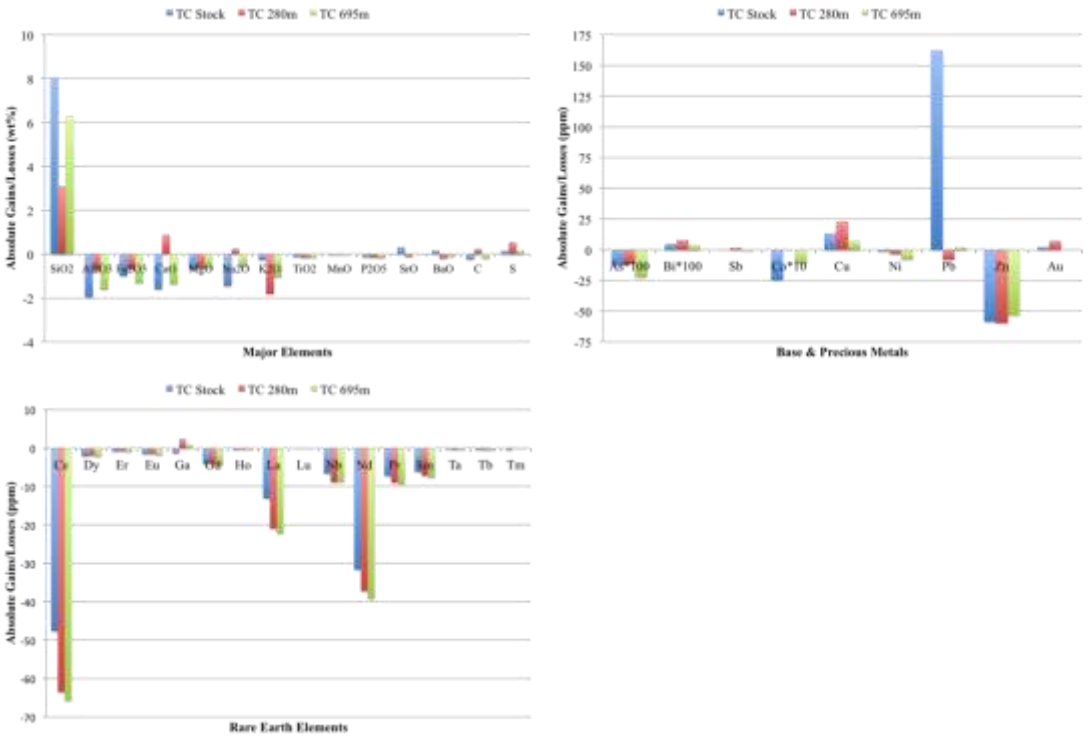

Figure 7.8: Mass balance calculations comparing alteration at the TC stock, TC 280m level and TC695m level.

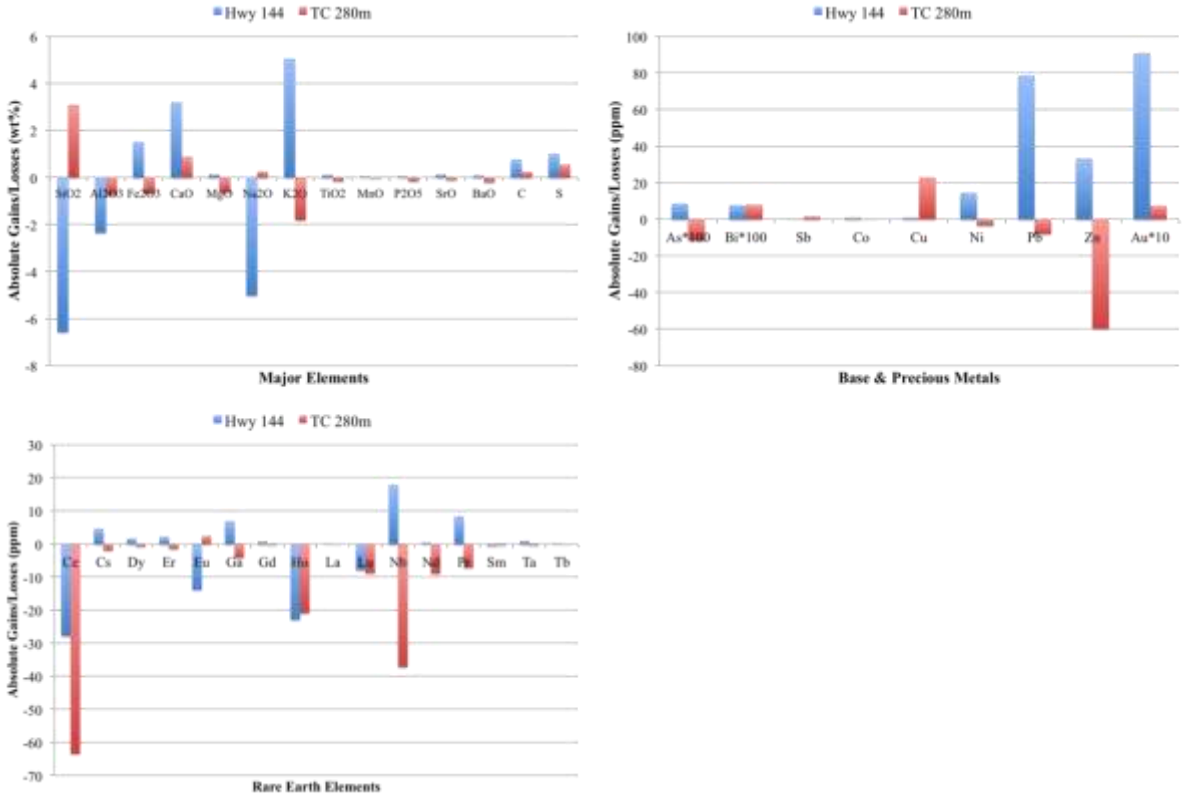

Figure 7.9: Mass balance calculations comparing alteration at Hwy-144 to Thunder Creek.

The results of the mass balance calculations are consistent with obsevations in both drill core and thin section. In the Alteration chapter it was noted that carbonate, hematite and potassic alteration are present in the Hwy-144 syenite. Looking at the major element changes we see an increase in FeO, CaO and K_2O which are the main elements responsible for these alteration phases. At Thunder Creek it was noted that visible carbonate, hematite and potassic alteration were absent in most locations. The mass balance calculations show that FeO and CaO change little, but there is a significant loss of K_2O. The loss of potassium likely occurred during silica replacement.

7.5 Mineral Chemistry

The compositions of pyrite and feldspar grains were determined for both Thunder Creek and Hwy-144 using Westerns electron microprobe. Pyrite grains were analyzed for Fe to compliment the laser ablation calculations by acting as an internal standard. Both potassium feldspar and plagioclase grains were analyzed to determine what composition of each phase was present, and to better understand the temperature of feldspar crystallization. All samples from both localities are end member K-feldspar and albite. Table 3 below provides examples of both feldspars from each site. Feldspars were analyzed from the unaltered Thunder Creek stock and the Thunder Creek mine, there is no significant chemical difference between the two.

Table 7.3: Representative electron microprobe analyses of albite grains from both Thunder Creek and Hwy-144.

	TC Stock Least altered	TC 280m Altered	Hwy-144 Least altered	Hwy-144 Mineralized
SiO_2	68.30	68.06	68.71	67.98
Na_2O	9.74	9.56	9.21	10.13
Al_2O_3	21.16	20.21	21.33	20.81
FeO	0.01	0.34	0.05	0.47
MnO	0.01	0.03	0	0
K_2O	0.07	0.09	0.08	0.08
BaO	0	0.02	0	0

CaO	0.09	0.01	0.05	0.03
TiO_2	0.01	0	0	0
Total	99.37	98.34	99.41	99.47

Table 7.4: Representative electron microprobe analyses of K-feldspar grains from Thunder Creek and Hwy-144.

	TC Stock Unaltered	TC 280m Altered	Hwy-144 Least Altered	Hwy-144 Mineralized
SiO_2	63.93	63.83	64.03	63.53
Na_2O	0.18	0.14	0.16	0.29
Al_2O_3	19.56	19.40	19.41	19.05
FeO	0.05	0.01	0	1.69
MnO	0	0	0.01	0.03
K_2O	16.31	16.08	15.43	15.33
BaO	0.25	0.58	0.82	0.15
CaO	0.02	0.01	0.01	0
TiO_2	0	00	0.01	0
Total	100.31	100.04	99.89	100.07

7.6 Whole Rock Geochemistry Discussion

Whole rock geochemistry of both properties reveals clear differences in alteration. Using Miyashiro's (1978) alkalinity plot it is apparent that both syenites are alkaline, however they both plot in separate domains. Major element analyses of the Thunder Creek syenite are homogeneous, while the concentrations of Ca, Na, K and Si change substantially at Hwy-144. This variability is also visually apparent in drill core. The chemical changes represent carbonate, hematite and potassic alteration noted in drill core. While it is clear that the two syenite intrusions underwent different degrees of alteration, REE profiles suggest that the two intrusions were likely fed from a similar source. Hwy-144 is elevated in REE compared to the least altered Thunder Creek

stock. This suggests that the Hwy-144 syenite is either more fractionated or has undergone mass loss. The mineralized Thunder Creek syenite is depleted in REE compared to the least altered Thunder Creek stock. This suggests the unit has under gone mass gain. It is unlikely that it is a more primitive based on field relationships (albite alteration, disseminated pyrite). Finally mineral chemistry of the feldspars reveals two things. The albite and K-feldspar grains at the Thunder Creek Stock, Thunder Creek Mine and Hwy-144 property are all very similar. Secondly, all mineral analyses on plagioclase grains were albite indicating that every intrusion underwent low temperature re-equilibration.

7.7 Pyrite Mapping

At both the Thunder Creek and Hwy-144 pyrite and gold mineralization have a close spatial relationship with one and other. Detailed petrographic work on mineralized samples indicates that the vast majority of gold mineralization is present as inclusions or along fractures within vein-hosted pyrite grains. However, there is still an anomalous component of gold present in disseminated pyrite. Based primarily on the location, but also considering shape and inclusions, 3 stages of pyrite have been determined. Trace element electron microprobe mapping was completed to determine if mineralized pyrite have a unique signature. Previous studies by (Large 2009, Martin 2012) show a correlation between gold and trace element geochemical zoning in pyrite. These studies were conducted on Carlin and lode gold deposits. The results provide insight into the mechanism of gold transport and precipitation.

Thunder Creek and Hwy-144 both demonstrate similar stages of pyrite growth. Both contain fine to medium-grained disseminated pyrite and medium to coarse-grained vein-hosted pyrite. However, Hwy-144 contains a third stage of fine to medium grained fracture filling pyrite. Texturally the pyrite at Thunder Creek and Hwy-144 are different as well. At Thunder Creek, medium-grained disseminated pyrite is anhedral and corroded with abundant silicate inclusions. Vein-hosted pyrite at Thunder Creek contains less abundant silicate inclusions but is still generally anhedral. At Hwy-144, disseminated, vein-hosted and fracture filling pyrite is subhedral to euhedral and contains minor sulfide inclusions, with less abundant silicate inclusions. From whole rock gold analyses of background syenite and V_1, V_2 and V_3 veins anomalous gold values suggests that both vein-hosted and disseminated pyrite are mineralized. Pyrite grains were selected for WDS/EDS mapping based on reconnaissance petrographic analyses. The sampling strategy targets both mineralized and non-mineralized pyrite grains.

7.7.1 TC 695m Disseminated

The disseminated pyrite at the TC deposit is fine to medium grained and commonly corroded. Pyrite mineralization on average occupies 0.5-2% modal rock volume and increases in the vicinity of abundant veining. Based on petrographic analyses pyrite grains have inclusion-rich cores containing: K-feldspar, carbonate, magnetite, quartz, albite and rutile. Trace element geochemical mapping indicates that strong elemental zoning is not associated with this variety of pyrite (Figure 7.10). Figure 7.10 displays a weak Ni-rich zone on the pyrite grain margin and a Ni-poor core. During microprobe mapping no gold grains were located.

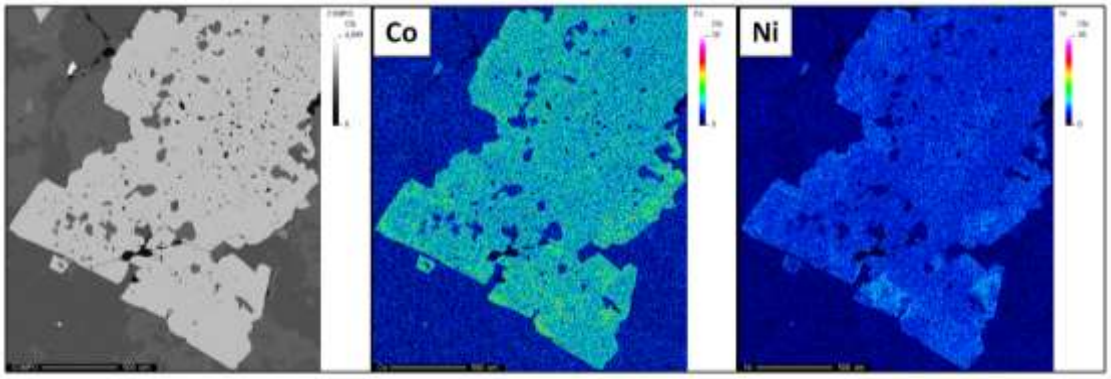

Figure 7.10: Disseminated pyrite trace element maps from TC 695m. Note that the rims are slightly enriched in Co and Ni. Both Ni and Co are anomalous compared to the background matrix.

7.7.2 TC 280m Disseminated

In the upper portion of the TC deposit the syenite is present as protruding fingers that coalesce at depth with the larger syenite pluton. Disseminated pyrite in this area is fine to medium grain generally occupying approximately 0.5% modal rock volume. Pyrite grains are generally sub to euhedral with abundant inclusions throughout the grain. Inclusions are primarily rutile, albite and orthoclase with minor muscovite. Rarely grains are inclusion free. The pyrites are not strongly zoned, however some samples display Co & Ni enrichment along the grain margin (Figure 7.11) and isolated zones of enrichment (Figure 7.12). Microprobe analyses did not detect any gold inclusions.

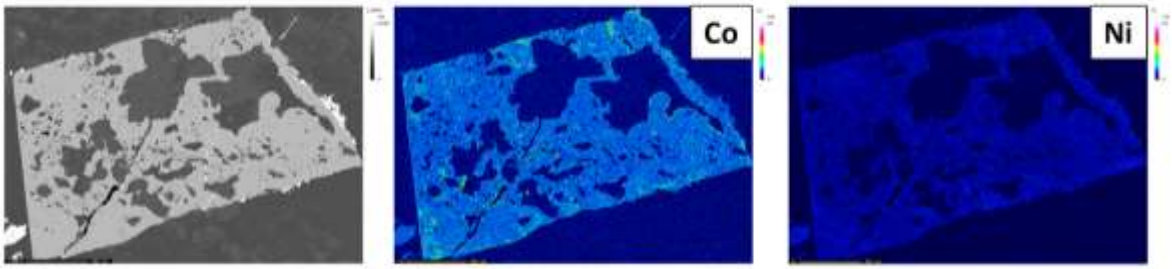

Figure 7.11: Backscatter, Co, and Ni trace element geochemical maps. Corroded pyrite grain with abundant inclusions lacking any distinct chemical zonation.

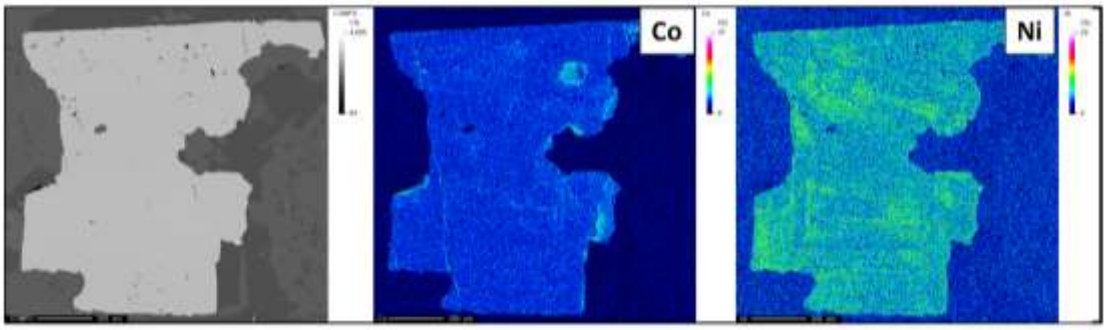

Figure 7.12: Inclusion free disseminated pyrite grain with Co & Ni enrichment along the margin. Ni & Co maps show discrete zones of enrichment within the grain.

7.7.3 TC 695m & 660m Vein-Hosted

Strategic sampling described earlier revealed that vein-hosted pyrite at the 695m level of Thunder Creek is very prospective for gold mineralization. During petrographic analyses gold grains were routinely located. Gold is primarily present as inclusions, or along fractures in pyrite. In addition, a significant amount of free gold in quartz veins was noted as well. Four pyrite samples from V_2 veins were trace element mapped. None of the samples displayed obvious Co or Ni zones (Figure 7.13). However, the only Te anomalies noted were present in these samples (Figure 7.14).

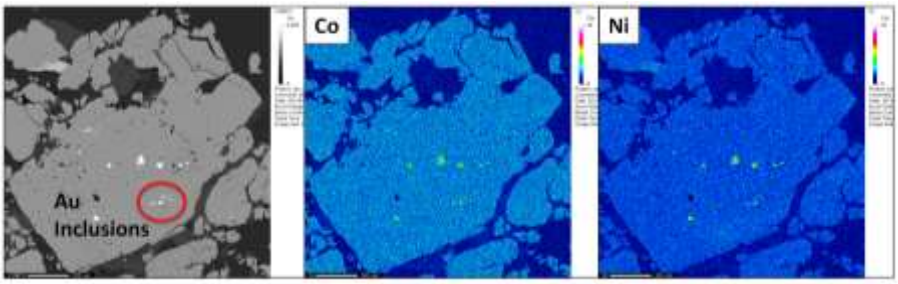

Figure 7.13: Electron microprobe images of TC 660m level vein-hosted pyrite. Note the pyrite is mineralized but does not show zoning.

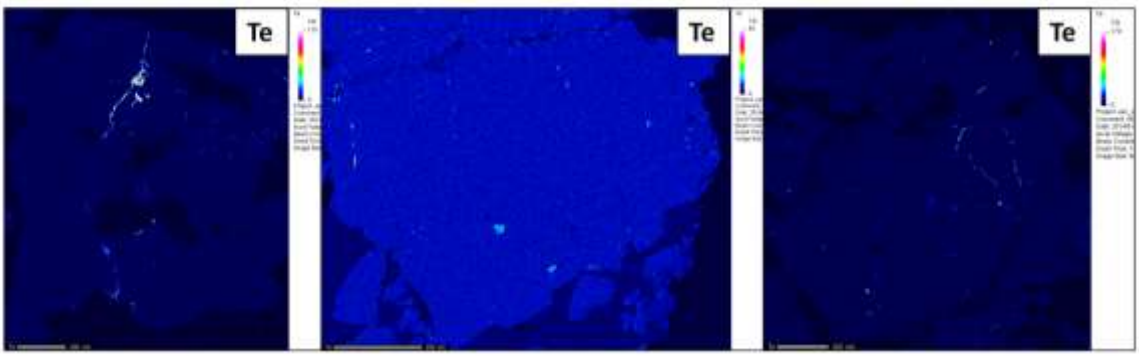

Figure 7.14: Electron microprobe images of three separate pyrite grains from the TC 660m level. The Thunder Creek deposit contains the only examples of anomalous tellurium.

7.7.4 TC 280m Vein-Hosted

Two samples from the 280m level were analyzed: sample M191372 represents coarse irregular pyrite associated with a quartz veinlet, while sample M191378 contains medium to coarse grained pyrite associated with a V_2 quartz vein. Both samples contain inclusions of orthoclase, albite, carbonate and quartz. Neither sample displays strong zoning, however the V_2 vein-hosted sample appears to have slight Co enrichment present along the grain margin (Figure 7.15).

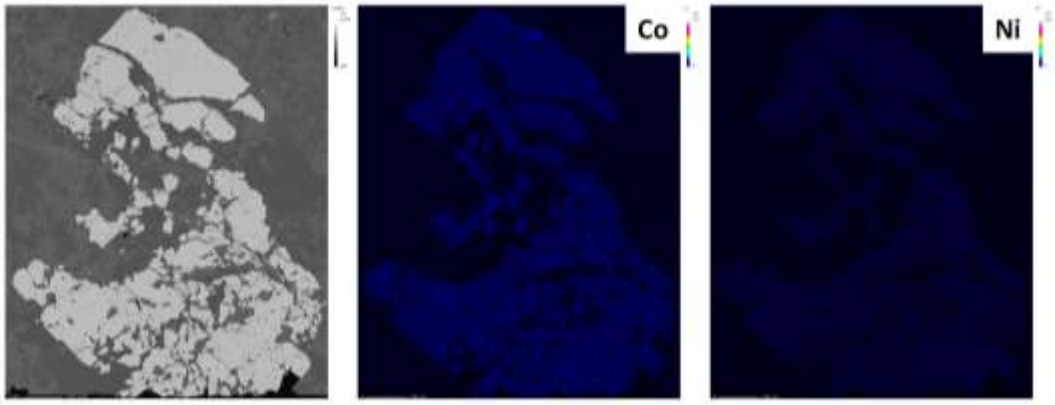

Figure 7.15: Backscatter, Co and Ni trace element geochemical maps of V_1 quartz vein pyrite at the 280m level of the Thunder Creek deposit. Note the Co and Ni values are only slightly above background.

7.7.5 Hwy-144 Disseminated

Disseminated pyrite is patchy within the syenite at Hwy-144. Pyrite is generally fine to medium grained, often euhderal, but also irregular with inclusions. WDS pyrite

mapping was performed on five grains believed to be representative of the larger pyrite population. Out of the four samples analyzed two are strongly zoned with elevated levels of gold inclusions (Figure 7.16). However, whole rock gold analyses in "zoned" samples were just above the 0.005ppm detection limit.

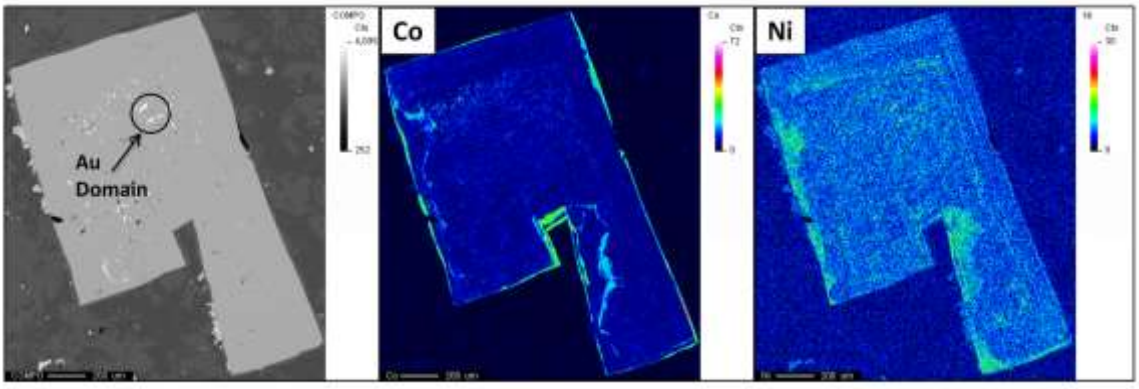

Figure 7.16: Electron backscatter, Co and Ni trace element maps/images of disseminated pyrite. The area of increased Au content is outlined in the backscatter image and corresponds to a Co & Ni zone of depletion.

7.7.6 Hwy-144 Fracture Controlled

Fracture controlled pyrite is a minor occurrence at the Hwy-144, but is easily identifiable in drill core. Pyrite forms discrete lineation's controlled by the fracture surface. Pyrite grains are generally medium grained, sometimes corroded, sometimes inclusion free. Trace element maps indicate that mineralized pyrite samples have irregular Co-rich "fracture" like patterns. These patterns do not correspond with any visual feature in BSE imaging.

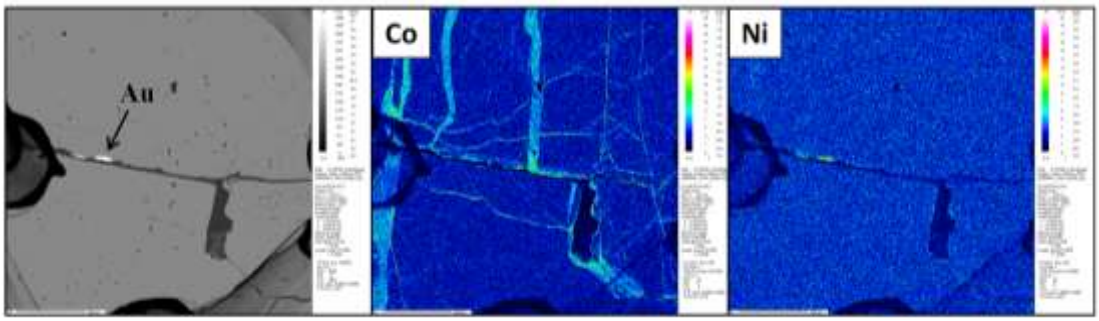

Figure 7.17: Electron backscatter, Co and Ni trace element geochemical maps. The location of gold is outlined in the backscatter image and correlates with a Co-rich fracture.

7.7.7 Hwy-144 Vein-Hosted

Drill core logging at Hwy-144 has determined vein-hosted pyrite to be the most prospective for gold mineralization. Consequently vein-hosted pyrite samples exhibit

the most numerous examples of gold inclusions located during petrographic reconnaissance. Six pyrite grains were mapped for trace elements; four of these grain contained elevated levels of gold. Each sample containing elevated gold is either zoned with respect to Ni & Co, or has Ni/Co enrichment along fractures (Figure 7.18 & 7.19). Gold mineralization as a whole appears to preferentially be hosted in Co-poor cores of pyrite grains, but as seen in Figure 7.18 this is not always the case.

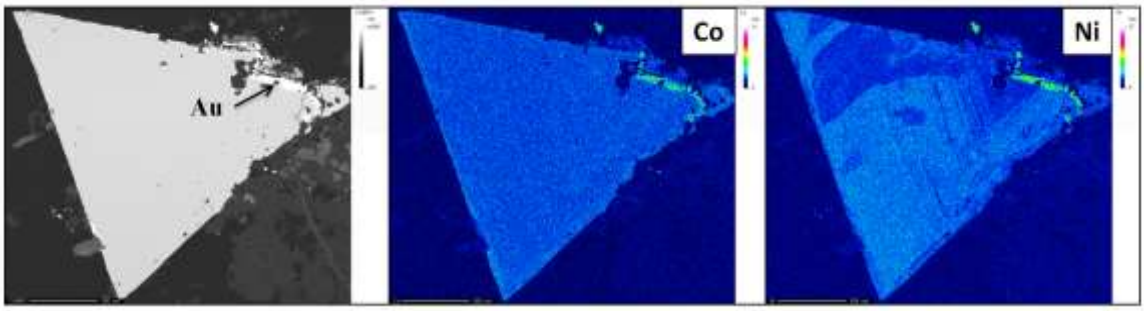

Figure 7.18: Electron backscatter, Co & Ni trace element maps. Euhedral gold bearing pyrite is situated within complex Ni zoning. The gold transects Ni-rich and Ni-poor domains.

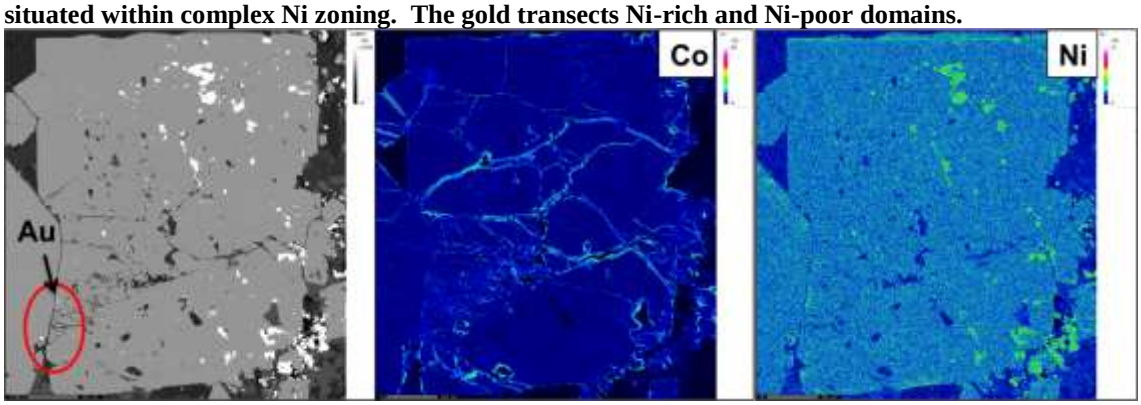

Figure 7.19: Electron backscatter, Co & Ni trace element maps. Highly reflective minerals in backscatter are Ti-bearing phases. The sample contains a small zone of gold enrichment. Co is enrichment along grain margin and along fractures. Gold corresponds to a Co low in the pyrite grain.

7.8 Pyrite Geochemistry

Laser ablation provides two key attributes that compliment the WDS trace element maps. First, the detection limits of laser ablation are significantly lower (~0.5 ppm for Au) compared to EMPA (~200ppm), and laser ablation provides continuous data across a pyrite grain transect, not just spot analyses. In effect laser ablation provides continuous element concentration across the mineral grain. Comparing the gold grade within pyrite to a large suite of elements can help us better understand the composition of the fluid that carried the gold. Laser ablation targeted the following trace and major elements in pyrite: Al, Si, Ca, Ti, Fe, Co, Ni, Cu, Zn, As, Se, Mo, Te, Ag, Cd, Sn, Sb,

Te, W, Re, Au, Pb, and Bi. Laser ablation transects were designed perpendicular to any visible zoning determined from EMP maps. The methodology and instrument specifications are given in the Methods chapter.

7.8.1 Thunder Creek Pyrite

The trace element compositions of both disseminated and vein-hosted pyrite samples were determined to evaluate whether these are genetically or temporally similar or different. Pyrite grains were analyzed from the 280m, 660m and 695m level to see if there was a difference between the top and bottom of the mine. Disseminated pyrite from the 280m and 695m level are visually very similar. Both levels contain inclusion-rich corroded pyrite. Petrographic work indicates that these inclusions are primarily feldspar and quartz with minor carbonate and rutile. When analyzing the laser ablation transect it becomes apparent that gold is preferentially located near inclusion-rich zones (Figure 7.20). The chemical dissolution texture within the pyrite coupled with common alteration minerals as inclusions suggests a late gold-rich fluid phase altered early disseminated pyrite. Gold values between 20 and 80ppm are well above the limit for gold held within the pyrite structure without significant arsenic (Cook & Chryssoulis, 1990) and consequently are determined to be invisible (nano) inclusions. However, there is a significant amount of background gold in disseminated pyrite in the range of 0.5-10 ppm Au. Using the combined Au/As concentrations for these zones and the Au saturation limit determined by Reich et al., 2005 it appears there is a significant amount of gold within the pyrite structure from the 280m and 695m levels. While pyrite grains at Thunder Creek contain what appears to be a significant amount of solid solution gold, the low arsenic concentrations indicate these are not arsenian pyrites.

The gold content of disseminated pyrite does not change significantly between the bottom and top of the intrusion. Both levels of the intrusion contain on the order of 0.5 to 10 ppm gold in the background pyrite, both as inclusions and probably part of the pyrite structure. At the 280m level two grains were analyzed. The first grain had an average background gold content of 1.04 ppm while the second was 0.37 ppm. Another two grains were traversed at the 695m level. One grain had an average gold content of 3.05 ppm while the other grain contained 0.20 ppm with multiple analyses falling below the 0.29 ppm detection limit. From our results we see that the majority of disseminated pyrite grain are strongly mineralized where the pyrite grain has been corroded. A larger sample size is needed to truly test this hypothesis and determine the actual variance within the deposit.

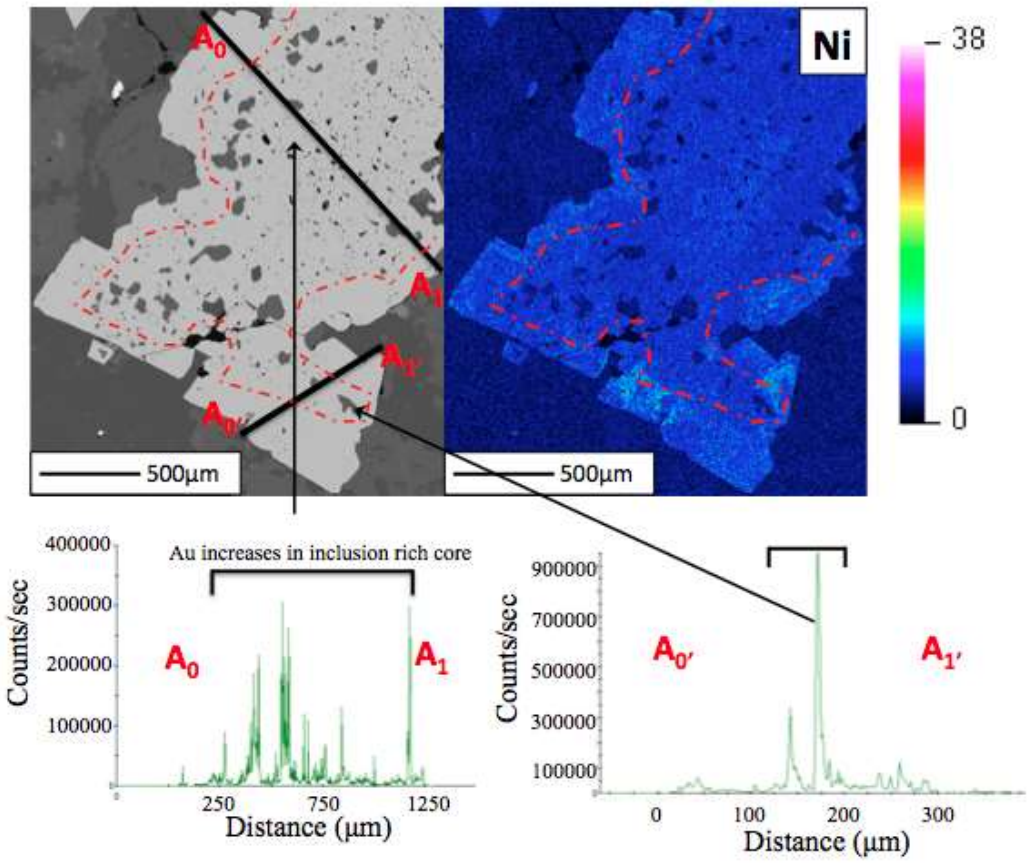

Figure 7.20: Thunder Creek 695m level disseminated pyrite. Note that in this case the gold-rich, inclusion-rich core corresponds to a Ni-poor zone. The green spectra represents counts/sec of Au.

V_1 and V_2 vein-hosted pyrite is the most prospective for gold mineralization and contains more gold inclusions compared to disseminated pyrite. However, vein-hosted pyrite has a more massive texture and does not display the same amount of inclusions seen in disseminated pyrite. At the 280m level two V_2 vein-hosted pyrite grains were analyzed. One grain was fine-grained (200-400µm), while the other was coarse (3-5mm). The fine-grained sample has fewer silicate inclusions. In the fine-grained sample gold is concentrated in the core of the pyrite grain, while the coarse-grained pyrite hosts gold nears the margin (Figure 7.21 & 7.22). Two laser ablation transects were completed on the coarse grained sample. The top transect intersects are relatively homogeneous portion of pyrite; the bottom traverses through an area of more intense fractures/increase in inclusions. Comparing the two spectra in Figure 7.23, it is evident that both contain elevated Au peaks, but the bottom transect contains a more consistent elevated gold spectra.

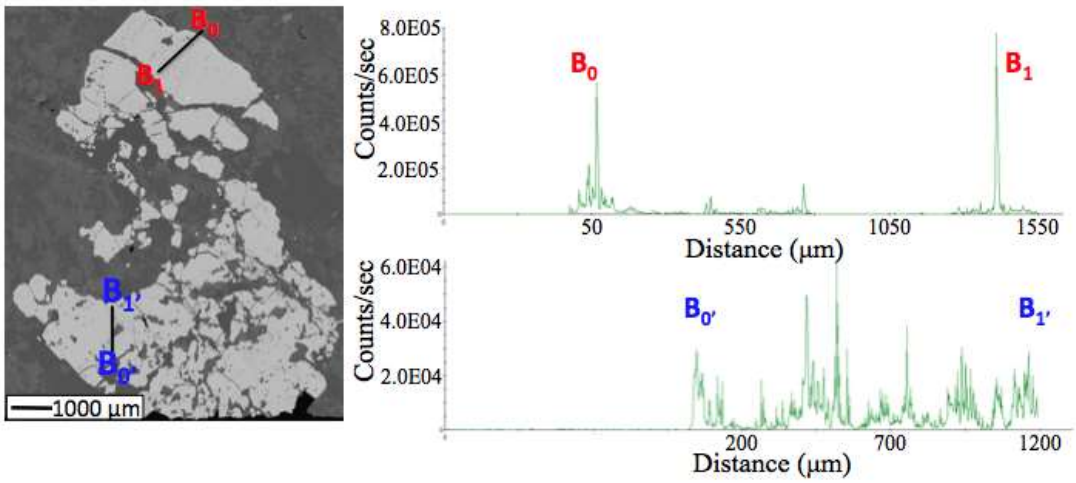

Figure 7.21: Pyrite and laser ablation spectra for coarse-grained vein-hosted pyrite from the 280m level. Gold is focused along grain margin. Au is represented by the green spectra.

At the 660m level two V_2 vein-hosted pyrite samples were analyzed. The first sample contains visible gold in thin section. Laser ablation transects avoided visible gold grains (Figure 7.22), but still intercepted significant nanoparticles of gold. Similar to the upper level, vein-hosted pyrite grains does not contain the abundant silicate inclusions as seen in disseminated samples. In Figure 7.22, the pyrite grain contains significant gold across the transect; almost consistently above 1.2ppm. The distribution of gold seems to favor the margin with the highest number of counts occurring there. This sample also does not contain many inclusions and appears uniform throughout the grain. The pyrite grain in Figure 7.24 contains inclusions, however gold distribution does not correlate accordingly. The sample does not contain any visible gold grains. In comparison to the mineralized sample (Figure 7.22), Figure 7.23 contains a much lower gold content even though it is vein-hosted pyrite from the 660m level. Gold grade is not homogenous throughout vein-hosted pyrite in the lower levels of the mine.

7.8.2 Hwy-144 Pyrite

Three styles of pyrite were analyzed via laser ablation; disseminated, fracture controlled and vein-hosted. Within these styles both mineralized and unmineralized samples were tested. Hwy-144 pyrite grains are visually different than Thunder Creek. Thunder Creek pyrite is visually corroded and inclusion-rich. These inclusions are dominantly K-feldspar, quartz, albite and carbonate. Hwy-144 contains inclusions, however they are more commonly rutile and sulfides with minor quartz, K-felspar and carbonate. Pyrite grains at Hwy-144 are more commonly sub-to euhedral, and fine to medium grained.

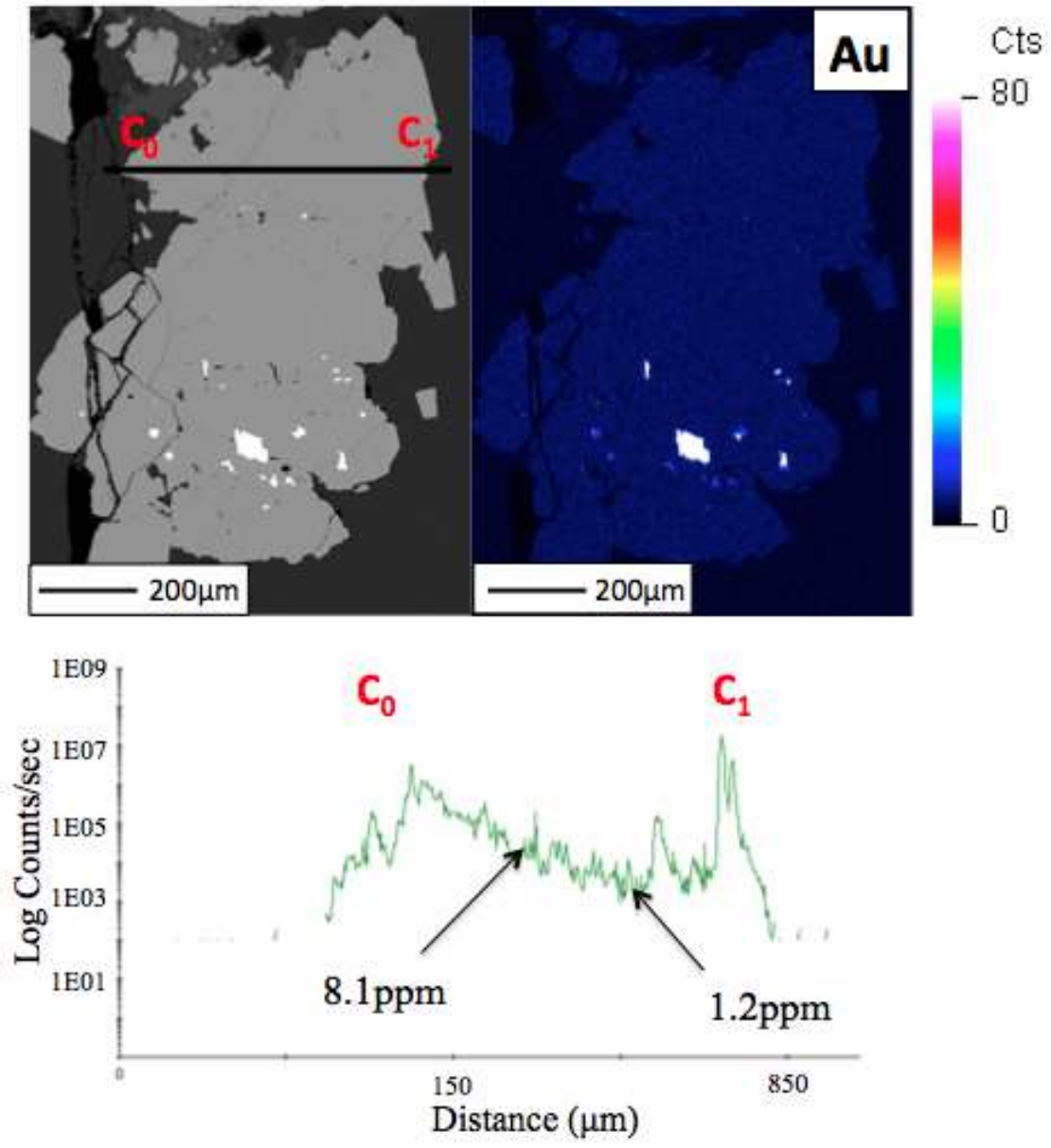

Figure 7.22: Gold bearing vein-hosted pyrite from the 660m level. The pyrite grain contains minimal silicate inclusions with a consistent gold grade above 1.2ppm. Gold concentration is represented by the green spectra.

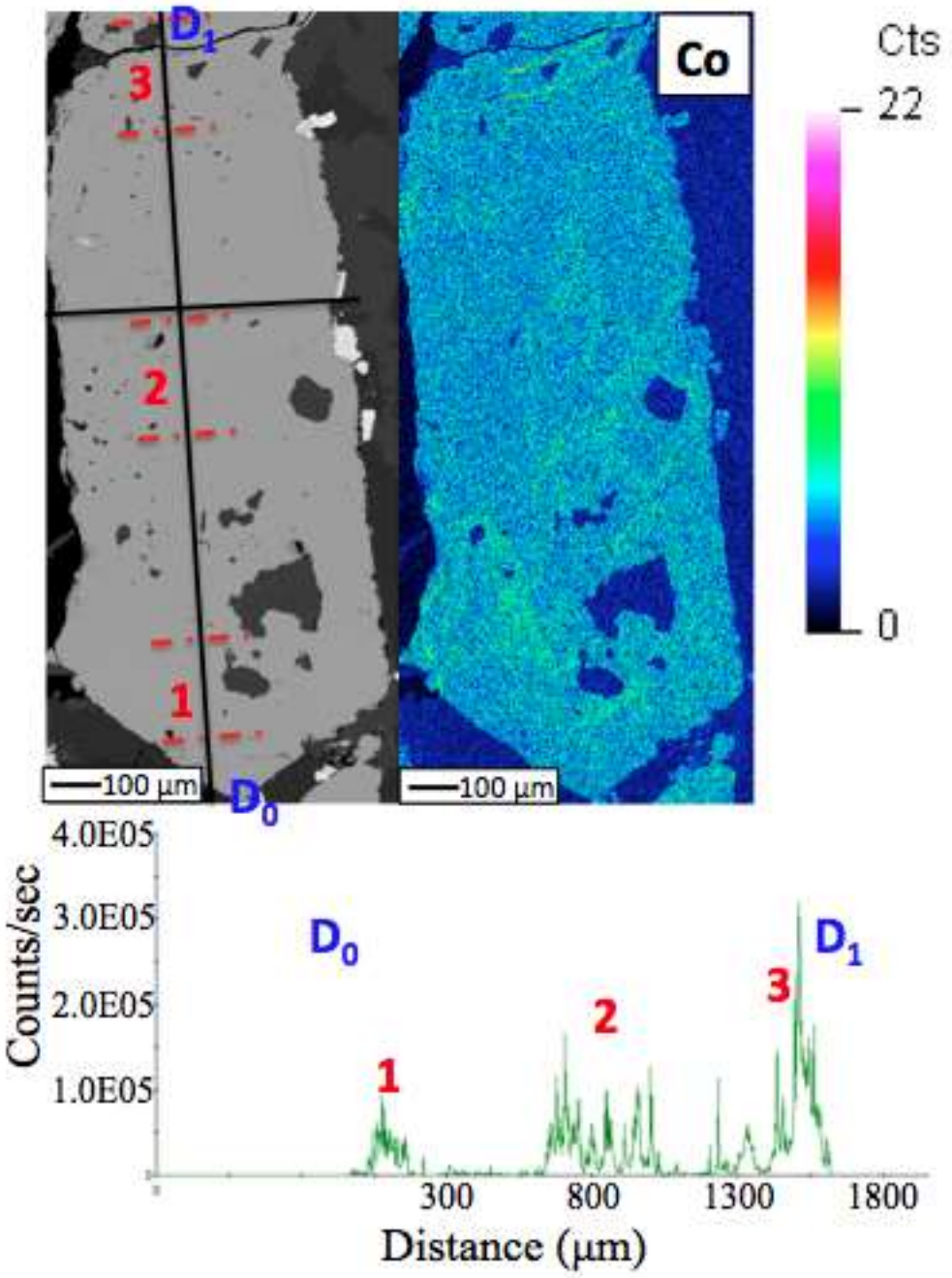

Figure 7.23: Gold free vein-hosted pyrite from the 660m level. Areas of gold enrichment are annotated with the dotted red lines. Gold grades between these domains are quite low and occasionally below the detection imit.

Two disseminated pyrite samples from Hwy-144 were analyzed. Both are euhedral pyrite grains, one medium-grained and the other coarse-grained (0.3-1.0 cm). Neither sample contains visible gold inclusions. Figure 7.24 contains an inclusion-rich core, however the inclusions are primarily galena and chalcopyrite with rutile present as well. The sample is visibly zoned with a Co-rich rim. Elevated gold concentrations are

present exclusively in the core of the E_0-E_1 pyrite grain, with elevated gold domains outlined by dashed red lines. The elevated gold spectra is still markedly lower than Thunder Creek.

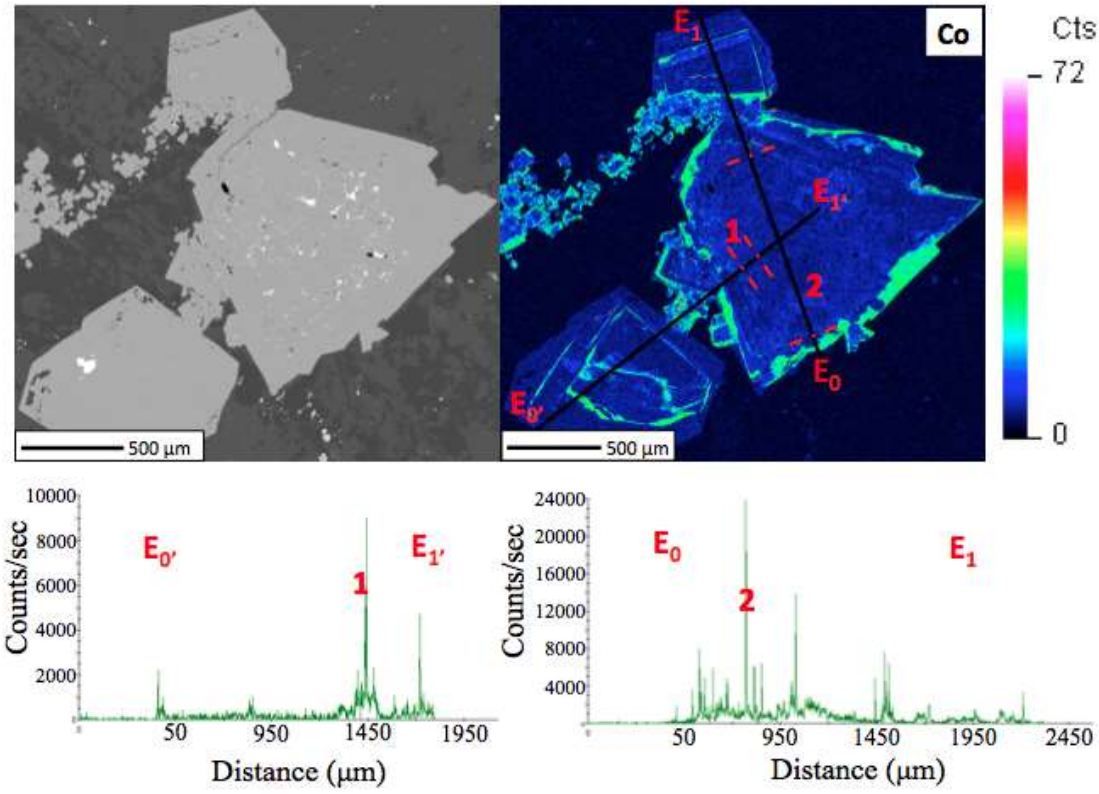

Figure 7.24: Disseminated pyrite grain from Hwy-144. Gold rich domains in between dashed red lines. Background gold content is often below machine detection limit.

Two samples of fracture filling pyrite from Hwy-144 were analyzed via laser ablation and compared to WDS trace element maps and backscatter images. One sample was mineralized with gold occurring along a fracture, the other was not mineralized. Both samples exhibit irregular, semi-linear Co enrichment bands that resemble a "fracture-like" pattern in the grain. These fractures generally do not correlate with any visible feature in BSE images, and visible fractures and are poorly correlated to Co-rich domains. Laser ablation data in the unmineralized pyrite grain indicates that gold is preferentially present along grain margins (Figure 7.25). These grain margins are irregular and corroded similar to gold rich zones in the disseminated Thunder Creek pyrite. In the mineralized sample gold is present along a fracture visible in both the BSE image and laser ablation spectra (Figure 7.26). The background gold content of the pyrite is quite low and very similar to the unmineralized pyrite grain. Gold distribution in the mineralized

sample does not follow any clear pattern. Looking at both the vertical and horizontal laser ablation transects it appears that gold grains are heterogeneously dispersed within pyrite. Gold present along the pyrite fractures indicates a relatively late deposition.

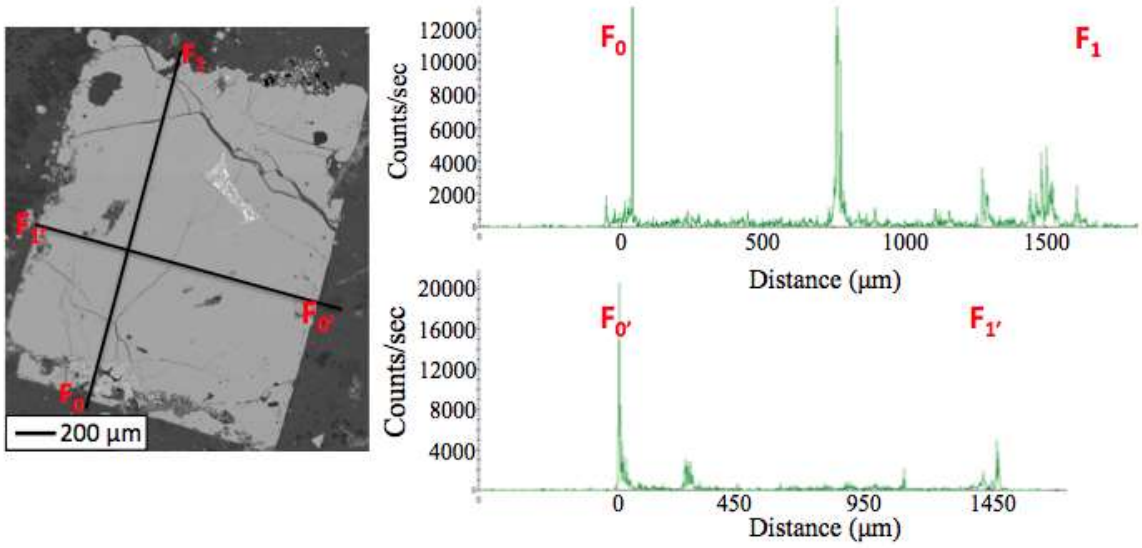

Figure 7.25: Unmineralized fracture filling pyrite from Hwy-144. Gold distribution is preferentially present along anhedral altered grain margins.

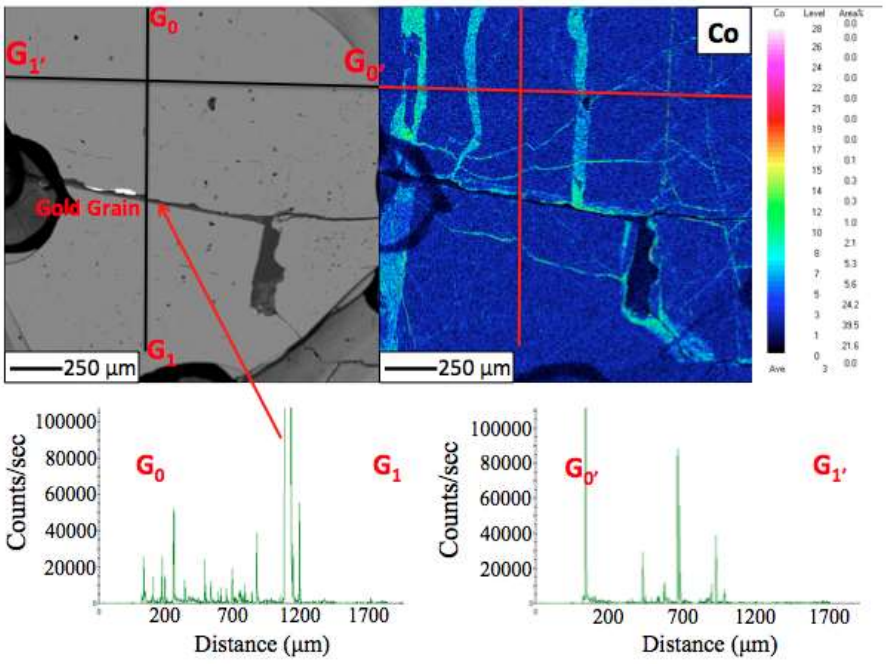

Figure 7.26: Mineralized fracture filling pyrite grain. Gold distribution is heterogeneous and shows no relationship to fractures, inclusions, or Co-rich fractures.

Lastly, two vein-hosted pyrite samples were analyzed to better understand gold distribution within this species of pyrite. Of the two samples analyzed, one is strongly zoned with respect to Ni, while the other displays no obvious trace element enrichment. The distribution of gold in the Ni zoned sample was correlated to the nickel map to determine if there was a preferential zone for gold deposition. Looking at Figure 7.27, gold appears to occur in both Ni-rich and Ni-poor zones. It is not possible to determine the exact gold content over the very thin zonations seen in domain "2". The second pyrite sample (Figure 7.28) is unmineralized and not zoned. The coarse-grained euhedral pyrite has sporadic gold distribution. Domain "1" is located right beside a fracture which is similar to the inclusion-rich and fractured pyrite grains seen at Thunder Creek/Hwy-144. Domains "2" and "3" do not have any visible features associated with elevated gold content. The background gold content of these pyrite grains is quite low compared to the Thunder Creek sample (~0.1ppm).

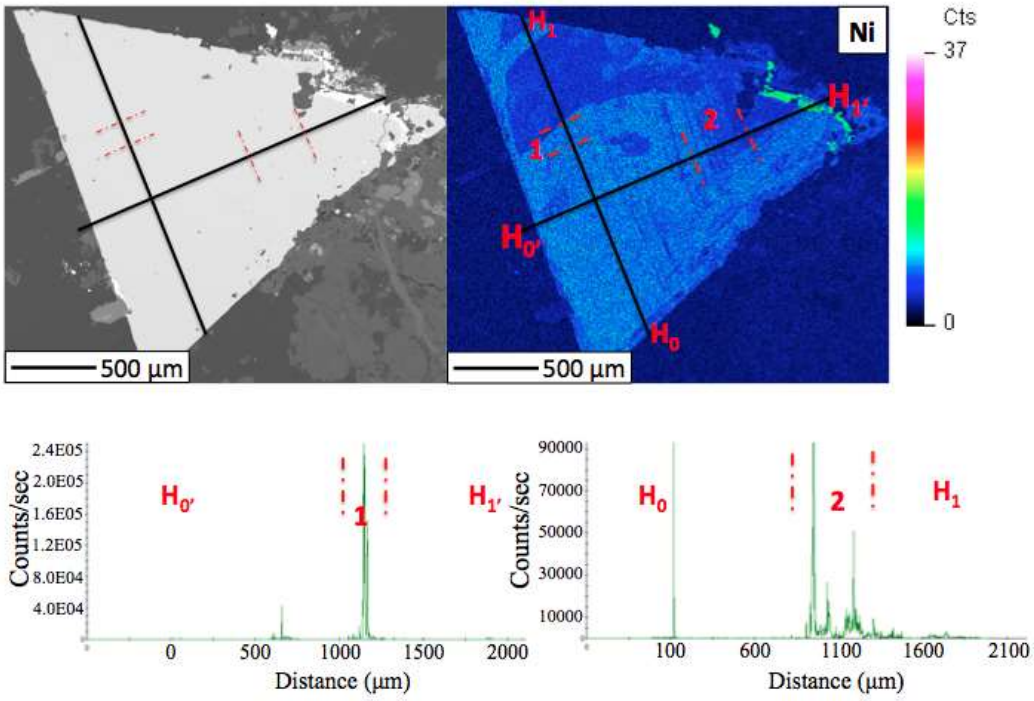

Figure 7.27: Zoned vein-hosted pyrite with gold rich domains highlighted by red dashed lines.

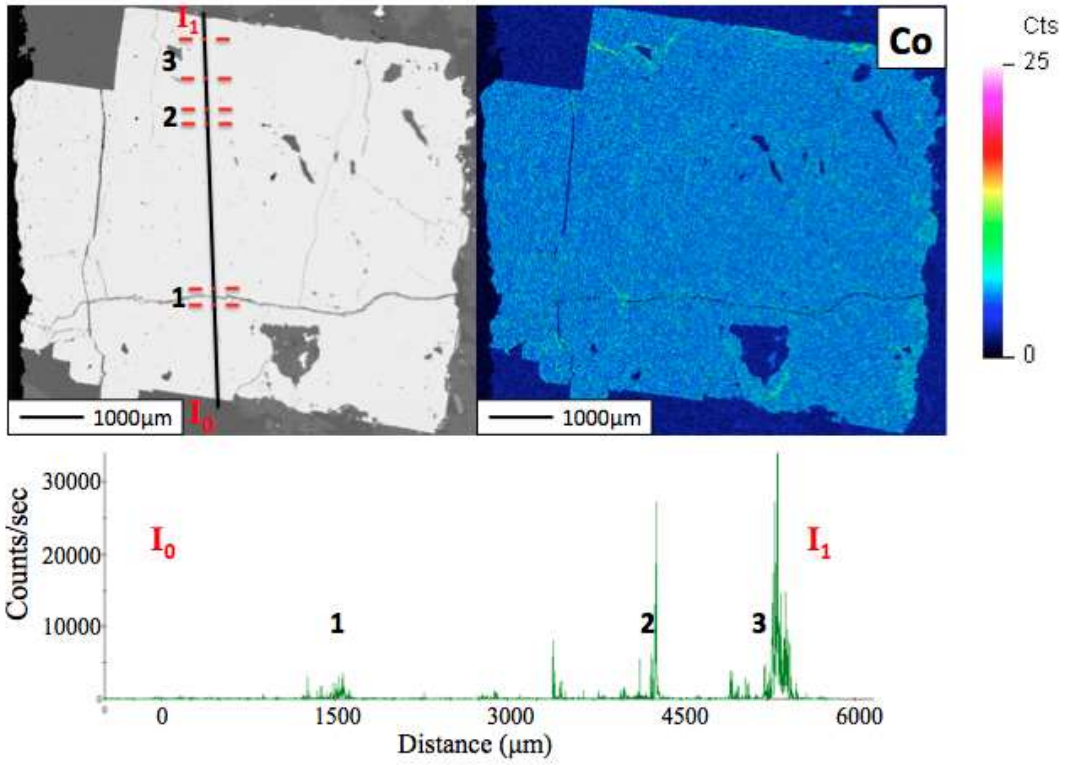

Figure 7.28: Vein-hosted, non-mineralized pyrite from Hwy-144. Mineralized domains outlined with red dashed lines.

7.9 Trace Element Correlations

The following trace elements were collected to see if they correlate with gold: Co, Ni, Cu, Zn, As, Se, Mo, Te, Ag, Cd, Sn, Sb, Te, W, Re, Pb and Bi. The elements Se, Sn, Sb, W and Re were generally present at concentrations near or below the detection limit. Suggesting that they have little or no affect on the gold concentration in pyrite. The rest of the trace elements were compared using the raw laser ablation spectra and actual quantitative data analyzed avoiding gold grains and nanoparticles of gold. Te, and Ag are the only elements that show a consistent tight relationship with gold. Copper shows a moderate relationship to gold at Thunder Creek. Pyrite generations (e.g. disseminated vs. vein-hosted) and location (TC vs. Hwy-144) were compared to try and determine what trace elements were transported with gold.

At Thunder Creek gold is tightly correlated with Te, Ag and shows a weaker relationship with Cu. The Te-Ag correlation is present in both vein-hosted and disseminated pyrite samples (Figure 7.29 & 7.30). Gold in pyrite (280m or 695m) never correlates with arsenic (Figure 7.31). Spikes in arsenic concentrations like occur

where the laser ablation transect has gone over an arsenide grain, the background concentration of As in the pyrite is similar to gold. The low arsenic concentrations of gold in pyrite indicate these pyrites are not "arsenian pyrites". Concentrations of Ag are often higher than Au, while concentrations of Te are lower than Au. The trace element concentration of the pyrites are elevated in the lower portion of the mine (more mineralized) compared to the top.

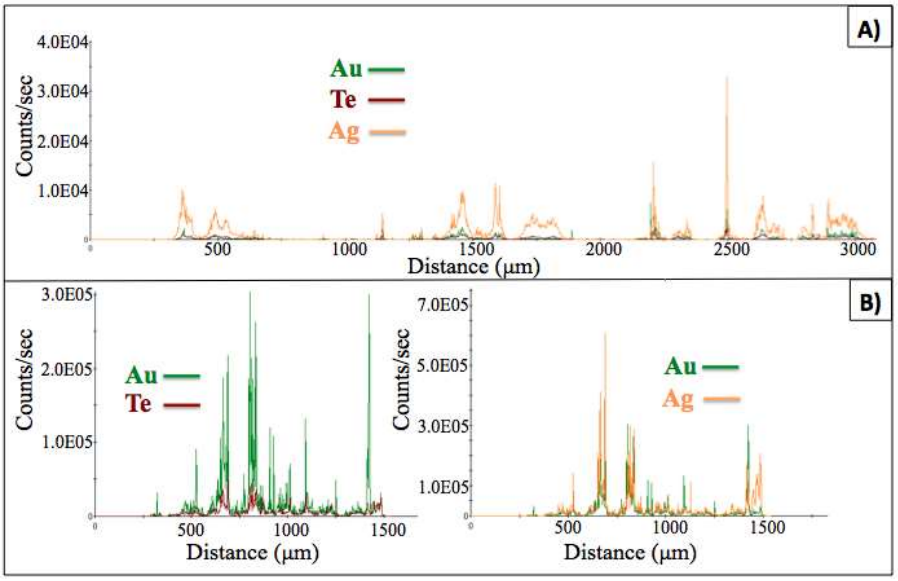

Figure 7.29: Strong gold correlations within Thunder Creek disseminated pyrite. A) is from the 280m level and B) is from the 695m level.

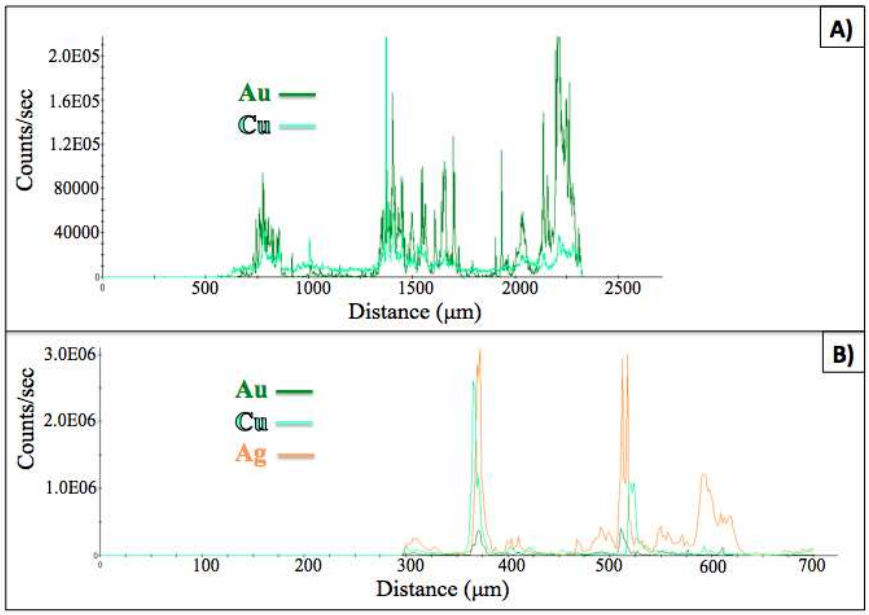

Figure 7.30: Moderate Cu-Au correlations from Thunder Creek pyrite. A) is vein-hosted pyrite from the 660m level, while B) is vein-hosted pyrite from the 280m level.

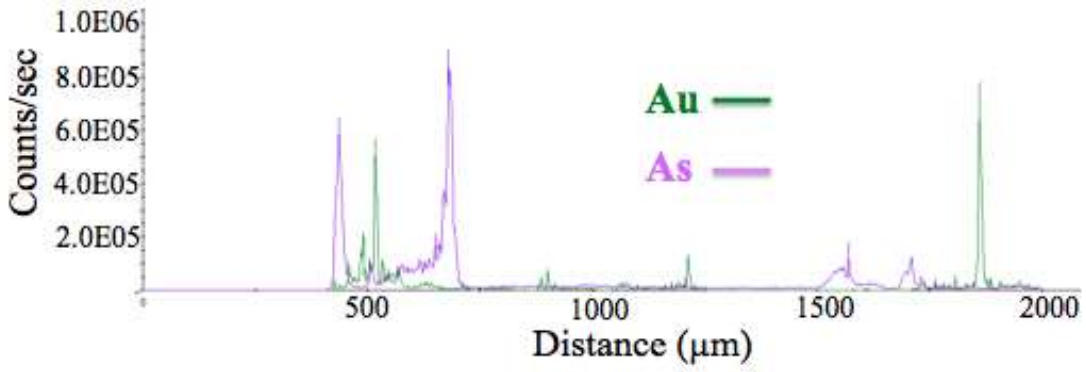

Figure 7.31: The laser ablation transect above displays that there is no correlation between As and Au in this 280m vein hosted pyrite sample.

Hwy-144 has a very different trace element composition compared to Thunder Creek. The strong correlations between Au and Te, Ag and Cu are not as evident at Hwy-144. Hwy-144 also contains zoned pyrite grains that contain 0.5-1.3 wt% Co and Ni. Pyrite grains at Hwy-144 contain a much lower gold content (often below the detection limit) and the trace element concentrations of Ag, Te, As and Cu is on average lower as well.

Disseminated pyrite at Hwy-144 is generally fine to medium grained and sub to euhedral. Pyrite grains often contain sulfide and rutile inclusions, but do not contain the same abundance of silicate and carbonate inclusions. In Figure 7.32, we see that Au correlates well with Ag and Te, but has no correlation with Cu or As. Another pattern that is only visible at Hwy-144 is the Co-As or Co-Ni-As correlation. Fracture filling pyrite at Hwy-144 shares many similar characteristics with disseminated pyrite. Mineralized samples show a moderate correlation with Ag and a strong Co-Ni-As correlation (Figure 7.33). Un-mineralized samples show a strong correlation with Te, except where nanoparticles of gold are present (Figure 7.34). Similar to disseminated pyrite there is no correlation between gold and Cu or gold and As. Lastly, vein-hosted pyrite samples were analyzed. The two samples chosen were not strongly mineralized, with one sampled Ni-zoned while the other was not. The unmineralized sample in Figure 7.35 shows a tight correlation of Au with Te and Ag, whereas the zoned sample shows a moderate Te correlation and weak Ag correlation with Au. Similar to all other Hwy-144 samples there is no correlation between Au and Cu or As (Figure 7.36). Finally the vein-hosted samples do not share the Co-As or Co-Ni-As correlation that has been noted in the disseminated and fracture filling samples.

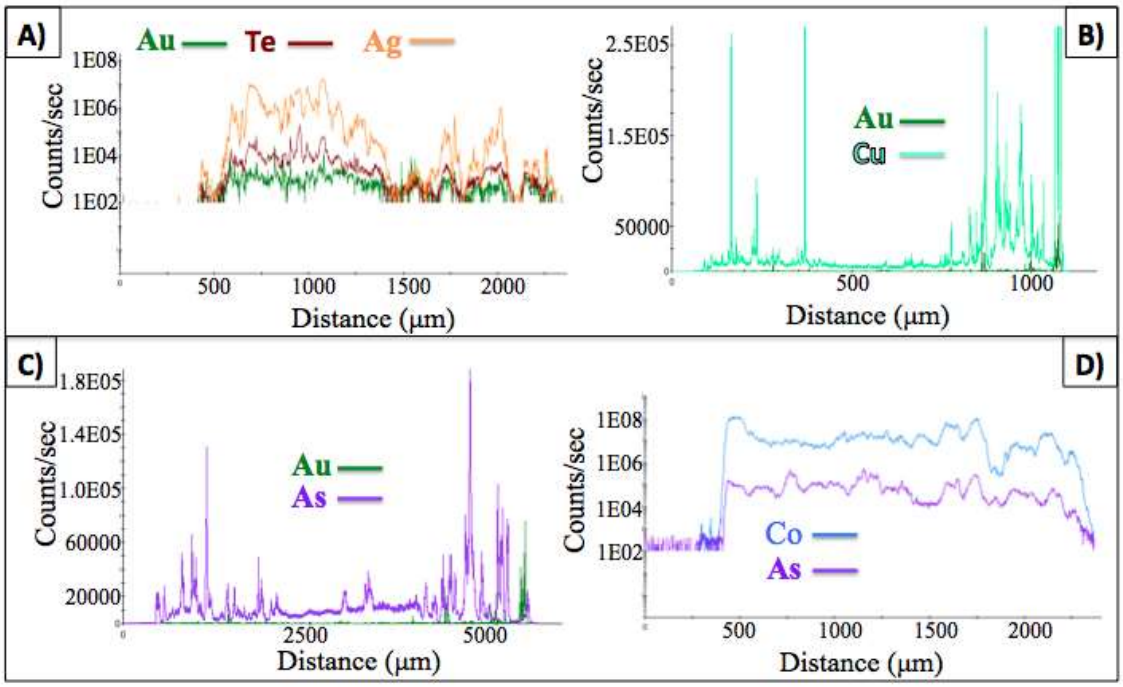

Figure 7.32: Hwy-144 Disseminated pyrite correlations. A) Strong correlation of Au, Te and Ag. B) No correlation between Au and Cu. C) No correlation between Au and As. D) Moderate correlation between Co and As.

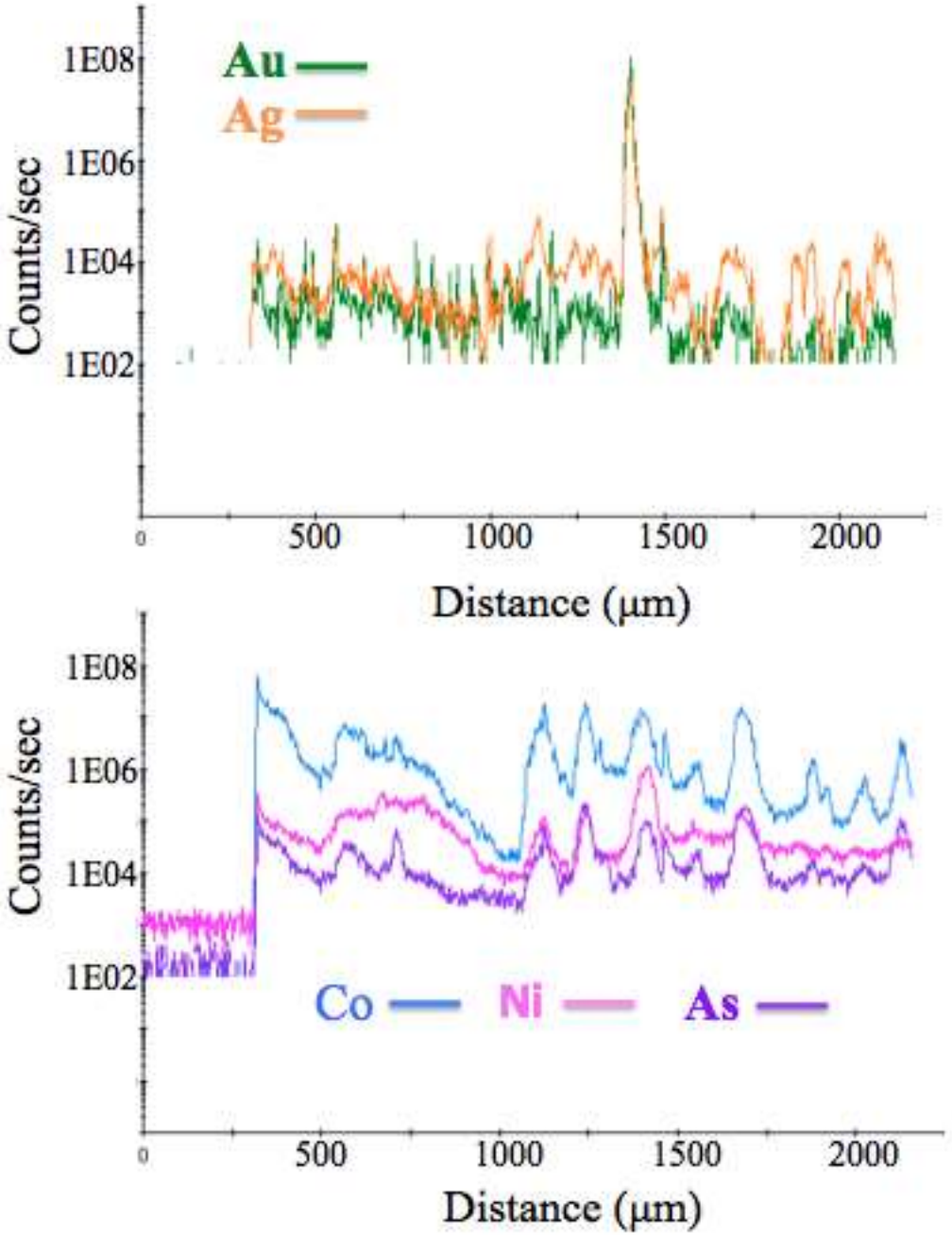

Figure 7.33: Laser ablation spectra for a mineralized fracture filling pyrite sample. Both mineralized and un-mineralized samples share a correlation between Au and Te/Ag. The Co-Ni-As correlation is only present in the mineralized sample.

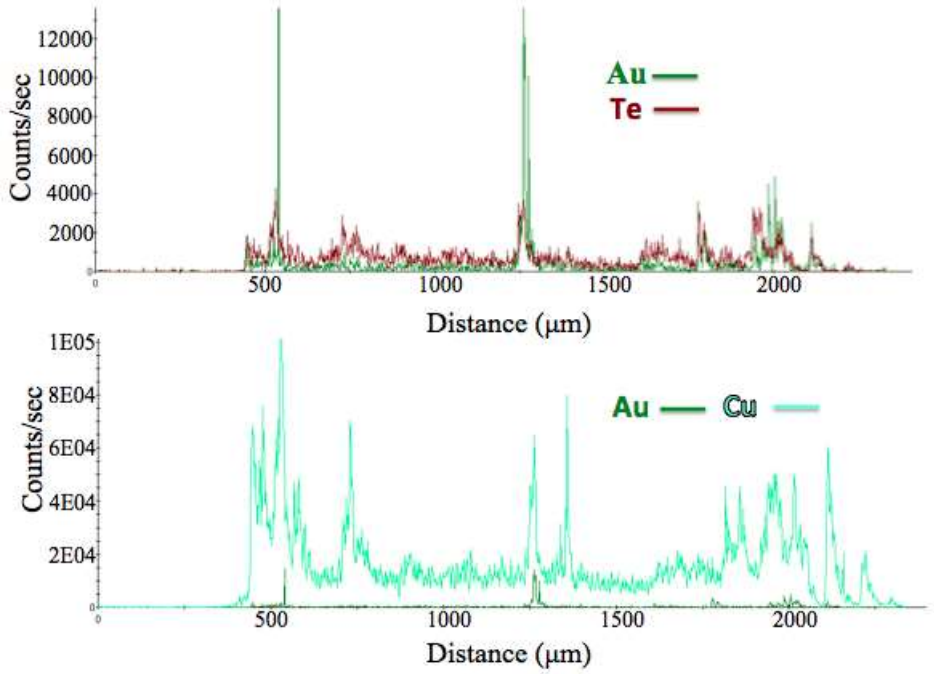

Figure 7.34: Un-mineralized fracture filling pyrite spectra. The top graph demonstrates the tight correlation between Te and Au. The bottom graph demonstrates that there is not Cu-Au correlation.

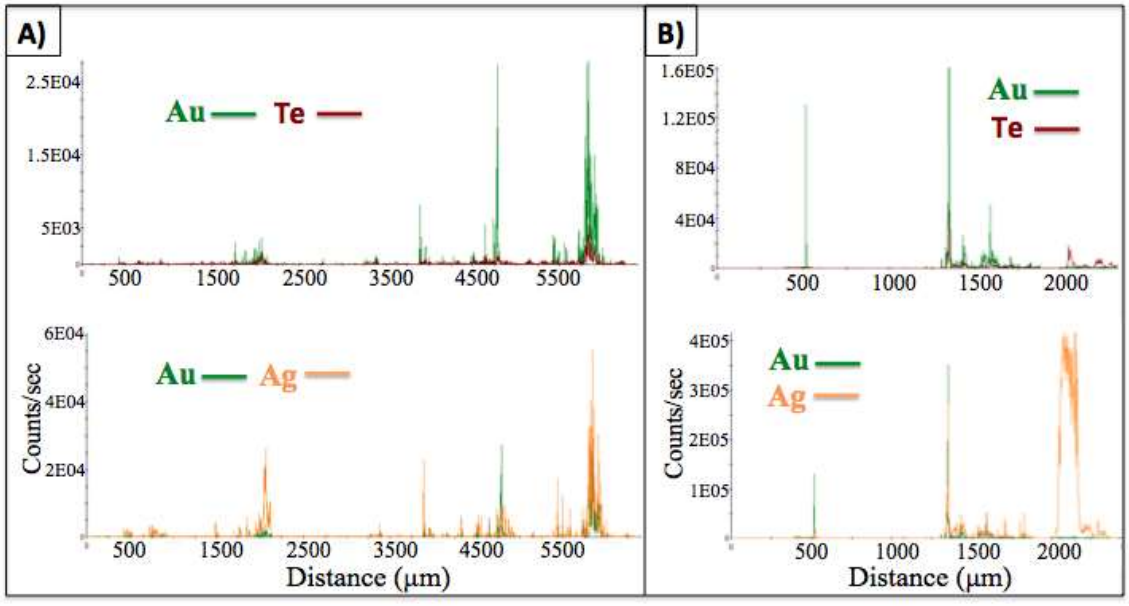

Figure 7.35: Vein-hosted laser ablation spectra from Hwy-144. A) Vein-hosted pyrite that is not zoned B) Ni-zoned pyrite sample.

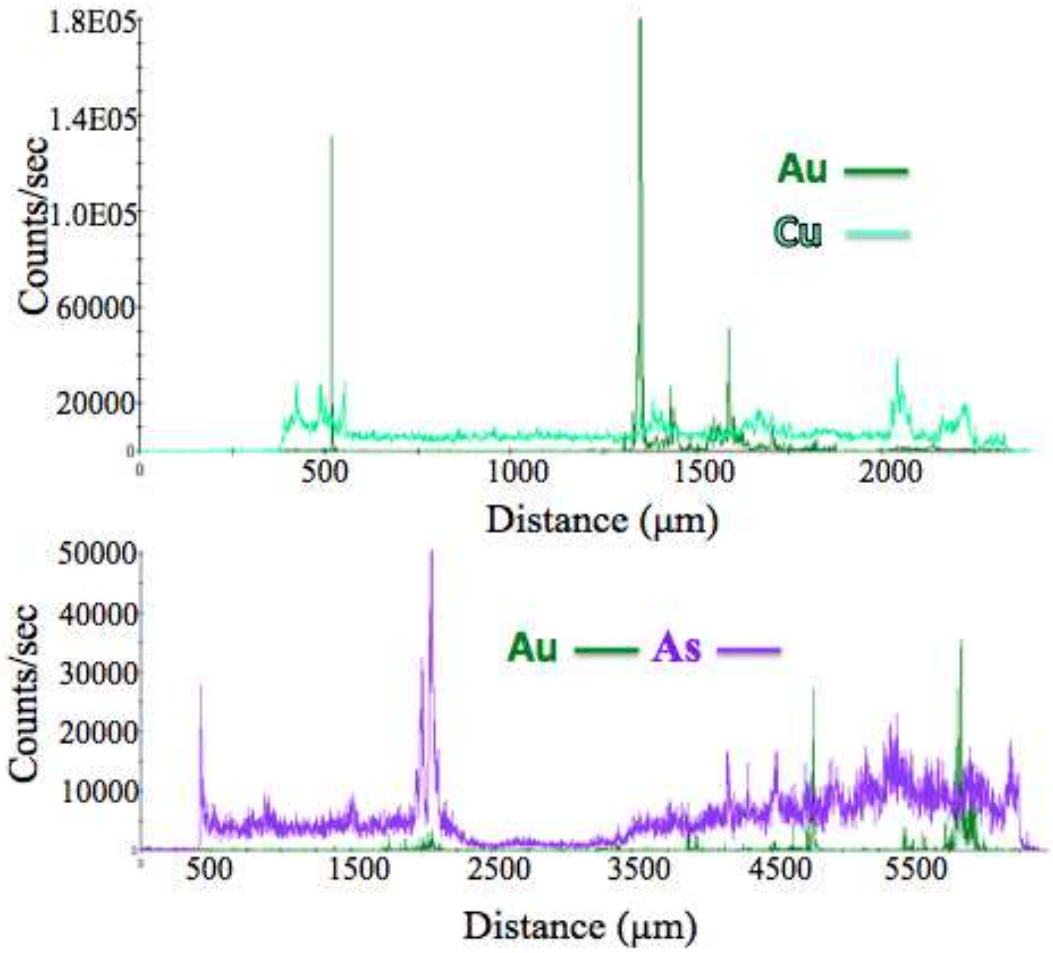

Figure 7.36: Unzoned vein-hosted pyrite showing no correlation between Au and Cu or As.

7.10 Gold Solubility In Pyrite

Reich et al. (2005), has shed light on the solubility of gold in pyrite based on arsenic concentration. Without the aid of arsenic, the solubility of gold in pyrite has been determined to be quite low (~0.2-4ppm)(Cook & Chryssoulis, 1990). Reich et al. (2005), determined an Au saturation line, where based on the concentration of Au and As, Au will either be held in the pyrite structure or as nanoparticles of gold. Ten background Au analyses from each pyrite grain laser ablated were plotted on the Reich et al. diagram to see if gold was more likely to be held in the pyrite structure or as nanoparticles of gold. Background laser ablation spectra were used because peaks in the spectra are clearly nano to visible particles of gold. The detection limits for gold was determined by the software program Plasma Lab Ver 2.5.5. Point analyses that fall below the detection limit were divided by two and then plotted on the graph so as to be easily distinguished. The work confirms the difference in gold content between Thunder Creek and Hwy-144. Thunder Creek, contains primarily gold below the

saturation line, but is strongly enriched in gold (~0.5-10ppm)(Figure 7.37). Hwy-144 on the other hand is extremely depleted in gold, with many examples plotting below the Au detection line(Figure 7.38). Looking at As content, Hwy-144 has on average a similar to higher concentration of arsenic compared to Thunder Creek. This indicates that As content is not the only control on gold solubility in these deposits.

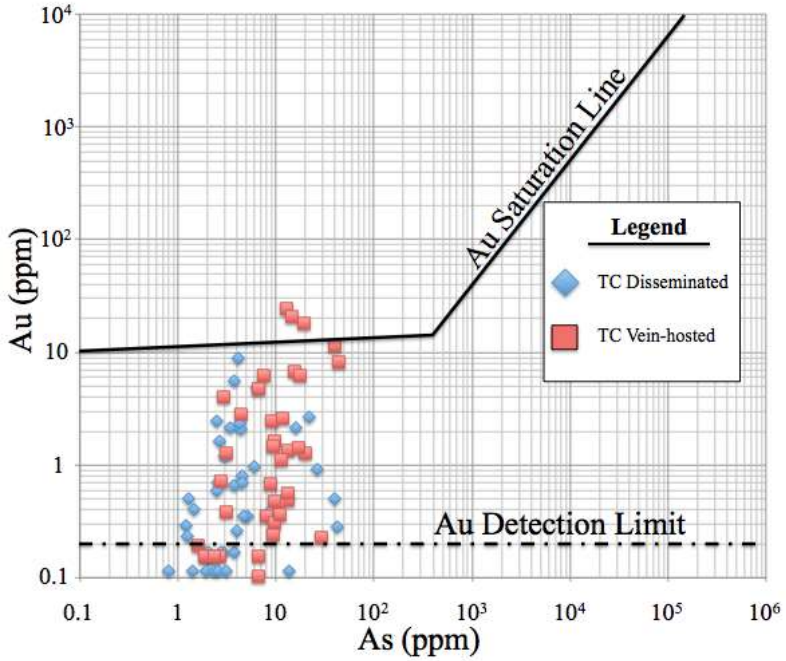

Figure 7.37: Graph of gold solubility in pyrite for Thunder Creek analyses (Modified from Reich et al., 2005)

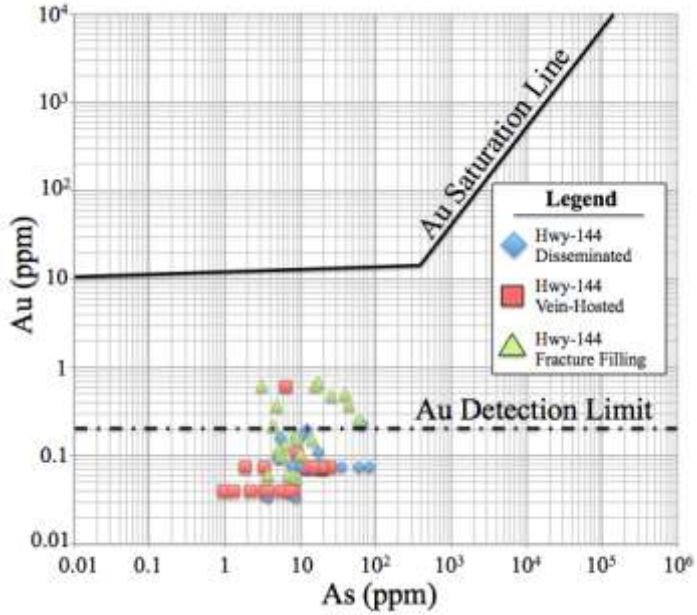

Figure 7.38: Graph of gold solubility in pyrite for Hwy-144 analyses (Modified from Reich et. 2005)

7.11 Pyrite Geochemistry Discussion

The results of the pyrite mapping and laser ablation study are consistent with prior geochemical and fieldwork conducted at both locations. The corroded nature of Thunder Creek pyrite was noted as very prospective while logging drill core. Using laser ablation transects we were able to confirm that a late fluid phase eroded portions of the pyrite grain depositing gold, sulfides and gangue minerals very similar to the host rock composition. Silicate minerals such as K-feldspar, quartz and albite are always associated with mineralized pyrite grains. Hwy-144 has a much smaller population of pyrite grains that are corroded, containing silicate inclusions. Pyrite grains that do contain inclusions are always mineralized, however this species of disseminated pyrite is not pervasive resulting in a lower average gold grade. Using the laser ablation spectra we were able to correlate trace elements with gold. Particularly in the case of Thunder Creek we noted a Te, Ag and Cu correlation with gold. This correlation is often associated with magmatic fluids. In the mass balance calculations done for Thunder Creek a positive Cu anomaly was also noted. The laser ablation data confirmed that while there is an anomalous amount of gold in the Thunder Creek pyrites, this is not directly affected by arsenic, and these are not arsenian pyrites. The actual gold content of the pyrites varies substantially between Thunder Creek and Hwy-144. Both disseminated and vein-hosted pyrite at Thunder Creek can contain up to 10 ppm gold. At Hwy-144 the insitu gold content of the pyrites is rarely above 2ppm. This suggests that the gold content of the fluid is much lower at Hwy-144.

7.12 Sulfur Isotopes

Sulfur isotopes were collected using a Secondary Ion Mass Spectrometer (SIMS) at Memorial University, Newfoundland. The machine specifications and running conditions are available in the Methods chapter. Sulfur isotopes were collected on the same pyrite grains that were WDS trace element mapped and laser ablated. By using the same pyrite grains for the three techniques we were able to combine and interpret all the data without making conclusions potentially based on sample variability. Sulfur isotopic work has been undertaken in the Kirkland Lake area, and the negative $\delta^{34}S$ values were used to infer the oxidative nature of some mesothermal Archean gold deposits (Cameron & Hattori, 1987). Strongly negative sulfur isotopic values along with Fe-carbonate, hematite, and hydrothermal barite suggest that gold-rich fluids were highly oxygenated. At both the Thunder Creek and Hwy-144 localities all of these oxide mineral phases are present in varying intensities. Gold tenor has also been linked to decreasing S isotopic compositions in the Yilgarn craton of Western Australia (Palin & Xu, 2000). Using spot analyses of S isotopes and laser ablation transects in the immediate vicinity, we are can correlate gold grade and sulfur isotopic composition quite accurately.

Two distinct sulfur isotopic populations were determined during the analyses (Table 7.6). The first population is strongly negative, with a per mil range of -3.5 to -6.1. Samples in this range are exclusively from Thunder Creek with one exception from Hwy-144. The second population has a per mil range of -0.1 to -3.3. These samples are exclusively from Hwy-144. This broad correlation initially suggests that strongly negative $\delta^{34}S$ values correlate with increasing gold grade, or that these are two mineralizing systems with different sulfur isotopic compositions. To test the first hypothesis, point analyses were compared with gold values from the laser ablation transects.

While some examples (Figure 7.39 & 7.40) do support the first hypothesis, an equal amount of samples do not (Figure 7.41). There is not sufficient evidence to suggest that gold tenor is related to decreasing sulfur isotopic values. Looking at the samples with trace element zoning, point analyses were taken inside each zone to determine if zoning recorded changing fluid composition. Only a few samples were zoned (three), and the results were inconclusive. Two of the three samples displayed increasing sulfur isotopic composition in Ni/Co-rich zones while the third sample displayed the opposite. Previous comparisons of gold grade to zoning indicated no clear connection. Further isotopic work is needed to accurately constrain the fluid composition, origin and evolution.

Table 7.5: Sulfur isotopic analyses from pyrite grains.

Location	Pyrite Generation	Delta ^{34}S Range (per mil)	Avg. Delta ^{34}S (per mil)	Number of Analyses
Thunder Creek	Disseminated	-3.0 to -6.1	-4.7	8
Thunder Creek	Vein-Hosted	-3 to -5.3	-4.3	14
Hwy-144	Disseminated	-1.8 to -3	-2.4	2
Hwy-144	Vein-Hosted	-0.1 to -3.3	-1.5	8
Hwy-144	Fracture Filling	-1.4 to -6.9	-3.7	9

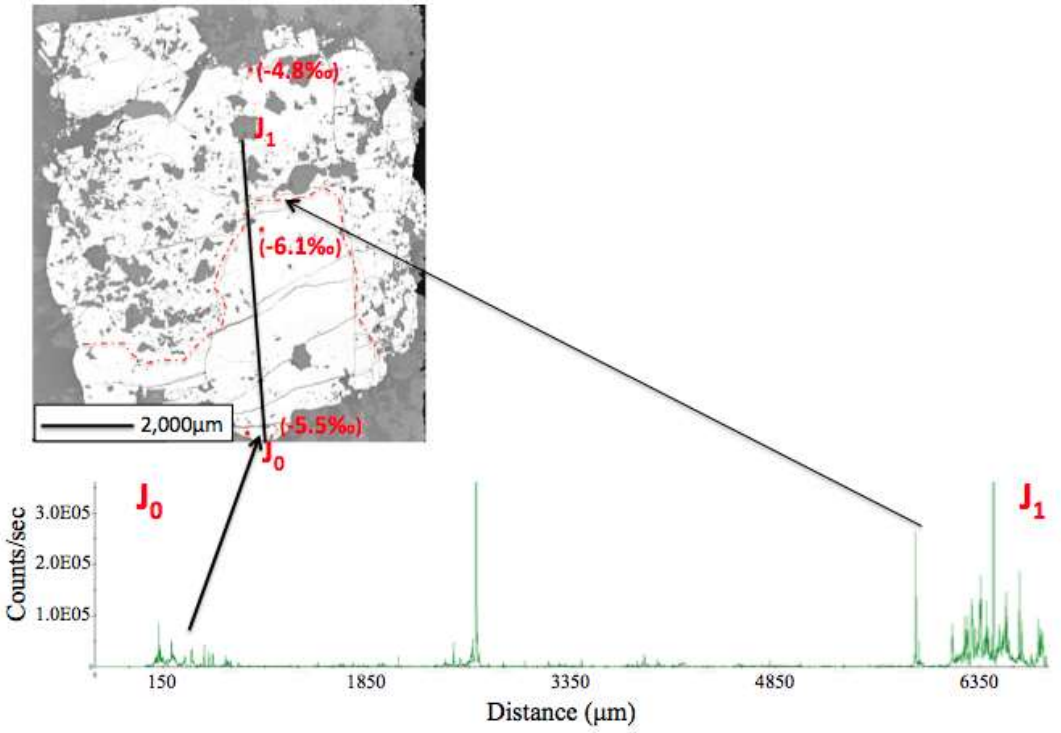

Figure 7.39: Disseminated pyrite from the 280m level. Sulfur isotope values are strongly negative and get increasingly negative approaching the corroded part of the pyrite grain. Gold spectra below the photo for reference.

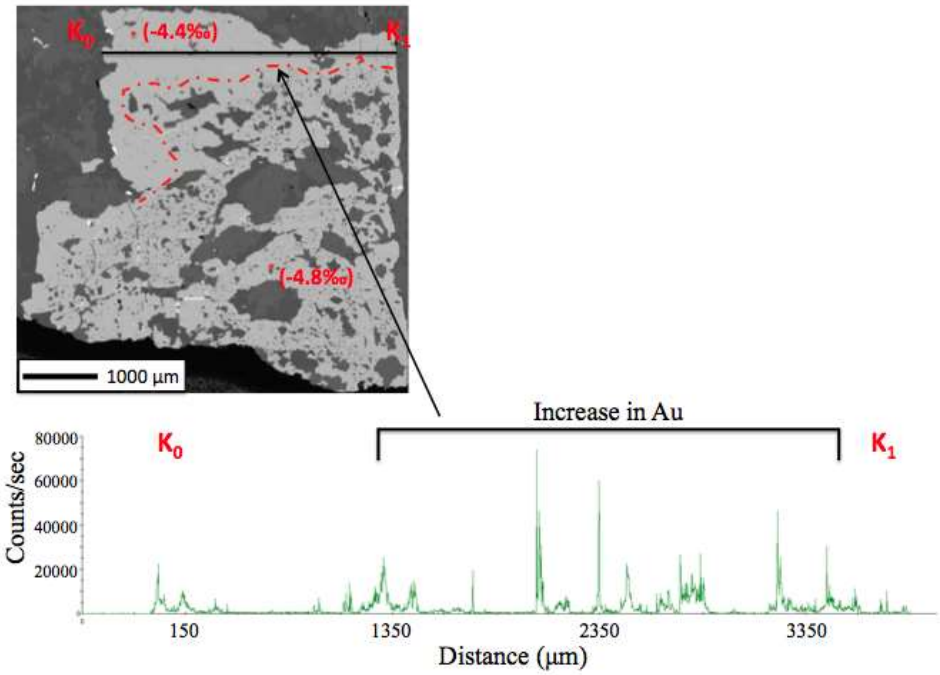

Figure 7.40: Disseminated pyrite from the 280m level at Thunder Creek. Sulfur isotopic values are more negative in the corroded and gold-rich portion of the pyrite grain.

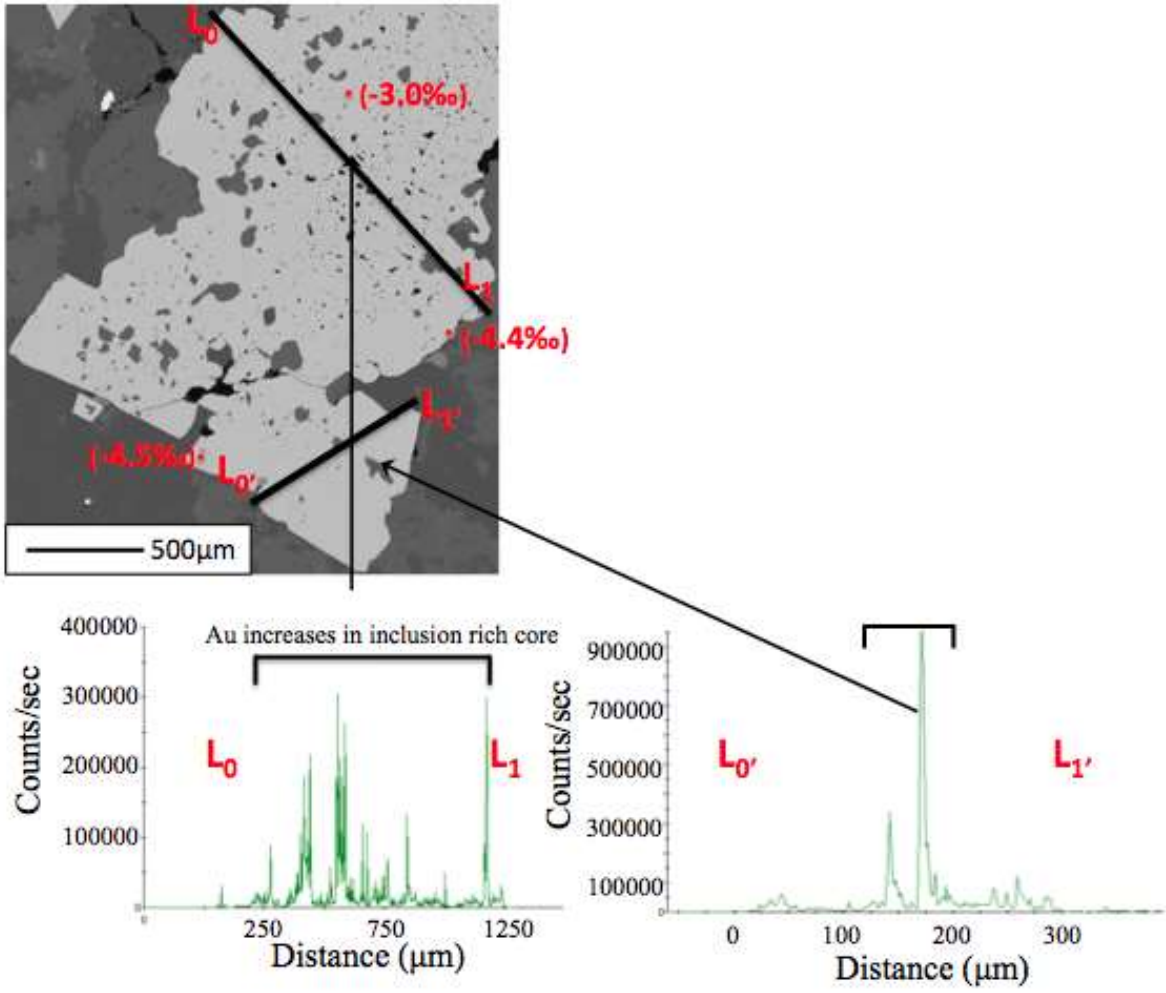

Figure 7.41: Disseminated pyrite from the 695m level of Thunder Creek. The inclusion and gold-rich portion of the pyrite has more positive sulfur isotopic values compared to the rim.

7.13 Sulfur Isotope Discussion

Sulfur isotopic analyses of pyrite grains did not provide empirical evidence to suggest the origin of mineralizing fluids. All isotopic analyses were near zero to fairly negative (-6.1 to -0.1 per mil). Negative $\delta^{34}S$ values can reflect oxidizing fluids (Cameron & Hattori, 1987), but can also reflect the dissolution of diagenetic pyrite. To differentiate between oxidation and fluid mixing another isotopic study (Pb isotopes) would need to be done. The prescence of hematite in the host rock also indicates oxidizing conditions. While it is clear that oxidation is proximal to mineralization, no grain scale connection between Au tenor and negative $\delta^{34}S$ values was found. On the property scale, the more mineralized Thunder Creek deposit has more negative $\delta^{34}S$ values compared to Hwy-144. Near zero isotopic values are also indicative of mantle derived fluids. The variation between near zero and strongly negative values could be caused by the mixing

of two isotopically distinct fluids. At this point further isotopic work is needed to determine the origin of the mineralizing fluids. Substantial barite was noted in equilibrium with pyrite in multiple samples. It would be useful to have sulfur isotopes of a sulfide-sulfate pair to determine the actual fluid isotopic composition and to determine a temperature of pyrite/barite crystallization. Pb-Pb isotopes are also suggested to determine if fluid mixing occurred. Pb-Pb isotopes can be performed on pyrite and orthoclase grains and their compositions compared. Orthoclase grains that are believed to be magmatic will share a similar Pb isotopic composition with magmatic-hydrothermal pyrite grains from the same origin.

8.0 Discussion

Using all the data collected it is possible to interpret how and when gold formed at Thunder Creek and Hwy-144. The most basic observation made during core logging at both sites is the relationship between increasing gold grade and increasing pyrite abundance and quartz vein density. Whole rock geochemistry confirms that there is a proportional relationship between Au and S in syenite samples at Hwy-144 (Appendix D). This observation suggests that gold travelled as a pervasive fluid depositing gold in disseminated pyrite aureoles and along brittle contacts as vein-hosted pyrite. At Thunder Creek strategic sampling of the background syenite and different vein arrays provided insight into the timing relationships of gold endowment. The mineralized and folded Rusk Shear zone represents mineralization during D_3/D_4 deformation (Dave Rhys, pers commun). V_1 veins in the syenite are folded probably occurring before or during the same deformation event. V_2 and V_3 veins are undeformed brittle vein sets younger than V_1 and the Rusk Shear zone. V_2 veins are strongly mineralized whereas V_3 veins are not. The sampling indicates that gold mineralization formed over a period of time beginning with ductile syn-metamorphic deformation (Rusk Shear Zone, V_1 veins) and transitioning to the brittle zone with undeformed V_2 quartz veins. The mineralization episode tapered off as V_3 veins formed. While this model accurately characterizes vein-hosted mineralization, there is still a significant component of disseminated gold mineralization. A similar sampling approach was used to determine the gold content within background syenite hosting disseminated pyrite. At Thunder Creek, the background syenite consistently carried between 0.5-2.0 g/t gold with the same proportional relationship between Au and S. At Hwy-144 there is minor amounts of disseminated mineralization, however, outside of small, mineralized lenses the syenite is barren. Where mineralized at Hwy-144, a proportional relationship between Au and S exists.

Both the Thunder Creek and Hwy-144 syenites were studied to determine if there was a link between gold mineralization and a particular alteration assemblage. At Thunder Creek, the syenite appears only weakly altered in hand sample and thin section. Many of the feldspars demonstrate Carlsbad twinning and polygonal grain boundaries. In addition there is very little carbonate, sericite and hematite alteration. The presence of disseminated pyrite in the syenite, and the presence of end member K-feldspar and albite (Table 7.3 & 7.4) in the syenite confirm the syenite is altered. It is possible that the syenite is only weakly altered,

or, altered by a fluid in equilibrium with the syenite. Whole-rock mass balance calculations were done to test this hypothesis. The mass balance calculations compared the syenite at the mine to the distal Thunder Creek syenite stock. The calculations indicate that silicification is the major alteration phase present during mineralization. Feldspar inclusions in mineralized pyrite grains do indicate the possibility of feldspathic alteration associated with mineralization. However there is not a broad albite or potassic replacement halo as seen in porphyry environments. At Hwy-144 the same calculations were performed, comparing a least altered, unmineralized sample to an altered and mineralized sample. These calculations determined that K_2O and CaO were added during mineralization. The comparison of mass balance calculations between the two properties suggest that two separate mineralizing systems are present. Albite was analysed in both altered samples from the TC Mine, Hwy-144, and unaltered Thunder Creek stock. The presence of albite in the least altered rocks studied suggests it occurred prior to gold mineralization and is unrelated. Mass balance calculations do not indicate that Na enrichment is related to gold mineralization.

At Hwy-144 alteration is visible in both hand sample and thin section. In localized domains pervasive hematite and carbonate alteration are present. Review of mineralized sample petrography and whole rock geochemistry provides no indication that gold mineralization is related to hemitization or carbonitization of the syenite. Samples with the strongest hematite alteration are not mineralized and Au values do not correlate with CaO in whole rock geochemistry. Whole rock geochemistry also indicates that portions of the Hwy-144 syenite have undergone potassic alteration. Again, there is no correlation between potassic alteration and gold mineralization as seen at the Young Davidson Mine (Martin, 2012).

Petrographic, microprobe and SEM analyses indicate that gold is present as anhedral grains within pyrite. A smaller proportion of gold occurs along fractures in pyrite, and an even smaller fraction is present as free gold. Gold hosted within pyrite has two possible origins. Early gold could have formed as poikiloblastic inclusions within the pyrite, whereas late gold could be deposited in voids within a pyrite grain corroded by mineralizing fluids. The irregular pattern of inclusions and deformed pyrite grains suggests a late mineralizing fluid deposited gold in porous pyrite grains. K-feldspar, albite and quartz are always present as inclusions that host mineralized disseminated pyrite. The composition of the inclusions likely reflects the composition of the mineralizing fluids. The laser

ablation study conducted on pyrite grains confirmed that at TC gold mineralization and pyrite crystallization are synchronous. Both vein-hosted and disseminated pyrite have appreciable (1-10 ppm) contents of Au in the pyrite structure, along with visible gold inclusions. This observation suggests that there is both an early deposition of gold during pyrite crystallization (vein-hosted + disseminated varieties) and a later deposition of gold into porous cavities of the pyrite (disseminated only). At Hwy-144, many of the pyrite grains have gold contents below the detection limit of LA-ICP-MS (0.05 ppm) suggesting that a large portion of the pyrites crystallized from a gold-poor fluid. In thin section, gold is present as inclusions in pyrite or along late fractures. Gold-bearing disseminated pyrite at Hwy-144 typically have the same suite of silicate inclusions as TC. Gold was likely only transported later when mineralizing fluids caused pyrite dissolution. Hwy-144 does not have the same widespread deposition of gold within disseminated pyrite, and Hwy-144 has reduced vein-density likely due to the weak nature of the shear zone along the pyroxenite-syenite contact. The combination of these two events may explain why Hwy-144 has a lower gold endowment compared to Thunder Creek.

The synchronous relationship between pyrite and gold mineralization provides the justification that sulfur isotopes can be used to evaluate the origin of mineralizing fluids. In-situ sulfur isotopic compositions were determined for each variety of pyrite present at both Thunder Creek and Hwy-144. From both deposits these range from near 0 to -6.1 suggesting a mantle origin. S isotopic compositions did not generally change drastically within the grain, and showed no correlation to Ni/Co zoning or presence of silicate inclusions. Two sulfur isotopic populations were determined: -6.1 to -3.5 per mil at Thunder Creek and -3.7 to -0.1 per mil at Hwy-144. Both populations potentially represent magmatic fluids or fluids leached from mantle derived rocks such as basalts. The strongly negative values at Thunder Creek could be a result of a partially oxidized fluid transitioning from H_2S to H_2S0_4 with a fractionation effect causing increasingly negative δS^{34} values. It's also possible that Hwy-144 and Thunder Creek were sourced from two separate sulfur reservoirs, but this is unlikely due to their close proximity. It is clear that the two deposits underwent different deformation/alteration histories. At Thunder Creek the trace element assemblage associated with gold in pyrite is Ag, Te, and Cu. These trace elements are often associated with gold sourced from magmatic fluids (Au-Cu porphyries; Sillitoe, 1972). Finally, microcline was observed in quartz vein samples from Thunder Creek. The presence of microcline indicates that K-feldspar (orthoclase) re-equilibrated with fluids at relatively high

temperature (>300 degrees; Nesse, 2009). Hwy-144 shares similar trace element associations (Au with Ag and Te) but lacks the association with Cu. The whole rock mass balance is association with Pb, Zn and Ni is also different compared to Thunder Creek. This base metal association may be a result of mineralizing fluids stripping metals from altered volcanic slivers within the syenite and depositing them within the altered Hwy-144 syenite.

The dominant complexes that transport gold in solution are $AuHS^0$ and $Au(HS)_2^-$ at low temperatures (~250-400°C) and $AuCl_2^-$ at higher temperatures (> 400°C) (Gilbert et al, 1998; Stefanson & Seward, 2003; Williams-Jones et al., 2009). Studies of typical orogenic lode gold deposits constrain the pressure temperature parameters between 1-3kbar and 160-700°C, with a near neutral pH and salinity between 0-35 wt% equivalent NaCl (McCuaig & Kerrich, 1998). It is likely that gold precipitation at Thunder Creek and Hwy-144 was controlled by one or more of the following; sulfidation of the host rock, boiling, oxidation, temperature decrease and fluid mixing.

Pyrite and gold mineralization are synonymous across most gold deposits in the Abitibi, including the Thunder Creek and Hwy-144 gold occurrences. As discussed in the Mineralization chapter, gold is commonly present as inclusions in pyrite alluding to the close spatial relationship between the two species. Sulfidation of the host rock occurs through the crystallization pyrite, with simultaneous consumption of Fe-oxides, Fe-silicates and Fe-carbonates. Crystallizing pyrite removes HS^- from the fluid reducing gold solubility promoting precipitation. Large disseminated pyrite halos are present around mineralized zones at Thunder Creek and to a lesser extent Hwy-144. For sulfidation of the host rock to be a valid gold precipitation mechanism we would expect to see replacement textures between pyrite and another iron bearing phase. While magnetite and ankerite are present in the syenite, an example of replacement was never observed. Hence for sulfidation of the host rock to be the primary mechanism of gold precipitation complete replacement of iron oxides and iron carbonates must have occurred with no relict intermediary phases preserved. Both magmatic and metamorphic fluids are potentially sulfur rich and could be responsible for sulfidizing the host rock. It is also possible that Fe, S and Au were added to the syenite from one fluid or the mixing of two fluids. Mass balance calculations from both locations indicate that Fe stays fairly immobile while sulfur is added to the system, suggesting sulfidation of the host rock is more likely. Looking at pyrite morphology there is a strong association between mineralized disseminated pyrite and irregular corroded grains with K-feldspar, quartz and albite inclusions. Two interpretations are possible: first, poikilitic pyrite formed after an early fluid stage with a higher silica content, or, pyrite

underwent dissolution from a later a silica + gold-rich fluid that deposited inclusions in pyrite voids. The second interpretation is favoured because the inclusions form irregular patterns and are not isolated to the core or rim of zoned pyrite grains. Silicate inclusions are not present in Hwy-144 samples that display strong Co/Ni zoning, making it difficult to fully evaluate the timing of the inclusions. While this process accurately describes disseminated pyrite halos, it cannot account for vein-hosted mineralization, or the remobilization of gold along fractures in pyrite.

The occurrence of boiling can reduce the activity of HS^- causing the precipitation of gold (William-Jones et al., 2009). Detailed fluid inclusion studies were not the focus of this research and firm conclusions regarding boiling cannot be made. While not a mechanism for gold precipitation, pressure drops in response to quartz vein formation and seismic pumping are common in lode gold style deposits (Bowers, 1991, Sibson et al., 1975). The unequivocal relationship between vein intensity and gold grades at both Thunder Creek and Hwy-144 supports ^{this} model for gold formation. The proximity of the Thunder Creek deposit to the Rusk Shear zone and the mineralized nature of the shear zone indicate that mineralized fluids traveled along this conduit. The Rusk Shear Zone represents D_3 deformation in the Timmins Camp, with the formation of V_1 and V_2 veins in the syenite forming in response to rheological stress on the pluton (Rhys, pers communication). The shear zone does not manifest as strongly at Hwy-144 and is one reason for the poor gold mineralization and low vein intensity in the syenite. Sibson et al., (1975) outlined the following criteria for mineralization in response to seismic pumping; cemented vein breccia, compositional vein layering, laminated vein arrays and crystal growth zoning. The Thunder Creek deposit does have cemented vein breccias and laminated vein arrays characteristic of seismic pumping, and has chemically different vein sets (V_1 vs. V_2 vs. V_3). In thin section the veins at Thunder Creek are visibly strained with undulose extinction and subgrain development visible.

The presence of hematite and negative $\delta^{34}S$ values suggest that oxidized fluids were present at both Thunder Creek and Hwy-144. Increasing fO_2 reduces gold solubility in the fluid causing gold precipitation. Cameron and Hattori (1987) determined a relationship between increasing gold grade and strongly negative $\delta^{34}S$ compositions in pyrite from the Kirkland Lake gold camp. While a direct correlation is not present at our study area, there do appear to be oxidized fluids in the vicinity of mineralization. Metamorphic fluids are reduced leaving the possible source for oxidized fluids coming from late magmatic fluids or meteoric fluids. The current understanding of the Archean atmosphere indicates it was strongly reduced with mildly oxidized shallow sediments and felsic plutons as the only

likely source for oxidized fluids. Magmatic and hydrothermal fluids are interpreted as the source of oxidized fluids in the study area. In Kirkland Lake strongly negative $\delta^{34}S$ values are related to gold mineralization. Hwy-144 pyrites have weakly negative $\delta^{34}S$ values with visible hematite alteration that is locally intense. ICP-MS analyses of disseminated and vein-hosted pyrites indicate they formed from a gold poor fluid. Thunder Creek pyrites have more negative $\delta^{34}S$ values with very little hematite alteration present. These pyrites often contain 1-10ppm Au in the background excluding visible gold grains and Au nanoparticles. These observations suggest that oxidized fluids were not solely responsible for the precipitation of gold.

Cooling is one of the mechanisms for gold precipitation considered at Thunder Creek and Hwy-144. Based on the greenschist metamorphic assemblage, presence of microcline in quartz veins, and sulfur isotopic composition of pyrites suggesting magmatic fluid involvement we can infer that the mineralizing fluids were not high temperature (<450°), but were also above 250° Celsius. In this temperature range a gold sulfide complex is most stable. Using Figure 8.1 we can see that only a gold-chloride complex will cause gold precipitation with decreasing temperature. The solubility of gold in solution at the interpreted temperature suggests that cooling did not play a major role in gold precipitation at Thunder Creek and Hwy-144.

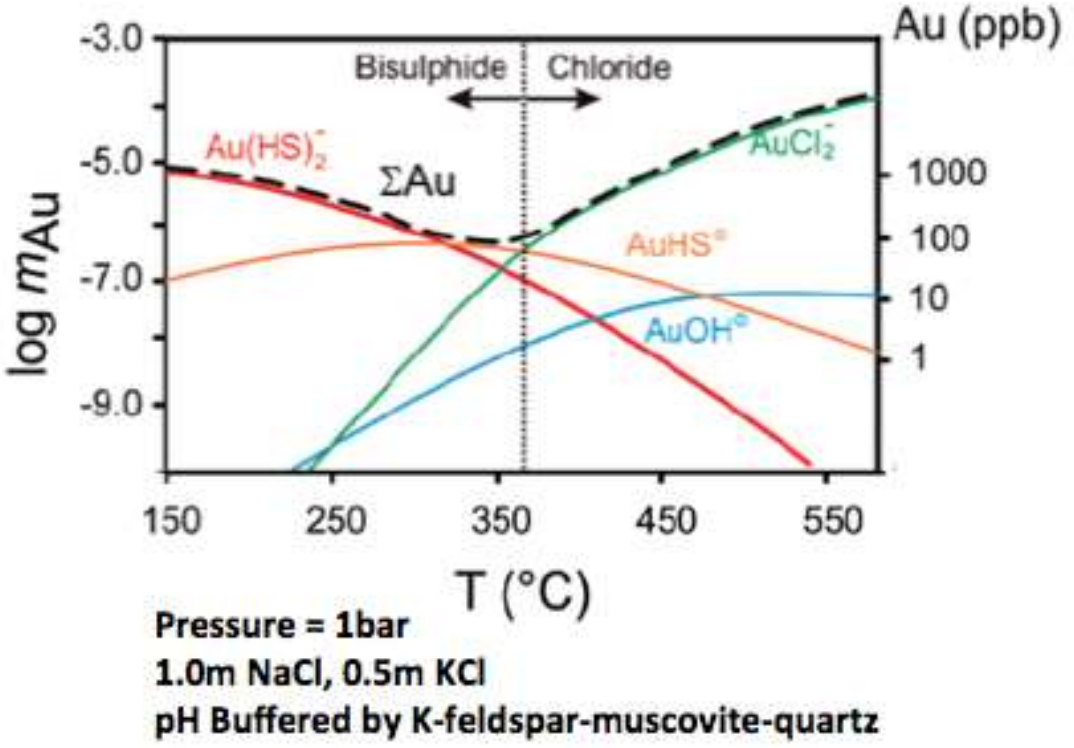

Figure 8.1: Gold complex solubility with changing temperature. The stability constants for gold are from Stefansson and Seyward (2004), and thermodyanic data for other species are from the SUPCRT92 database (Johnson et al., 1992). Modified from William-Jones et al., 2009.

Metamorphic fluids have often been thought to play a role in the formation of mesothermal gold deposits (Groves et al., 2003). Large lode gold camps in the Yilgarn, Superior and many other Archean cratons are hosted in green schist metamorphic facies rocks (Groves et al., 2003). In modern porphyry environments the involvement of magmatic fluids related to Cu and Au mineralization is well studied (Sillitoe, 1972). With both metamorphic and magmatic fluids present in the study area, understanding each fluids role in the mineralizing system is difficult. Sulfur isotopic compositions of the pyrites discussed above have a magmatic signature, but are easily re-equilibrated during alteration. The sulfur isotopic composition of Hwy-144 potentially suggests it did not interact with the same volume of metamorphic fluid and has thus retained an oxidized magmatic fluid signature. It is possible that a magmatic fluid has re-equilibrated with a metamorphic fluid resulting in the weakly negative sulfur isotopic values reported. Further work, involving more S isotopes on sulfates (barite/celestine) and Pb-Pb isotopes is needed to further constrain the origin of the mineralizing fluid at Thunder Creek and Hwy-144.

In order to assess the viability of Hwy-144 as a potential new gold deposit, it is important to compare it to Thunder Creek because of their spatial proximity. Initial interpretations based on location and geology suggested that Hwy-144 might be an extension of Thunder Creek. On a regional scale, both areas display similar alteration, lithologies, and an association of gold with pyrite and quartz veining. Morphologically, the Thunder Creek syenite is more continuous and geochemically uniform compared to Hwy-144. At Hwy-144 the syenite consists of numerous, thin, altered mafic volcanic slivers and syenite intrusions are typically 5-15m in thickness. With respect to alteration, both areas display hematite and carbonate alteration. Thunder Creek however, contains minimal alteration whereas the alteration at Hwy-144 ranges in intensity, and is overall more altered. Whole rock mass balance calculations distinctly identify two different mineralizing systems. At Thunder Creek mineralization is associated with silicification and Cu, Bi, Au enrichment. At Hwy-144 there is more potassic and carbonate alteration with increases in As, Ni, Pb, Zn and Au. This evidence facilitated the need to look at both deposits at higher resolution focusing on pyrite grains.

Mineralized pyrite grains at Thunder Creek have been noted by Lake Shore Gold geologists and come in two forms; corroded and ratty disseminated pyrite indicative of late auriferous fluids depositing gold in pyrite, and homogenous relatively inclusion-free vein-hosted pyrite. Laser ablation determined that these grains contain a significantly enriched background concentration of gold (~0.5-10 ppm) along with gold inclusions. At Hwy-144 disseminated pyrite grains are overall much more euhedral and do not display the same altered textures. Some pyrite grains display primary growth zoning in the form of Ni and Co zoning. Laser ablation of these pyrite grains determined that they are gold-poor, with many of the analyses falling below the 0.5ppm detection limit. The low gold content and euhedral nature of the pyrites at Hwy-144 suggests that they may not have mingled with late auriferous fluids and are subsequently gold poor.

To fully understand the controls on gold mineralization at Thunder Creek and Hwy-144 it is necessary to integrate all of the analytical techniques discussed in earlier chapters. To isolate gold at the Thunder Creek deposit vein and syenite specific samples were taken at multiple levels of the mine. The sampling determined that economic ore grades are hosted by V_1 and V_2 veins. However, heterogeneous disseminated pyrite distribution in the mineralized zone contains low grade but

consistent gold mineralization that plays a role in the total gold endowment. Looking at vein composition, pyrite is the most abundant ore mineral with minor galena, molybdenite and scheelite. Thin section microscopy confirmed that roughly 90% of the observable gold present is directly held within or adjacent to pyrite. Gold is present either as inclusions or along fractures in pyrite grains. This initial interpretation suggests that there is both an early (inclusion) and late (fracture-filling) episode of gold mineralization. Close inspection of pyrite grains via BSE imaging highlights pyrite grain architecture. At Thunder Creek, the bulk of disseminated and some vein-hosted pyrite samples are heavily corroded with silicate/carbonate inclusions. The irregular, inclusion-rich pattern within pyrite grains suggests a later fluid has irregularly passed through the pyrite grain. If there were an inclusion-rich core and inclusion-free rim, the argument could be made that two stages of pyrite growth have been recorded. At Thunder Creek the inclusion distribution is generally sporadic, negating the previous hypothesis. Petrographically, Thunder Creek appears relatively weakly altered. In thin section well-formed polygonal grain boundaries and Carlsbad twinning are common. However, the rocks in both the hanging wall (pyroxenite) and footwall (mafic volcanic) are visibly altered. This suggests that the syenite is at least weakly altered. The presence of disseminated pyrite within the mineralized portion of the syenite and endmember feldspar compositions confirms that late fluids have traveled through the rock. The composition of inclusions in pyrite (quartz, K-feldspar, albite and carbonate) suggests the late fluid was close to being in equilibrium with the host rock (i.e. near neutral pH and relatively high temperature). A late fluid similar in composition to the host rock would effectively mask visible alteration, especially if it was pervasive. A working hypothesis is that the late fluids represent a late magmatic-hydrothermal fluid phase tapping the same source as the syenite. The mineralogy of secondary phases in the vicinity of the syenite suggests the late fluid was oxygenated. This is confirmed by the presence of hematite and barite in the surrounding host rocks. Furthermore, the increasingly negative $\partial^{34}S$ values in pyrite grains is further evidence to suggest the fluid was oxygenated.

Robert (2001) characterized a significant portion of syenite-associated gold deposits in the Abitibi. At the time of publication, the Thunder Creek deposit and Hwy-144 gold prospect were not sufficiently developed to warrant study. The deposits studied in the paper share many characteristics with the syenite associated gold deposits researched in this study: disseminated sulfide zones, qtz-carb-K-spar vein stockworks, proximity to major fault structures, steeply plunging mineralization, total sulfide content less than 10%, presence of shallowly dipping extensional quartz veins, and predominance of albitization and K-spar alteration over sericite. While the deposits in this study are similar in a broad regional sense, distinct deposit scale differences are present. For

example, extensional veins analogous to V_2 in this study are classified as barren by Robert (2001), whereas at Thunder Creek they are consistently ore grade. Many of the deposits classified by Robert have albite, K-spar and carbonate alteration assemblages associated with ore halo. At Thunder Creek, silicification was determined through mass balance, with very little visible alteration detected in thin section. This is an outlier compared to the majority of deposits studied by Robert (2001), except for Malartic, which is also characterized by silicification. Hwy-144 on the other hand contains increased carbonate, K-spar and albite alteration similar to the deposits in the Robert (2001) study. While these alteration assemblages are spatially proximal to the mineralization at Hwy-144, none of them appear to be directly related to the mineralization. Texturally, the generations of ore related pyrite at Hwy-144 and Thunder Creek are different from the majority of syenite-associated deposits in the Abitibi. At Thunder Creek and Hwy-144 coarse corroded disseminated pyrite, and coarse vein-hosted pyrite are associated with mineralization while other deposits in the Abitibi host very fine- to fine-grained pyrite.

9.0 Conclusions

Mass balance calculations indicate that Fe stayed immobile while S was added to the system. While visible replacement textures were no observed, they do not discount the possibility of sulfidation forming the disseminated pyrite halo which late auriferous fluids targeted as a host for mineralization. Thus sulfidation of the host rock is interpreted to play an important role in the precipitation of gold. At Thunder Creek pervasive fluid flow resulted in increased mineralization compared to Hwy-144. The similar sulfur isotopic compositions of disseminated and vein-hosted pyrite, along with quartz, carbonate and feldspar inclusions in pyrite similar to the composition of veining suggest a cogenetic source. Quartz vein sampling determined that V_1 and V_2 veins consistently contain economic grades of gold mineralization. Seismic pumping resulted in quartz vein formation, the main contributor to gold mineralization. Vein density studies suggest that the strongest mineralization is associated with the highest vein density. While seismic pumping appears to be important in forming gold mineralization the importance of boiling is untested. The proximity to the Rusk Shear zone caused brittle deformation in the Thunder Creek syenite while the Hwy-144 syenite was more altered but not as deformed. Finally the variable sulfur isotopic signatures suggest fluid mixing. The mixture of a low temperature, reduced, S-rich metamorphic fluid with higher temperature, oxidized and near neutral magmatic fluid could have caused gold precipitation. A long lived, multi episode mineralization model consisting of the interaction of both magmatic and metamorphic fluids controlled by regional and property scale crustal structures suits this style of syenite-hosted gold mineralization best.

References

Ayer J.A. Thurston, P.C. Bateman, R. Dubé, B. Gibson, H.L. Hamilton, M.A. Hathway, B.Hocker S.M. Houlé, M.G. Hudak, G. Ispolatov, V.O. Lafrance, B. Lesher, C.M., MacDonald, P.J. Péloquin, A.S. Piercey, S.J. Reed L.E. Thompson, P.H. 2005. Overview of Results from the Greenstone Architecture Project: Discover Abitibi Initiative. Open File Report 6154, Ontario Geological Survey, Sudbury, Ontario.

Barron, K.M. 1991. Relationship of Archean gold to alkaline magmatism, Superior Province, Canada. BRAZIL GOLD91'.

Bateman, R. Ayer, J.A. Dube, B. 2008. The Timmins-Porcupine gold camp, Ontario: anatomy of an Archean greenstone belt and ontogeny of gold mineralization. Economic Geology, **103**: 1285-1308.

Bateman, R. Bierlein, F.P. 2007. On (Kalgoorlie), Timmins-Porcupine(Canada), and factors in intense gold mineralization. Ore Geology Reviews, **32**: 187-206.

Beakhouse, G.P. 2011. The Abitibi Subprovince plutonic record: tectonic and metallogenic implications. Open File Report 6268. Ontario Geological Survey, Sudbury, Ontario.

Bowers, T.S. 1991. The deposition of gold and other metals: pressure induced fluid immiscibility and associated stable isotope signatures. Geochemica, **55**: 2417-2434.

Cameron, E.M. Hattori, K. 1987. Archean gold mineralization and oxidized hydrothermal fluids. Economic Geology, **82**: 1172-1191.

Cathelineau, M. 1986. The akali hydrothermal metasomatism on granitic rocks: quartz dissolution and related subsolidus changes. Journal of Petrology, **27**: 945-965.

Card, K.D. 1990. A review of the Superior Province of the Canadian Shield, a product of Archean accretion. Precambrian Research, **48**: 99-156.

Cook, N.J. Chryssoulis, S.L. 1990. Concentrations of "invisible gold" in common sulfides. Canadian Mineralogist, **28**: 1-16.

Cox, S.F. Wall, V.J. Etheridge, M.A. Potter, P.F. 1990. Deformation and metamorphic processes in the formation of mesothermal vein-hosted gold deposits-examples from the Lachland Fold Belt in central Victoria, Australia. Ore Geology Reviews, **6**: 391-423.

Diment, R. Craig, S. 1998. Brewery Creek gold deposit, central Yukon. Yukon Exploration and Geology, 225-230.

Gibert, F. Pascal, M.L., Pichvant, M. 1998. Gold solubility and speciation in hydrothermal solutions: Experimental study of the stability oh hydrosulfide complex of gold (AuHS°) at 350 to 450°C at 500 bars. Geochemica et Cosmochemica Acta, **62,** 2931-2947.

Grant, J.A. 1986. The isocon diagram- a simple solution to Gresens' equation for metosomatic alteration. Economic Geology, **81**: 1976-1982.

Gresens, R.L. 1967. Composition-volume relationships of metasomatism. Chemical Geology, **2**: 47-65.

Groves, R. I. Goldfarb, R. J. Robert, F. Hart, C.J.R. 2003. Gold deposits in metamorphic belts: Overview of current understanding, outstanding problems, future research, and exploration significance. Economic Geology, **98**: 1-29.

Kerrich, R. Fyfe, W.S. 1981. The gold-carbonate association: source of CO_2 , and source of CO_2 fixation reactions in Archean lode deposits. Chemical Geology, **33**: 265-294.

Jamtveit, B. Ragnarsdottir, K.V. Wood, B.J. 1995. On the origin of grossular-andradite garnets in hydrothermal systems. European Journal of Mineralogy, **7**: 1399-1410.

Large, R.R. Danyushevsky, L. Hollit, C. Maselnnikov, V. Meffre, S. Gilbert, S. Bull, S. Scott, R. Emsbo, P. Thomas, H. Singh, B. Foster, J. 2009. Gold and trace element zonation in pyrite using a laser imaging technique: implications for the timing of gold in orogenic and Carling style sediment-hosted deposits. Economic Geology, **104**: 635-668.

_Linnen, R. Lin, S. Martin, R. Naderi, N. Davis, D. Hamilton, M. Creaser, R. Berger, B. Bannerjee, N. Wing, B. Wu, C. 2012. Section 3: A synthesis of the structure, petrology, geochronology and geochemistry of the Young-Davdson gold deposit and surrounding area; report in Results from the Shining Tree, Chester township and Matachewan Gold Projects and the Northern Cobalt Embayment Polymetallic Vein Project, Ontario Geological Survey, Miscellaneous Release-Data 294.

López-Moro, F.J. 2012. EASYGRESGRANT- a Microsoft Excel spreadsheet to quantify volume changes and to perform mass-balance modeling in metosomatic systems. Computers and Geosciences, **39**: 191-196.

Ludden, J. Hubert, C. 1986. Geologic evolution of the late Archean Abitibi greenstone belt of Canada. Geology, **14**: 707-711.

MacDonald, P.J. 2010. The geology, lithogeochemistry and petrogenesis of intrusions associated with gold mineralization in the porcupine gold camp, Timmins, Canada. Msc Thesis, Geology Department, Laurentian University, Sudbury, Ontario.

MacLean, W.H. Barret, T.J. 1993. Lithogeochemical techniques using immobile elements. Journal of Geochemical Exploration, **48**: 109-133.

Martin, R.D. 2012. Syenite-hosted gold mineralization and hydrothermal alteration at the Young Davidson deposit, Matachewan, Ontario. Msc Thesis, Earth Science Department, University of Waterloo, Waterloo, Ontario.

Micucki, E.J. 1998. Hydrothermal transport and depositional processes in Archean lode-gold systems: A review. Ore Geology Reviews, **13**: 307-321.

Miller. 2008. A contribution to the geology of the Thunder Creek property, northern volcanic zone, Abitibi subprovince, Canada: litholgies, metamorphism, overprinting hydrothermal alteration assemblages, precious metals mineralogy based on petrography, ore microscopy and scanning electron microscope investigation of selected drill core samples from drill holes TC-04-13, TC-07-27, TC-07-30, TC-07-36, TC-07-37 with comparison to the Timmins West Gold Property. Internal Lake Shore Gold Report, Timmins, Ontario.

McCuaig, T.C. Kerrich, R. 1998. P-t-t-deformation-fluid characteristics of lode gold deposits: evidence from alteration systematics. Ore Geology Reviews, **12**: 381-453.

Miyashiro, A. 1978. Nature of alkalic volcanic rock series. Contributions to Mineralogy and Petrology, **66**: 91-104.

Palin, J.M. Xu, Y. 2000. Guilt by association? Origins of pyritic gold ores in the Victory mesothermal gold deposit, Western Australia. Economic Geology, **95**: 1627-1634.

Reich, M. Kesler, S.E. Utsunomiya, S. Palenik, C.S. Chryssoulis, S. L. Ewing, R.C. 2005. Solubility of gold in arsenian pyrite. Geochemica, **69**: 2781-2796.

Rhys, D. 2010. Structural study of gold mineralization in portions of the Timmins Mine and Thunder Creek projects, Porcupine Mining District, Ontario. Internal Lake Shore Gold Corp Report, Timmins, Ontario.

Rhys, D. 2011. Technical report on the initial mineral resource estimate for the "Thunder Creek Property", Bristol Township, West of Timmins, Ontario, Canada. Internal Lake Shore Gold Corp Report, Timmins, Ontario.

Rhys, D. 2012. Evaluation of structural styles of mineralization in the ultramafic and footwall zones at the Timmins West Mine, with additional comments about the Thunder Creek mineralization. Internal Lake Shore Gold Corp Report, Timmins, Ontario.

Robert, F. 2001. Syenite-associated disseminated gold deposits in the Abitibi greenstone belt, Canada. Mineralium Deposita, **36**: 503-516.

Robert, F. Poulsen, K.H. 1997. World-Class Archaean gold deposits in Canada: an overview. Australian Journal of Earth Sciences, **44**: 329-351.

Shaheen, M. Gagnon, J.E. Yang, Z. Fryer, B.J. 2008. Evaluation of analytical performance of femtosecond laser ablation inductively coupled plasma mass spectrometry at 785nm glass with reference materials. Journal of Analytical Atomic Spectrometry, **23**: 1610-1621.

Sibson, R.H. Mcm. Moore, J. Rankin, A.H. 1975. Seismic pumping- a hydrothermal fluid transport mechanism. Journal of Geological Society, **131**: 653-659.

Sillitoe, R. 1972. A plate tectonic model for the origin of porphyry copper deposits. Economic Geology, **67**: 184-197.

Snyder, D.B. Bleeker, W. Reid, L.E. Ayer, J.A. Houle, M.G. Bateman, R. 2008. Tectonic and Metallogenic Implications of Regional Seismic Profiles in the Timmins Mining Camp. Economic Geology, **103**: 1135-1150.

Stanley, C.R. Russell, J.K. 1989. Petrologic hypothesis testing with Pearce element ratio diagrams: derivation of diagram axes. Contributions to Mineralogy and Petrology, **103:** 78-89.

Sylvester, J. P. 2008. Martix effects in laser ablation ICP-MS. Mineralogical Association of Canada Short Course, **40**: 67-78.

Thurston, P.C. 2002. Autochthonous development of Superior Province greenstone belts? Precambrian Research, **115**: 11-36.

Thurston, P.C. Ayer, J.A. Goutier, J. Hamilton. M.A. 2008. Depositional gaps in the Abitibi greenstone belt stratigraphy: a key to exploration for syngenetic mineralization. Economic Geology, **103**: 1097-1134.

William-Jones, A.E. Bowell, J.B. Migdisov, A.A. 2009. Gold in Solution. Elements, **5**: 281-287.

Appendix A

Drill Hole Information

This appendix contains the location and orientation of the diamond drill holes used for geochemical and thin section samples in the study.

Drill Hole Information:

Drill Hole	Azimuth	Dip	Easting (UTM)	Northing (UTM)	Elevation	Zone	Coordinate System
HWY-10-03	129.74	-51.68	457553.76	5357029.81	316.64	17	NAD83
HWY-11-12	128.98	-58.3	457427.17	5357054.25	317.54	17	NAD83
HWY-11-13	130.90	-49.2	457330.49	5357226.05	314.72	17	NAD83
HWY-11-20	132.10	-75.13	457335.87	5357289.53	316.84	17	NAD83
TC05-21-EXT	166.99	-43.98	458862.99	5357912.08	319.26	17	NAD83

Appendix B

Hand Sample Descriptions

This appendix contains a brief description of samples taken for geochemistry and petrography. The samples are from four diamond drill holes used to make a composite cross section through the Hwy-144 gold prospect. Samples are also from a transect taken across the Thunder Creek deposit on the 695m level of the Timmins West Mine. Finally samples are taken from the diamond drill hole TC-05-21-EXT which intersects the Thunder Creek stock and represents a least altered syenite.

Hwy 11-12			
Sample Number	Depth (m)	Purpose	Description
N969051	553.72-554	TS & Geochem	Grey, diabase dyke. Large epidote phenocrysts, only weakly altered.
N969052	491-491.25	TS & Geochem	Light grey, fine-grained sediment. Fracture filling fine-grained Py present. Well sorted, with no apparent bedding.
N969053	454.6-455	TS & Geochem	Altered sediment with extensive fracturing and infill veining. Fracture filling Py is present occupying 1% volume. Py is fine- to medium-grained, corroded and irregular.
N969054	436-436.4	TS & Geochem	Syenite dyke, hosted within volcanics. Red porphyritic syenite. Fine-grained disseminated Py, less than 1%. Hematite alteration along fractures.
N969055	434.87-435.12	TS & Geochem	Altered m. volcanic near shear zone. Foliation present, with thin syenitic veinlets parallel to foliation. 1% dissem fine-grained Py.
N969056	410-410.3	TS & Geochem	Least altered m. volcanic. No foliation, dark green with some light green epidote alteration.
N969057	383-383.3	TS & Geochem	Least altered m. volcanic. Dark green with light green epidote alteration.
N969058	369.8-370.2	TS & Geochem	Syenite, near contact with m. volcanic. Red, highly fractured with large (0.3cm) feldspar phenocrysts. Phenocrysts are fractured with red hematite staining.

			Porphyritic. Chlorite fills fractures, less than 1% fine-grained dissem Py.
N969059	350-350.4	TS & Geochem	Red syenite, fine-grained (1mm). Small qtz-carb veinlets occupying 1% volume. No visible sulphides, very homogenous.
N969060	329.6-330	TS & Geochem	Red porphyritic syenite. Red potassic/hematitic alteration overprint. Thin qtz-carb veinlets (5%) which appear barren. No visible sulphides.
N969061	311.6-312	TS & Geochem	Red porphyritic syenite with pervasive ankerite alteration occurring as stringers. No visible sulphides, qtz-carb veinlets occupying 1%.
N969062	291.6-292	TS & Geochem	Red porphyrtitic syenite with larger feldspar phenocrysts up to 1.0 cm. Ankerite stringer alteration. 5% qtz-carb veinlets perpendicular to core axis.
N969063	267.1-267.5	TS & Geochem	Red porphyrtitic syenite with smokey qtz phenocrysts. Fracture filling hematite, ankerite stringers. 2% qtz-carb veinlets with no visible sulphides.
N969064	252.4-252.8	TS & Geochem	Extensive hematite/potassic alteration occurring as a bright red equigranular, fine-grained syenite. Possible foliation with trace amounts of fine-grained dissem Py.
N969065	232.56-233	TS & Geochem	Red porphyritic syenite, with fractured phenocrysts. Minor hematite/potassic alteration. No visible sulphides with trace amounts of qtz-carb veinlets.
N969066	214.8-215.19	TS & Geochem	Very red porphyritic syenite. Tabular feldspar phenocrysts. Fracture filling Py (3%) occurring as med-coarse grained corroded and irregular crystals.
N969067	195.1-195.5	TS & Geochem	Red porphyritic syenite. Thin 0.1cm to 0.3cm yellow ankerite-carb veinlets. Py is associated with veinlets (5-8% total Py). Py is mainly cubic and corroded with mainly vein hosted.

N969068	174.6-175.1	TS & Geochem	Red porphyritic syenite with patchy hematite/potassic alteration. Small amount of mafic contamination (dark minerals) with a small amount of qtz-carb stringers. Ankerite stringers present as well. Py is mainly cubic sometimes irregular. Med-coarse grained and corroded.
N969069	158-158.4	TS & Geochem	Red syenite, equigranular. Both alb-carb and qtz-carb veinlets (2% total) Small smokey qtz grains. No visible sulphides.
N969070	143.4-143.85	TS & Geochem	Red porphyritic syenite. Highly fractured. Fractures are filled with chlorite and hematite stringers. Alb-carb veinlets contain cubic Py (1%) and are corroded. This portion of the syenite is near the contact with mafic volcanic xenoliths.
N969071	122.55-122.95	TS & Geochem	Porphyritic red syenite. Mafic phenocrysts, and some smokey qtz. Slight foliation/allignment of feldspar phenocrysts. Qtz-carb veinlet (1%) and barren. Trace amounts of fine-grained dissem Py.
N969072	104.8-105.2	TS & Geochem	Red, fine grained syenite woth resorbed/altered phenocrysts. Extensive Hem/Pt alteration Small car-ank stringers. Locally a strain zone (5 cm wide) has a foliation 60 deg to core axis.
N969073	90.7-91.1	TS & Geochem	Red, strongly altered syenite. Pervasive Fe-carb alteration. Deformed qtz-carb veinlets. Chlorite infilling fractures. Mostly equigranular. No visible sulphides.
N969074	70.6-71	TS & Geochem	Pink, porphyritic syenite. Some mafic grains, k-spar phenocrysts. No veining, no sulphides.
N969075	47.6-48	TS & Geochem	Pink syenite near mafic contact. Porphyritc with large tabular feldspar phenocrysts. Chlorite infilling fractures.

N969076	28.2-28.6	TS & Geochem	Red porphyritic syenite. Chlorite infilling fractures with qtz-carb veinlets. No visible sulphides patchy Hem/Potassic alteration.
N969082	170.8-171.29	TS & Geochem	Min Zone 1. Porphyritic syenite. Mafic phenocrysts. Coarse Py (5%) fracture filling associated with alb-carb veins. Minimal qtz-carb veins. Ankerite stringers and minor dissem Py.
N969083	220.3-220.7	TS & Geochem	Min Zone 2. Red porphyritc syenite. Qtz-carb veinlets 15%. Coarse Py (5%) is mostly dissem. Py has qtz inclusions. Minor amounts of Py are qtz-carb vein hosted, minor py in alb-carb vein. Py is corroded and irregular.
N/A (thin Section only)	156-156.3	TS	Min Zone 3. Red equigranular. Patchy Hem/Potassic alteration. Abundant 5% sulphides. Both Cpy and Py present. Py is mainly found in coarse disseminated clots that are corroded and irregular. To a lesser extent Py is found filling fractures (medium-grained). This Py is usually found with qtz-carb stringers and veinlets. A small portion of the Py is found disseminated (med grained).
N/A (thin Section only)	171.7-172	TS	Min zone 4. Pale pink porphyritic syenite. Abundant qtz-carb veins to veinlets (15-20%). Qtz-carb and Py have a strong association. Total Py content is 4%. Py is mainly found as inclusions and on the margins of qtz-carb veinlets, med-coarse grained, irregular and corroded. Small amounts of fine-grained disseminated Py are present as well.
N/A (thin Section only)	185-185.3	TS	Min zone 5. Pale pink to dark red syenite. Patchy Hem/Potassic alteration. Unit is porphyritic in the pale pink portion. Total Py content is 3-4%. Py is mainly fracture controlled and medium-grained.

Hwy 11-20			
Sample Number	Depth (m)	Purpose	Description
N969077	197.1-197.4	TS & Geochem	Massive dark green, fine-grained pyroxenite. Chlorite fractures. Least altered sample, magnetic.
N969078	224-224.4	TS & Geochem	Green, fine-grained pyroxenite with large magnetite phenocrysts. Large pink slender phenocrysts (Apatite?) Some small carbonate stringers. Dissem fine-grained Py (1%). Biotite clots present as well.
N969079	250-250.4	TS & Geochem	Green, fine-grained pyroxenite with magnetite rich bands. Bands range from 2-7 cm thick. Carbonate stringer veins occupy 1% of whole rock.
N969080	313-313.4	TS & Geochem	Green fine-grained pyroxenite with large garnet domains (10-20cm). More pervasive carb stringers (15%) of rock.
N969081	325.5-326	TS & Geochem	Pyroxenite near structural zone. More pervasiv carb stringer alteration (15%). Green and fine grained. Large biotite and magnetite phenocrysts. No visible sulphides.
N969084	329.9-330.5	TS & Geochem	Mineralized sample. Strongly altered/sheared pyroxenite unit. The rock is strongly bleached by carbonate alteration. Compositional banding is present and the mafic rock is fine-grained. There is a trace amount of Py (fine-grained) associated with qtz-carb veinlets. Py is usually found on the vein margin.
N969085	338-338.5	TS & Geochem	Mineralized sample. Red syenite. Fine-grained, equigranular with pervasive Hem/Potassic alteration. 15-20% ankerite stringers. Fine-grained Py found in the ankerite stringers, coarse-grained Py associated with fractures. Coarse Py forms clots. No qtz-carb veinlets. Py is mainly cubic and appears to have K-spar

			inclusions? Total Py content is about 5%.
N969086	360.5-361.05	TS & Geochem	Red, slightly porphyritic syenite. Intense, pervasive Hem/Potassic alteration. Chlorite is found filling fractures, some ankerite-carb stringers giving a localized foliation at 120 degrees tca. Mainly fine-grained, with no sulphides or qtz-carb veinlets.
N969087	385.75-386.3	TS & Geochem	Pink-red porphyritic syenite. Fractures filled with chlorite. Smokey qtz and mafic grains. Grains are approximately 1mm. Some Alb-carb veinlets (yellowish) (3-5%). No visible sulphides.
N969088	408.7-409.4	TS & Geochem	Red, porphyritic syenite. Patchy Hem/Potassic alteration with minor chlorite infilling stringer sized fractures. Fe-carb stringers. Smokey qtz phenocrysts. No visible sulphides. Qtz-carb veinlets are barren and account for 1-3% of total rock volume.
N969089	435.4-436	TS & Geochem	Dark red syenite. Phaneritic (1mm phenocrysts) with Hematite stringers and chlorite filling fractures. 1% thin qtz-carb veinlets. Trace amount of Py found in veinlet.
N969090	455.5-456	TS & Geochem	Intensly hematized/potassically altered syenite. Porphyritic with large phenocrysts. Chlorite fills fractures, small mafic grains. No veining, no sulphides.
N969091	478-478.5	TS & Geochem	Red, fine-grained syenite. Extensive Hem/Potassic alteration. Equigranular, with chlorite filling fractures. Trace amounts of carbonate stringers. No visible sulphides.
N969092	496.3-496.75	TS & Geochem	Porphyritic, pink syenite. Large phenocrysts along with ankerite and hematite stringers. Smokey qtz phenocrysts. 1% qtz-carb veinlets. Py (fine-grained) found inside the veinlet. Trace amounts of Py.
N969093	521-521.5	TS &	Porphyritic syenite with larger (0.5-1.5cm) white feldspar phenocrysts. Phenocrysts

		Geochem	are fractured with red staining. Thin, 1mm qtz-carb veinlets that contain Cpy. Trace amount of sulphides.
N969094	546.5-547.05	TS & Geochem	Mineralized sample. Porphyritic syenite, with large phenocrysts. Hem/Potassic alteration found as stringer veins. Qtz-carb veinlet (0.4cm) wide with Py associated. Veinlets account for 3-5% volume of the sample. Py is coarse and generally cubic with qtz inclusions. Py accounts for 3% of the rock and is mainly associated with qtz-carb veinlets.
N969095	564.5-565	TS & Geochem	Mineralized sample. Porphyritic pink-purple syenite with large phenocrysts. Py is found in veinlets and fractures. Py is present in both qtz-carb veinlets and alb-carb stringers. Py is fine- to coarse-grained accounting for 5% total rock volume. Smokey qtz grains and inclusions of qtz in Py.
N969096	575-575.5	TS & Geochem	Mineralized sample. Red, slightly porphyritic syenite. Carbonate stringers are present along with patchy orange ankerite staining. Qtz-carb veinlets occupy 3-5%. Coarse Py is associated with veinlets. Py is corroded, with inclusions of qtz, and usually irregular in shape. Py accouts for 4-5% of the sample, with a minor amount occurring as fine-grained disseminated Py.
N969097	621-621.5	TS & Geochem	Strongly altered (Pot/Hem) syenite. Locally there are large phenocrysts (1cm) of white feldspars. Phenocrysts are fractured and have hematite staining. There are both stringers of hematite and qtz-carb stringers present. Qtz-carb stringers appear barren of sulphides. Chlorite is found filling fractures.
N969098	659.15-659.65	TS & Geochem	Mineralized sample. Red porphyritic syenite, highly fractured. Fractures are occupied by qtz-carb veinlets and chlorite stringers. Two sets of qtz-carb veinlets, perpendicular to eachother. Py is primarily associated with one orientation of the

			vein sets. However most veinlets appear barren. Py is coarse and often found associated with chlorite filled fractures. Qtz-carb veinlets occupy 5-8%. Py occupys 4-5% and is corroded.
N969099	688.5-689	TS & Geochem	Red, strongly altered syenite. Porphyritic, with apparent deformed stringer veins that appear ductile. These fractures are filled with stringer chlorite. Alb-carb (yellow) veinlets found along fractures. Medium-grained irregular Py is found in chlorite filled fractures. (1%). The syenite unit is found near the basal contact with mafic volcanics.
N969100	717.2-717.7	TS & Geochem	Dark green, fine-grained mafic volcanic. Epidote stringers. Minor carbonate stringer alteration. Fracture filling Py is present as fine-grained clots accounting for 0.5%. Possible garnets fill fractures present in this sample as well.
Hwy 10-03			
Sample Number	Depth (m)	Purpose	Description
N969101	19.3-19.85	TS & Geochem	Red, slightly porphyritic syenite. Hem/Ank fractures, pervasive alteration. Chlorite is found filling fractures (stringers). Qtz-carb veinlets are present, less than 1% rock volume. Trace amount of fine-grained dissem Py.
N969102	34.7-35.36	TS & Geochem	Red, equigranular syenite. Locally intense Hem/Ank stringers overprinting syenite. Fracture controlled Py-Cpy. Fine-med grained Py found associated with stringers. Py-Cpy appear corroded and irregular. One qtz-carb veinlet with possible tourmaline/specularite (needle shape). Fracture filling chlorite. Total Py-Cpy content is 2-3%.

N969103	54.4-54.9	TS & Geochem	Mineralized Zone. Red, equigranular syenite. Strong Hem/Potassic alteration. Locally intense stringers of Hem/Ank. Mafic and smokey qtz grains. Fine- to med-grained Py is present as clots (2-4% rock volume).. Qtz-carb veinlets account for 1-3%. Veinlets overprint alteration and are late. Vein Py is irregular and corroded. Minor amounts of fine-grained Py are disseminated. Disseminated Py is corroded and cubic. Finally, Py is present on the margin of 1cm Ank alteration zone.
N969104	63.9-64.4	TS & Geochem	Mineralized Zone. Red, strongly altered syenite. Porphyritic, with intense carbonate-Hem/Potassic alteration. Carbonate veins/veinlets (1cm) Host Py and Cpy. Veins are highly deformed and irregular. Carbonate veins account for 5% total rock volume and host a black mineral that may be tourmaline/specularite. Py is coarse, mainly cubic, occasionally irregular. Py is mainly disseminated, sometimes associated with qtz-carb veinlets. Py is corroded with qtz inclusions.
N969105	95.9-96.4	TS & Geochem	Red, porphyritic syenite. Minor mafic contamination, from nearby (1m) mafic unit. Tabular white feldspar phenocrysts (2mm). Pervasive Hem/Ank stringers. Chlorite is present filling fractures. Trace amount of disseminated Py. Trace amount of Py along chlorite fractures. 1 qtz-carb veinlet hosts a spec of Py.
N969106	106.1-106.7	TS & Geochem	Mineralized Zone. VG seen as an inclusion in med-grained, irregualr Py. Py is corroded and disseminated. Red porphyritic syenite. Patchy Hem/Potassic alteration. Hematite stringers are locally intense. Py associated with Ank/Hem stringers (med-fine grained). Py associated with qtz-carb veinlets (coarse-grained). Disseminated Py (med-grained). Total Py content is 5%. Chlorite is present filling fractures. Py is present occasionally as clots, but often disseminated.
N969107	124.4-125	TS &	Mineralized Zone. Red porphyritic syenite. Locally pervasive chlorite filled fractures. Some Py is proximally associated with these fractures. Small stringers of

		Geochem	qtz-carb have coarse Py associated. Med-grained dissem Py accounts for majority of Py present. Py is mainly corroded, med-grained and cubic. Occasionally Py is irregular. Py occasionally has inclusions of qtz.
N969108	142.15-142.6	TS & Geochem	Red, porphyritic syenite. Qtz-carb veinlets (3-5%) cut hematite stringers. Black mineral in veinlets? Tourmaline/specularite? White feldspar grains found in veinlet. Vein is barren of sulphides. Trace amount of fine-grained Py on vein margin. Rock is fairly homogenous, minimal alteration.
N969109	165.1-165.7	TS & Geochem	Red, mostly equigranular syenite. Fine-to medium-grained. Locally, pervasive/intense Hem stringers. Qtz-carb veinlets account for 5% and have irregular med- to coarse-grained Py along the margin. Fine to- med-grained Py is present inside Hem stringer network. Minor amounts of dissem, cubic, fine-med Py.
N969110	181.5-182	TS & Geochem	Strong Hem/Pot overprint on a fine grained, equigranular felsite. Small dykelets of porphyritic syenite are present (5-8%). Chlorite is present filling fractures. Fine-grained Py is associated with small Hem veinlets? No qtz-carb veins. Looks similar to felsic dyke in TC 695 UG.
N969111	193.5-194	TS & Geochem	Mineralized Zone. VG seen as inclusion in Py on margin of qtz-carb veinlet. Qtz-carb veinlet accounts for 15-20% of the rock. Porphyritic red syenite, with smokey qtz grains (1-2mm) Py is strongly associated with qtz-carb veinlets. Py is coarse, cubic and corroded. Fine-grained Py appears to be related to a deformed chlorite band. Band cross cuts/overprints qtz-carb vein. Total Py content 4%.
N969112	213.5-214.05	TS & Geochem	Locally porphyrtic but also equigranular syenite. Pervasive and intense Hem/Pot alteration. Minor fractures are present, mainly filled by chlorite. Qtz-carb veinlets (3% rock volume). Fine-grained Py is found in these veinlets. A minor portion of Py

			present is disseminated. Total Py content is about 1%.
N969113	235.5-236	TS & Geochem	Pink to purple/black syenite. Dark colour is due to mafic minerals present as phenocrysts. The syenite is also becoming proximal to basal mafic contact. The syenite is equigranular and medium grained. Fractures are filled by chlorite, and ank-carb stringers. There is no foliation present, and no visible sulphides were seen.
N969114	251-251.5	TS & Geochem	Very red (bright) porphyritic syenite. White fldspars phenocrysts are 1-3mm in size. Significant fracturing is present and filled by chlorite stringers. There is a strong-uniform, pervasive Hem/Pot alteration. What is the yellow stringer mineral?
N969115	266-266.6	TS & Geochem	Red, porphyritic syenite near contact with diabase dyke. Moderately intense, uniform Pot/Hem alteration. Unit is highly fractured. Fractures are almost exclusively filled by chlorite. Minor qtz-carb veinlets(2-3%) with no visible sulphides. Phenocrysts within the syenite are fractured and filled with hematite.
N969116	332.2-332.5	TS & Geochem	Dark green to dark grey, fine-grained, massive mafic volcanic. Carbonate and epidote alteration. Mainly present as stringers, accounting for 15% of the total rock. There is a trace amount of disseminated fine-grained Py.
N969117	357.7-358	TS & Geochem	Dark green, medium grained massive mafic volcanic. Epidote alteration forming haloes present. Unit is wekaly to non magnetic. Some k-spar grains are found near alteration zones. No visible sulphides or qtz-carb veinlets. Minimal carb stringers. Sample represents least altered m. volcanic.
N969118	371.9-372.4	TS & Geochem	Grey, fine-grained iron stained altered sediment. Strong foliation present, perpendicular to the core axis. Ankerite stringers are found parallel to the foliation. Crenulations are present in the foliation. Py is present in qtz-carb veinlets. Py present in ankerite stringers is fine-grained. Ankertite alteration overprints the qtz-

			carb veinlets. Total Py content is 1%.
N969119	373.2-373.7	TS & Geochem	Syenite dyke cross cuts altered sediments. Red, medium-grained and equigranular. Fractures are filled with chlorite and ankerite. Qtz-carb veinlets (2-4%) have a small amount of fine-grained Py. There are clots of disseminated, irregular fine-grained Py. Total Py content is 2% and mostly disseminated.
N969120	400.7-401	TS & Geochem	Weakly altered sediment. Grey, fine-grained. Fractures are filled by chlorite and carbonate. Fine-grained Py is present in fractures along margins, intergrown with chlorite. There is a local foliation and alignment of fracture planes. 1% total Py content.
N969121	425-425.4	TS & Geochem	Least altered sediment. Grey, fine- to medium-grained poorly sorted wacke. No visible bedding. Tiny fracture planes visible. These planes contain abundant sulphides (5-8%). The sulphides range from bornite to chalcopyrite to pyrite. These fracture planes are schistose.

Hwy 11-13			
Sample Number	Depth (m)	Purpose	Description
N969122	38-38.35	TS & geochem	Mafic Vol. least altered. Green, fine-grained and massive. Remnants pillow selvages. Rock is highly fractured and filled in with carbonate and chlorite stringers. There

			appears to be some replacement of pink k-spar within carbonate.
N969123	113-113.45	TS & geochem	Pyroxenite unit near contact with diabase dyke. Medium to fine grained, massive, dark green rock. Magnetic, with biotite grains. Carbonate stringers are found filling fractures (3%). Some red alteration stringers (Hematite?) Least altered, no foliation.
N969124	260-206.5	TS & geochem	Altered pyroxenite. More intense carbonate alteration. Pink k-spar veinlets (10-15%). Medium-grained, dark green to black massive rock. Magnetic with biotite phenocrysts. Appears to be some epidote alteration. Unit is close to syenite dyke (10-15m)
N969125	271.8-272.35	TS & geochem	Syenite dyke within altered pyroxenite unit. Dyke is proximal to main syenite body. Unit is megacrystic and trachyitic. Feldspar phenocrysts are +3cm. Phenocrysts are fractured with hematite stringers filling the space. Dissem coarse Py (1%) is irregular and corroded. Some fracture filling Py is found associated with chlorite. Patchy Hem/Pot alteration.
N969126	287.6-288.15	TS & geochem	Syenite at the margin of the syenite body. Near pyroxenite contact. Porphyritic, red, with strong Hem/Pot alteration. Hematite stringers fill fractures. Coarse Py found within Ank/Chlorite bands (0.5cm). Fine Py is found in Ank stringers. Medium Py is associated with qtz-carb veinlets, and medium-grained Py is disseminated. Total Py content is 2-3%. Qtz-carb veinlet content is 5%.
N969127	304.5-305	TS & geochem	Mineralized zone. Porphyritic red syenite with patchy localized Hem/Pot alteration. Qtz-carb veinlets occupy 5%. Py content is 3-4%. Py is associated with qtz-carb veinlets, and is coarse, irregular with qtz inclusions. Py is also found associated with chlorite bands and fractures. Py is coarse and irregular. Py is also disseminated, coarse and irregular. Alb-carb veinlets 2%

N969128	324.9-325.3	TS & geochem	Red porphyritic syenite. Uniform, moderate Hem/Pot alteration. Grain size are 1-2mm. Black mineral in qtz-carb veinlets? Veinlets occupy 3%. Ankerite stringers fill fractures. Py occupies 0.5%, is medium grained and disseminated. Py is corroded and usually cubic.
N969129	339.5-340	TS & geochem	Red, mainly equigranular syenite. Disseminated Galena? Fine-grained disseminated Py (less than 1%). Med-grained Py associated with yellow Alb-carb veinlets (Less than 1%). Qtz-carb veinlets (2%) appear barren. Minor amount of fracture filling chlorite.
N969130	359.55-360.15	TS & geochem	Red porphyritic syenite. Strong interstitial hematite stringers. The majority of phenocrysts appear to be smokey qtz. Fine Py is present associated with hematite stringers (fracture control). Qtz-carb veinlets have minor Py on margins. Veinlets occupy 2-3% total rock volume. Py is evenly disseminated, not in clusters.
N969131	382.9-383.6	TS & geochem	Mineralized sample. Strongly altered (Pot/Hem) porphyritic syenite. Intense zones of alteration overprint equigranular syenite. Intensely fractured and filled with Hematite and minor qtz-carb veining (1%). Veinlets appear barren of mineralization. Trace amount of dissem, medium grained cubic Py. Free gold?
N969132	399.5-400	TS & geochem	Porphyritic red syenite. Moderate Hem/Pot alteration. Hematite stringers fill in fractures. Qtz-carb veinlets (8-10%) are present with a trace amount of sulphides (Ga-Py). Ankerite vein (4cm across). No visible dissem Py.
N969133	403.2-403.8	TS & geochem	Mineralized Sample. Red equigranular syenite. Strong overprint of Ank-Hem/Pot alteration. Fracture controlled Py fills chlorite fractures. This cross cuts qtz-carb veinlets. Qtz-carb veinlets appear barren of Py, but may have specularite? 2 sets of qtz-carb veinlets. Py is found as med to fine grained clots, strongly related to Ank

			stringers/chlorite fracture fills. Py is corroded and irregular. Qtz-carb veins (10%)
N969134	423.4-423.8	TS & geochem	Porphyritic red syenite. Moderate Hem/Pot alteration. Extensive fractures, filled by chlorite that cuts across qtz-carb veinlets. Chlorite fractures host fine-grained Py (1%). Py is corroded and irregular. Qtz-carb veinelts occupy 2% modal rock volume. Yellow-orange Ank-carb stringers occupy 2% modal rock volume.
N969135	444-444.5	TS & geochem	Red porphyritic syenite. Strong Hem/Pot alteration. Trace qtz-carb veinlets, no visible sulphides. Homogeneous appearance, Poor RQD, very broken up/fractured.
N969136	458-458.6	TS & geochem	Mineralized sample. Highly altered and bleached. Unrecognizable protolith. Syenite? Mafic unit? Brecciated texture filled by chlorite and qtz-carb veinlets. Foliated. Qtz-carb veinlets hosts Cpy and specularite? Py is found associated with chlorite in large (1-3cm) fine-grained clots.
N969137	481.2-481.9	TS & geochem	Pink-orange porphyritic syenite. Qtz-carb veinlets occupy 5% and appear to be barren of mineralization. Minimal fracturing and minimal hematite stringers. Fairly massive and homogeneous. MAY be the least altered syenite, within the suite.
N969138	511.7-512.3	TS & Geochem	Syenite near contact with mafic volcanics. Red, prophyritic with moderate Hem/Pot alteration. 5% qtz-carb veinlets that appear barren. No visible sulphides. Hematite stringers, no fracture filling chlorite.
N969139	532.2-533	TS & Geochem	Altered mafic volcanics. (20% sulphides, Cpy and Py). Pyrite forms fracture filling thick clots or bands. Py is fine-grained, but swarms. Py veins are 0.2 to 1.5 cm thick. Py is corroded and contains interstitial Cpy. Mafic volcanic is dark green to black and fine-grained. There appears to be a slight foliation. Large black phenocrysts? Some minor syenitic stringers. Carbonate alteration increases with depth through the

			sample, none at the top.
N969140	589.2-589.7	TS & Geochem	Altered sediment. Compositionally banded and crenulated. Fine-grained grey to pink rock. Pink could be alteration from nearby syenite. Ank staining, parallel to foliation. Fine-grained Py is found parallel to the foliation. Minor chlorite found filling fractures. Total Py content is 1%
N969141	613.3-614	TS & Geochem	Weakly altered sediment. Grey fine-grained. Slightly bleached and extensively fractured. Fractures are filled with chlorite and Py/Cpy. Py is corroded and med-coarse grained. Sulphides account for 10% of the rock (70%Py/30%Cpy)
N969142	630.6-631	TS & Geochem	Least altered sediment. Grey, fine-grained. Massive with minimal fractures. No visible sulphide mineralization. Small calcite veinlets (less than 1%).

Thunder Creek 695m			
Sample Number	Distance from survey station (m)	Purpose	Description
N605041	-30.5	TS & Geochem	Dark green biotite rich pyroxenite. Massive, equigranular, medium grained.
N605042	-20	TS &	Dark green massive pyroxenite, medium grained, unaltered.

		Geochem	
N605043	-16.5	TS & Geochem	Dark green massive pyroxenite medium grained, unaltered.
N605044	-14	TS & Geochem	Altered pyroxenite, foliated (shear zone) with 1% dissem fine-grained Py (parallel to foliation).
N605045	-9	TS & Geochem	Altered pyroxenite, foliated with potassic alteration overprint.
N605046	-3	TS & Geochem	Rusk Zone, tan (sericite/carbonate) alteration overprinting mylonite foliation.
N605047	1.5	TS & Geochem	Rusk Zone, Potassic alteration overprint with galena stringers, mylonite fabric
N605048	5.1	TS & Geochem	Rusk Zone, Tan alteration overprinting mylonite fabric, 1% dissem fine-grained Py
N605049	8.2	TS & Geochem	Syenite dyke. Red, hematite/potassic alteration. Equigranular with 2% dissem coarse Py
N605050	11	TS & Geochem	Rusk Zone, foliated mylonite, magnetite bands.
N605051	13	TS & Geochem	Syenite at contact with Rusk. Pink, equigranular with 1% med-grained dissem Py.

N605052	18.5	TS & Geochem	Syenite. Pink, equigranular with 2% med-grained dissem Py. (In area of grab sample mineralization)
N605053	29.4	TS & Geochem	Syenite. Pink, silicified equigranular with 1% coarse dissem Py. (low-grade grab sample mineralization)
N605054	37.2	TS & Geochem	Syenite. Pink, silicified, equigranular with 1% med-grained dissem Py. (Significant mineralization)
N605055	47.2	TS & Geochem	Syenite. Pink-white, silicified, equigranular with 2% med-coarse dissem Py & Cpy (mineralized)
N605056	56.8	TS & Geochem	Syenite. Pink-white, silicified, equigranular with 1% med-grained dissem Py.
N605057	63.3	TS & Geochem	Syenite. Red, equigranular with 1% dissem Py.
N605058	65	TS & Geochem	Syenite. Pink, equigranular, silicified? With 1% med-grained dissem Py. At contact with mafic volcanic.
N605059	66	TS & Geochem	Mafic volcanic, near contact with syenite. Foliated/tan sericite alteration. 2% dissem fine-grained Py
N605060	75.25	TS & Geochem	Mafic volcanic, altered, dark green.
N605061	77	TS & Geochem	Mafic volcanic, dark green with light green epidote alteration, least altered.

Thunder Creek 280m			
Sample Number	Location	Purpose	Description
M191366	280L RZ3a Rnd 63 RW	TS & Geochem	Background syenite, no veining. Deep red (hematite) medium-grained, homogeneous. 1% med grained dissem Py
M191367	280L RZ3a Rnd 30 RW	TS & Geochem	Rusk Zone, Strongly foliated with strong ankerite alteration parallel to the foliation. Syenitic dykelets, 3% med grained Py parallel to foliation, qtz veinlets
M191372	280L RZ3a Rnd 16 LW	TS & Geochem	Background syenite. Deep dark red colour, 1% med-coarse grained dissem Py. High vein intensity in the area. Homogeneous.
M191374	280L RZ3a Rnd 07 RW	TS & Geochem	Background syenite, Red and homogeneous with a trace amount of fine- to medium-grained dissem Py.
M191376	280L RZ3a Rnd 16 RW	TS & Geochem	Rusk sample. Strong foliation, strong ankerite/sericite alteration. Syenitic dykelets parallel to the foliation. No sulphides.

Thunder Creek Stock			
Sample Number	Depth (m)	Purpose	Description (1= least altered, 4=strongly altered)
Q694651	473.8-474	TS & Geochem	(2) Slightly altered syenite. Dark purple to grey with "lighter" alteration coming through in an irregular pattern. The rock is medium-grained and porphyritic.
Q694652	465.6-465.7	TS	Thin section only. Good sample of alteration bands cutting the syenite.
Q694653	464.25-464.65	TS & Geochem	(1) Least altered syenite. Primary biottie phenocrysts (med-grained). Medium-grained feldspars, Grey to purple in colour and equigranular.
Q694654	824.2-824.8	TS & Geochem	(2) Slightly altered syenite. Mafic biotite crystals, medium-grained and equigranular. Purple-grey in colour. There is a small amount of pink alteration penetrating the rock.
Q694655	820.9-821.1	TS & Geochem	(3-4) Moderately altered syenite. Full destruction of mafic phenocrysts. More pervasive pink colour with some hematite alteration along fractures. Med-grained, equigranular. Trace amount of med Py and small qtz veinlets.

Q694656	808.5-809	TS & Geochem	(3) Intermediate alteration. Dark zones of the syenite are being overprinted by lighter domains. Small unknown med-grained mafic phenocrysts. Pink to grey in colour. Med-grained equigranular.
Q694657	802.4-802.6	TS & Geochem	(4) Strongly altered syenite. Pink to red in colour. Full destruction of mafic phenocrysts. Red hematite alteration present in wisps (fractures?). Medium-grained and equigranular (looks similar to Hwy-144).
Q694658	461-461.5	TS & Geochem	(4) Strongly altered syenite. Pink to red in colour. Some quartz veinlets intrude (not sampled). Full destruction of mafic phenocrysts. Silicified?
Q694659	586.5-587	TS & Geochem	(1) Least altered syenite. Purple to grey in colour, medium grained and equigranular. Primary biotite phenocrysts, no visibile hematitic or potassic alteration.

Appendix C

Thin Section Descriptions

In this appendix thin section descriptions for each of the samples from Hwy-144, Thunder Creek Mine and the Thunder Creek stock are compiled. Due to the length and large file size, these descriptions and the pictures included are available on a jump drive provided by the author. If you are accessing this document from outside the University of Western Ontario please contact the author for any necessary thin section descriptions.

Appendix D

Whole Rock Geochemical Data

This appendix contains the whole rock geochemical data for each of the samples outlined in Appendix B. The appendix contains whole rock geochemical data for over 200 samples analyzed for 64 elements. Geochemical data was collected from Hwy-144, Thunder Creek Mine and the Thunder Creek stock. Due to the amount of data, a master excel file has been created to view the data. If you are retrieving this document from outside of the University of Western Ontario you will have to contact the author to get a copy of the excel file. Along with the geochemical data, raw rock density data is also presented in this appendix. This data was used to perform the Gresens' mass balance calculations.

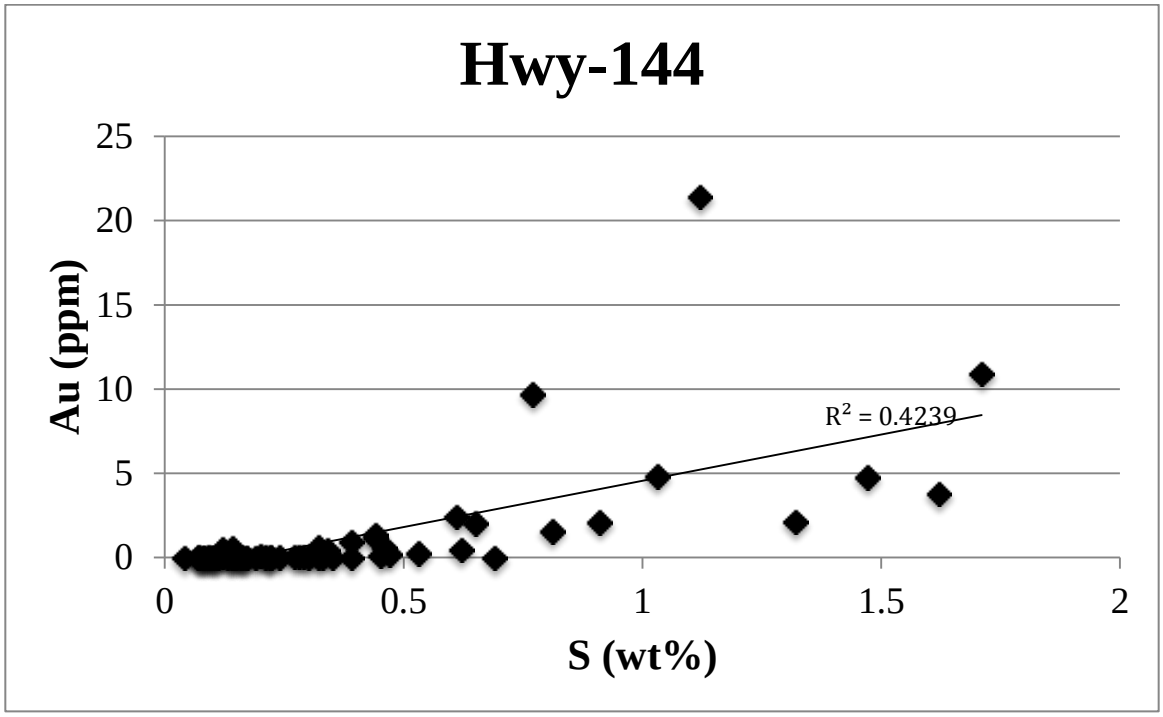

Figure 1: Correlation between sulfur and gold in whole rock geochemical samples from Hwy-144.

Appendix E

Electron Microprobe Data

In this appendix electron microprobe data is presented. The electron microprobe was used to create trace element maps of pyrite grains and to determine the mineral composition of selected minerals. Trace element map images have been stored on a USB jump drive accompanying the thesis. IF you have accessed this document from outside of the University of Western Ontario you will need to contact the author to obtain these images. Mineral chemistry data is presented below.

Albite	TC Stock Q694659 W. Altered	TC Stock Q694659 W. Altered	TC Stock Q694659 W. Altered	TC Stock Q694658 Altered	Hwy-144 N969133 Mineralized	Hwy-144 N969133 Mineralized	Hwy-144 N969144 W. Altered	Hwy-144 N969144 W. Altered	Hwy-144 N969144 W. Altered
SiO_2	68.30	68.55	67.87	68.34	69.00	67.98	68.53	68.38	68.39
Na_2O	9.74	8.05	8.47	9.65	8.05	10.13	9.14	9.23	9.37
Al_2O_3	21.17	21.41	21.34	20.1	20.84	20.81	21.29	20.81	20.86
FeO	0.01	0.28	0.21	0.14	0.44	0.47	0.1	0.05	0.04
MnO	0.01	0.02	0.02	0.02	-0.02	-0.03	0.02	-0.04	0
K_2O	0.07	0.13	0.27	0.09	0.06	0.08	0.06	0.29	0.13
BaO	-0.01	0.03	0.04	-0.01	-0.01	0.00	0	0	0.02
CaO	0.09	0.10	0.33	0	0.02	0.03	0.08	0.03	0.02
TiO_2	0.01	0	0.003	0	0.01	0	0	0.01	0.01
Total	99.38	98.56	98.55	99.29	98.37	99.47	99.22	98.76	98.82

	Hwy-144	Hwy-144	Hwy-144	Hwy-144	Hwy-144	Hwy-144	TC 280m	TC 280m	TC 280m
	N969098	N969098	N969106	N969106	N969126	N969126	M191372	M191372	M191374
Albite	Mineralized	Mineralized	Mineralized	Mineralized	?	?	W. Altered	W. Altered	W. Altered
SiO_2	68.04	67.95	68.15	68.53	68.25	68.29	68.23	67.95	67.97
Na_2O	8.63	9.70	9.71	9.11	8.81	9.22	8.68	8.55	8.77
Al_2O_3	20.15	19.98	20.26	20.83	20.17	21.14	20.87	21.08	20.71
FeO	0.41	0.01	0.01	0.012	0.47	0.07	0.23	0.15	0.21
MnO	0.01	-0.02	-0.01	0	0.01	0	-0.01	-0.02	0
K_2O	0.1	0.07	0.05	0.07	0.04	0.08	0.06	0.08	0.08
BaO	-0.02	-0.01	-0.01	0.01	0.01	0.02	0	0	0
CaO	0.03	0.03	0.01	0.03	0.023	0.17	0.03	0.13	0.11
TiO_2	0	-0.01	-0.01	0	0.01	0.03	0.01	0	-0.01
Total	97.34	97.69	98.15	98.59	97.78	99.01	98.09	97.94	97.84

	TC Stock	TC 280m	Hwy-144	Hwy-144	TC 280m
Albite	Least altered	Altered	Least altered	Mineralized	W. Mineralized
SiO_2	68.30	68.06	68.72	67.98	68.06
Na_2O	9.74	9.56	9.22	10.13	9.56
Al_2O_3	21.17	20.22	21.34	20.81	20.22
FeO	0.01	0.35	0.05	0.47	0.35
MnO	0.01	0.04	-0.02	-0.03	0.04
K_2O	0.07	0.01	0.08	0.08	0.01
BaO	-0.01	0.02	-0.01	0	0.02
CaO	0.09	0.01	0.05	0.03	0.08
TiO_2	0.01	0	0	0	0
Total	99.38	98.35	99.42	99.47	98.35

	TC Stock Q694659	TC Stock Q694659	TC Stock Q694659	TC Stock Q694658	TC Stock Q694658	TC Stock Q694658	Hwy-144 N969133	Hwy-144 N969133	Hwy-144 N969133
K-Feldspar	Unaltered	Unaltered	Unaltered	Altered	Altered	Altered	Mineralized	Mineralized	Mineralized
SiO_2	63.96	64.01	63.94	63.88	64.17	64.36	64.61	64.52	64.42
Na_2O	0.19	0.23	0.18	0.17	0.11	0.16	0.17	0.12	0.13
Al_2O_3	19.48	19.69	19.57	19.28	19.21	19.54	19.21	19.5	19.18
FeO	0.04	0.01	0.05	0.06	0.18	0.06	0.39	0.00	0.28
MnO	-0.01	-0.01	0.00	-0.02	-0.01	0	0.01	0.04	-0.02
K_2O	16.28	16.02	16.32	16.05	16.44	15.48	15.52	15.93	16.03
BaO	0.39	0.84	0.26	0.53	0.02	0.77	0.25	0.07	0.09
CaO	0	0.01	0.02	0.01	-0.00	0.00	0.00	0	0.01
TiO_2	-0.01	-0.01	-0.00	0.01	0.09	0.01	0.01	0	0.01
Total	100.32	100.78	100.32	99.95	100.11	100.38	100.18	100.18	100.13

	Hwy-144 N969133	Hwy-144 N969114	Hwy-144 N969114	Hwy-144 N969114	Hwy-144 N969114	Hwy-144 N969098	Hwy-144 N969098	Hwy-144 N969106	Hwy-144 N969106
K-Feldspar	Mineralized	Least Altered	Least Altered	Least Altered	Least Altered	Mineralized	Mineralized	Mineralized	Mineralized
SiO_2	63.53	63.97	64.03	63.85	64.27	64.29	63.91	64.65	64.73
Na_2O	0.29	0.17	0.17	0.15	0.16	0.12	0.21	0.14	0.12
Al_2O_3	19.05	19.22	19.41	19.33	19.2	18.96	18.16	19.35	19.25
FeO	1.69	0.03	0	0.24	0.06	0.13	0.49	0	0.02
MnO	0.03	0.01	0.01	0.01	0.02	0	0.01	0	-0.02
K_2O	15.33	15.52	15.43	15.32	15.46	15.90	16.77	15.51	16.18
BaO	0.16	0.69	0.82	0.65	0.18	0.01	0	0.53	0.04
CaO	0	0.02	0.01	0.03	0.05	0.01	0.01	0.02	0.01
TiO_2	0	0.02	0.01	0.01	0.01	0	0.01	-0.01	0
Total	100.07	99.65	99.89	99.57	99.39	99.41	99.57	100.18	100.34

	Hwy-144 N969126	Hwy-144 N969126	TC 280m M191372	TC 280m M191372	TC 280m M191374	TC 280m M191374	TC 660m	TC 660m
K-feldspar	?	?	Altered	Altered	Altered	Altered	V host Min	V host Min
SiO_2	65.05	64.29	64.34	64.39	63.83	63.4	64.4	64.87
Na_2O	0.16	0.15	0.14	0.1	0.14	0.13	0.13	0.16
Al_2O_3	19.34	19.68	19.53	19.49	19.4	18.47	18.97	19.39
FeO	0.24	0.02	0.1	0.07	0.01	0.33	0.06	0.11
MnO	0	-0.02	0	0.01	-0.01	-0.01	0.02	0
K_2O	15.8	15.41	16.12	15.93	16.08	16.49	16.91	15.88
BaO	0.02	0.98	0.17	0.09	0.58	0.07	0.05	0.29
CaO	0.02	0.01	0	0.01	0.01	0.01	0.01	0.01
TiO_2	0	0.01	-0.01	0.01	0	0	0	0
Total	100.67	100.52	100.39	100.1	100.04	99.42	100.56	100.71

	TC Stock	TC 280m	Hwy-144	Hwy-144
K-feldspar	Unaltered	Altered	W. Altered	Mineralized
SiO_2	63.94	63.83	64.03	63.53
Na_2O	0.18	0.14	0.17	0.29
Al_2O_3	19.57	19.4	19.41	19.05
FeO	0.05	0.01	0	1.69
MnO	0	-0.01	0.01	0.03
K_2O	16.32	16.08	15.43	15.33
BaO	0.26	0.58	0.82	0.16
CaO	0.02	0.01	0.01	0
TiO_2	0	0	0.01	0
Total	100.32	100.04	99.89	100.07

Appendix F

Pyrite Geochemical Data

This appendix contains the raw data used to determine the concentration of trace elements in pyrite grains. Trace element data was collected at the University of Windsor, Ontario and processed with the program Plasmalab. The raw data can only be manipulated with this program. The raw data is provided on a jump drive, if you would like access to the raw data please contact the author.

Appendix G

Sulfur Isotopic Data

This appendix contains a table that outlines where the sulfur isotopic values were taken from, the type of pyrite and whether there was gold in the whole rock sample. The appendix also contains a powerpoint with the BSE image of the pyrite grain and the location of each of the insitu sulfur isotope locations. To obtain the electronic copy of the powerpoint, please contact the author.

Sample Number	Location	Pyrite Type	δS^{34}	Gold in Sample?
M191366	TC280	Disseminated	-4.4	No
M191367	TC280	Disseminated	-4.8	No
M191372	TC280	Disseminated	-4.8	No
M191372	TC280	Disseminated	-6.1	No
M191372	TC280	Disseminated	-5.5	No
M191374	TC280	Vein Hosted	-4.3	No
M191374	TC280	Vein Hosted	-3	No
M191374	TC280	Vein Hosted	-5.3	No
M191378	TC280	Vein Hosted	-3.9	No
M191378	TC280	Vein Hosted	-3.3	No
M191378	TC280	Vein Hosted	-3.4	No
TC695 39m	TC695	Disseminated	-3	No
TC695 39m	TC695	Disseminated	-4.4	No
TC695 39m	TC695	Disseminated	-4.5	No
TC407	TC660	Vein Hosted	-4.8	No

TC407	TC660	Vein Hosted	-4.8	No
TC407	TC660	Vein Hosted	-4.2	No
TC407	TC660	Vein Hosted	-3.4	No
TC406	TC660	Vein Hosted	-5	Yes
TC406	TC660	Vein Hosted	-4.3	Yes
TC406	TC660	Vein Hosted	-5.2	Yes
TC406	TC660	Vein Hosted	-5	Yes
N969095	Hwy 144	Disseminated	-3	No
N969095	Hwy 144	Disseminated	-1.8	No
N969098	Hwy 144	Fracture Filling	-2.9	Yes
N969098	Hwy 144	Fracture Filling	-3.7	Yes
N969098	Hwy 144	Fracture Filling	-1.5	Yes
N969098	Hwy 144	Fracture Filling	-1.4	Yes
N969126	Hwy 144	Fracture Filling	-6.1	No
969126	Hwy 144	Fracture Filling	-6.9	No
N969126	Hwy 144	Fracture Filling	-4.4	No
N969126	Hwy 144	Fracture Filling	-3.7	No
N969126	Hwy 144	Fracture Filling	-2.5	No
N969106	Hwy 144	Vein Hosted	-1.7	Yes
N969106	Hwy 144	Vein Hosted	-0.1	Yes
N969106	Hwy 144	Vein Hosted	-1.2	Yes
N969106	Hwy 144	Vein Hosted	-1.1	Yes
N969106	Hwy 144	Vein Hosted	-0.3	Yes